

Development of a Bisphosphonate Delivering Hydrogel for the Augmentation of Impaired Peri-Implant Bone

THÈSE N° 6370 (2014)

PRÉSENTÉE LE 24 OCTOBRE 2014

À LA FACULTÉ DES SCIENCES ET TECHNIQUES DE L'INGÉNIEUR
LABORATOIRE DE BIOMÉCANIQUE EN ORTHOPÉDIE EPFL-CHUV-DAL
PROGRAMME DOCTORAL EN BIOTECHNOLOGIE ET GÉNIE BIOLOGIQUE

ÉCOLE POLYTECHNIQUE FÉDÉRALE DE LAUSANNE

POUR L'OBTENTION DU GRADE DE DOCTEUR ÈS SCIENCES

PAR

Ulrike KETTENBERGER

acceptée sur proposition du jury:

Prof. G. Fantner, président du jury
Prof. D. Pioletti, directeur de thèse
Prof. J.-M. Bouler, rapporteur
Prof. Ph. Procter, rapporteur
Prof. H. van Lenthe, rapporteur



ÉCOLE POLYTECHNIQUE
FÉDÉRALE DE LAUSANNE

Suisse
2014

“Don’t just stand there; make something happen.”

- Lee Iacocca

Acknowledgements

I would like to express my deep gratitude to my thesis director Prof. Dominique Pioletti for giving me the opportunity to perform this research project in his laboratory, for his patient guidance, useful critiques and endless optimism during the last four years.

Furthermore, I want to thank my thesis committee, Prof. Jean-Michel Bouler, Prof. Philip Procter, Prof. Harry van Lenthe, and Prof. Georg Fantner for their availability, precious time, and motivation to examine my work.

I also want to thank all my former and current colleagues from the LBO for the great atmosphere in the lab, the uncounted coffee breaks, lunch discussions, and social events. You made working in the lab a pleasure for me. Special thanks should be given to Sandra Jaccoud for her help with the cell culture experiments, the histology, and the surgeries and to Eric Thein from the CHUV for assisting and teaching me how to operate and suture correctly. I am also particularly grateful for the assistance with the animals given by Gisèle Ferrand, Simone Duis, Laetizia Baud, Maury Duany, and Stéphanie Marro. My special thanks are extended to Julien Ston and Christoph Engelhardt for their availability whenever I had problems with the computers or software and to Valérie Malfroy Camine for all the fruitful discussions and her support with the microCT. I also want to thank Caroline Fernandes for her valuable help with statistics and Matlab as well as for English-language proofreading. Salim Darwiche was always there for pimping my abstract titles, sharing his sweets, and analyzing my histology slides together with Karina Klein and Prof. Brigitte von Rechenberg from the University of Zürich. Furthermore, I want to thank Gisela Kuhn from the ETH Zürich for introducing me to the dynamic histomorphometry and to Adeliya Latypova and Alexandre Terrier for realizing the microFE study with me under heavy time pressure. Special thanks should be given to Philippe Abdel-Sayed, who always has an open ear to share joy and pain and became a close friend.

I also want to express my great appreciation to Virginie Kokocinski who helped me wherever she could with organizing my project and dealing with Swiss bureaucracy. Marc Jeanneret and the team from the mechanics workshop also contributed significantly to the success of the project with their precious work and expertise.

Furthermore, I wish to acknowledge the team from the CTI project for their collaboration, their precious feedback and input for the project. Not to be forgotten are also the students that contributed to this thesis; Raphael Obrist, Jules Bourgon, Stefania Rissone, and Adam Ouzeri, thank you very much for your work.

Last but not least I want to thank my friends and my family, especially my parents Lina and Michael Kettenberger, who always supported me in my ideas and plans and helped me to become what I am today. Finally and most importantly, I want to express immeasurable gratitude to Maxi for his love, understanding, and patience during four years that have not always been easy.

Lausanne, 08.10.2014

Abstract

Osteoporosis is a major health problem in our aging society. This metabolic disease, which is characterized by a deterioration of the bone microarchitecture and a significant loss of bone mass, is affecting a rising number of mostly elderly patients. The main clinical consequences are typical fragility fractures resulting in severe pain, morbidity, and mortality for affected patients. Osteoporosis does not only cause fractures, but also complicates fracture treatment, as implants are difficult to anchor in the impaired bone structure. Therefore, many mechanical and pharmaceutical approaches have been developed over the last decades to target this issue and improve implant anchorage in osteoporotic bone.

The overall goal of the present PhD thesis was the development of a bisphosphonate (BP) releasing hydrogel that can enhance implant fixation in osteoporotic bone. The project was divided into three major sections: the investigation of the BP effect on peri-implant bone, the development and testing of the drug delivering biomaterial, and the evaluation of its efficiency in terms of implant fixation improvement. An ovariectomized rat model of postmenopausal osteoporosis was utilized for the investigation of the spatio-temporal effect of locally released Zoledronate, the BP used in this study. The drug was delivered from a biodegradable hyaluronic acid (HyA) hydrogel matrix to the bone stock surrounding screws that were implanted in the femoral condyles of the rats. Static and dynamic bone histomorphometric parameters were monitored in four concentric bone layers around the screw with time-lapsed *in vivo* microCT scans. With this study, we were able to demonstrate a significant enhancement of early bone formation rate accompanied by an efficient inhibition of peri-implant bone resorption in a large range around the screw. In a second *in vivo* study, we incorporated Zoledronate-loaded hydroxyapatite nanoparticles in the HyA hydrogel resulting in an unexpected rapid mineralization of the hydrogel within 10 days after implantation. Histology performed 2 months after implantation revealed granule-shaped mineralized spots within the peri-implant bone serving as scaffolds for new bone formation. When using Zoledronate-loaded particles, we could demonstrate a strong inhibitory effect on both peri-implant bone resorption and mineralized hydrogel degradation. Finally, we used the *in vivo* microCT scans of the first animal study to create micro-finite element models for the analysis of the screw fixation time course. We were able to show that Zoledronate locally delivered from the hyaluronic acid hydrogel improved screw fixation significantly as soon as 17 days after implantation when compared to an untreated control group. This difference persisted until the end of the study at day 58.

Taken together, the studies performed for the present PhD thesis demonstrated an excellent suitability of HyA hydrogels for the local delivery of BPs intended to improve implant fixation in impaired bone. A Zoledronate triggered enhancement of screw fixation occurred early and persisted over a prolonged period,

an important aspect considering that osteosynthesis implants need a reliable bone anchorage from the time of implantation until complete fracture healing. Furthermore, it could be shown that an addition of hydroxyapatite particles to the HyA resulted in a rapid *in vivo* mineralization of the hydrogel, a promising feature for bone defect repair applications.

Keywords

Bisphosphonate; drug delivery; hydrogel; hydroxyapatite; implant fixation; microCT; microFE; OVX rat model; dynamic histomorphometry

Zusammenfassung

Die Skeletterkrankung Osteoporose ist ein ernsthaftes gesundheitliches Problem und betrifft aufgrund der aktuellen demographischen Entwicklung und der steigenden Lebenserwartung immer mehr Menschen. Diese Krankheit manifestiert sich typischerweise in einer signifikanten Verminderung der Knochenmasse gepaart mit einer veränderten Knochenstruktur. Als Folge dieser Knochenschwächung treten Frakturen bei Betroffenen oft schon bei geringen Belastungen, wie zum Beispiel einem Sturz aus Standhöhe, auf. Diese Knochenbrüche resultieren bei den oft älteren Patienten nicht selten in dauerhaften Behinderungen, einer eingeschränkten Mobilität und einer verringerten Lebenserwartung. Die Osteoporoseerkrankung erhöht aber nicht nur das Frakturrisiko, sie erschwert nach Auftreten eines Knochenbruchs auch die chirurgische Versorgung. Üblicherweise verwendete Osteosynthese-Implantate können in der der geschwächten Knochenstruktur oft nicht zuverlässig verankert werden und dislokieren. In den letzten Jahrzehnten wurden daher zahlreiche mechanische und pharmakologische Ansätze zur Verbesserung der Implantatverankerung in osteoporotischen Knochen entwickelt und getestet.

Das Ziel der vorliegenden Doktorarbeit war die Entwicklung eines Bisphosphonat-freisetzenden Hydrogels, das zur lokalen Verstärkung der Knochensubstanz in direkter Umgebung eines Implants eingesetzt werden kann. Das Projekt umfasste drei Hauptaufgabengebiete: Zunächst wurde der Einfluss des lokal applizierten Bisphosphonats auf den Knochen in Implantatnähe ermittelt. Danach wurde ein geeignetes System zur Freisetzung des Wirkstoffs entwickelt. In einem dritten Schritt wurde die Effizienz des gewählten Hydrogels bei der Verbesserung der Implantatverankerung getestet.

Für die *in vivo* Untersuchung der räumlich-zeitlichen Wirkung von lokal freigesetztem Zoledronat, dem für die vorliegende Arbeit verwendeten Bisphosphonat, wurden ovariectomierte Ratten als Modell für postmenopausale Osteoporose verwendet. Miniaturschrauben wurden in die Femurkondylen von Ratten implantiert und der Wirkstoff wurde dabei direkt mit einem Hyaluronsäure-Hydrogel in die Umgebung der Implantate eingebracht. Mit Hilfe von zeitversetzt erstellten MicroCT-Aufnahmen wurden die statischen und dynamischen Knochenparameter in vier konzentrisch um die Schraube angeordneten Knochenschichten ermittelt. In diesem Tierversuch konnte in den Zoledronat-behandelten Ratten im Vergleich zu den Kontrollratten eine deutlichen Zunahme der Knochenneubildung direkt nach Schraubenimplantation gepaart mit einer Verringerung der Knochenresorption während des ganzen Studienzeitraums beobachtet werden.

In einer zweiten *in vivo* Studie wurde der Wirkstoff vor Einbringung in das Hydrogel auf Hydroxyapatit-Nanopartikel absorbiert. Die Präsenz der Keramikpartikel, sowohl mit als auch ohne Wirkstoff, resultierte in einer unerwarteten, innerhalb weniger Tage nach Einbringung erfolgenden *in vivo* Mineralisierung des Hydrogels. Histologische Untersuchungen, die 2 Monate nach Implantation von Schrauben und Hydrogel erfolgten, zeigten granulatförmige mineralisierte Stellen eingebettet in neugebildeten Knochen. Bei gleichzeitiger Verwendung von Zoledronat und Hydroxyapatitpartikeln konnte ein starker inhibitorischer Effekt sowohl auf die Knochenresorption als auch auf den Abbau des mineralisierten Biomaterials gezeigt werden.

Im dritten Teil der Arbeit wurden die für den ersten Tierversuch erzeugten microCT Aufnahmen zur Erstellung von micro-Finite-Elemente Modellen verwendet. Diese Modelle dienten zur Untersuchung des zeitlichen Verlaufs der Schraubenverankerung im Rattenknochen. Es konnte gezeigt werden, dass die lokale Freisetzung von Zoledronat aus einem Hyaluronsäure-Hydrogel schon nach 17 Tagen die Ausreißfestigkeit der Schrauben signifikant erhöht. Der Unterschied zwischen den mit Zoledronat behandelten und unbehandelten Tieren blieb die folgenden 6 Wochen bis zum Studienende bestehen.

Zusammengefasst belegten die im Rahmen dieser Doktorarbeit durchgeführten Versuche die ausgezeichnete Eignung abbaubarer Hyaluronsäure-Hydrogele für die lokale Freisetzung von Bisphosphonaten zum Zweck der Verbesserung der Implantatverankerung in osteoporotischem Knochen. Es konnte gezeigt werden, dass die lokale Applikation von Zoledronat den Halt eines Implantats schnell und dauerhaft verbessern kann. Dies ist ein wichtiger Aspekt, da die Verankerung der zur Frakturbehandlung eingesetzten Osteosynthese-Implantate über den gesamten Zeitraum der Knochenheilung sichergestellt werden muss. Zusätzlich konnte gezeigt werden, dass die Zugabe von Hydroxyapatit-Partikeln zum Hyaluronsäure-Hydrogel in einer schnellen *in vivo* Mineralisierung der Gels resultiert. Dieses Ergebnis erweitert den Kreis der möglichen Anwendungsgebiete dieses Biomaterials auf die Reparatur von Knochendefekten.

Schlüsselwörter

Bisphosphonat; Wirkstofffreisetzung; Hydrogel, Hydroxyapatit; Implantatverankerung; microCT; microFE; Rattenmodell; Osteoporose; Dynamische Histomorphometrie

Acknowledgements	vii
Abstract	ix
Keywords	x
Zusammenfassung	xi
Schlüsselwörter	xii
Chapter 1 Introduction	17
1.1 Bone	17
1.1.1 Bone Structure.....	17
1.1.2 Bone Cells	18
1.1.3 Bone Modeling and Remodeling	19
1.1.4 Osteoporosis and Bone Loss.....	20
1.2 Implant Treatment in Low Quality Bone.....	21
1.2.1 Osteoporotic fractures	21
1.2.2 Improving Implant Fixation in Low Quality Bone	22
1.3 Bisphosphonates.....	23
1.3.1 Molecular Mechanisms and Mode of Action of Bisphosphonates.....	24
1.3.2 Local Release of Bisphosphonates.....	26
1.3.3 Delivery Systems for Bisphosphonates.....	26
1.4 Evaluation of Implant Outcome	27
1.4.1 Mechanical Testing of the Implant Stability	27
1.4.2 Numerical Evaluation of the Implant Stability.....	27
1.4.3 Bone Analysis with CT-Based Dynamic Bone Histomorphometry.....	28
1.5 Scope of the Thesis	29
1.5.1 Industrial Background.....	30
1.5.2 Objectives of the Thesis.....	30
1.5.3 Aim 1: Investigation of the Zoledronate Effect on Peri-Implant Bone	31
1.5.4 Aim 2: Development of a Drug Delivery System	31
1.5.5 Aim 3: Evaluation of the Implant Fixation with μ Finite-Element-Analysis	31

1.6	References	32
Chapter 2	Investigation of the Effect of Locally Delivered Zoledronate on Peri-Implant Bone	37
2.1	Abstract.....	38
2.2	Introduction	39
2.3	Materials and Methods.....	40
2.3.1	General Study Design.....	40
2.3.2	Hydrogel Preparation	41
2.3.3	Animal Model	41
2.3.4	Surgical Procedures	41
2.3.5	MicroCT Imaging, Data Processing and Analysis	42
2.3.6	Histology	44
2.3.7	Statistics.....	45
2.4	Results.....	45
2.4.1	Clinical Observations	45
2.4.2	Assessment of the Estrogen Deficiency Induced Bone Loss.....	45
2.4.3	MicroCT-based Dynamic Histomorphometry.....	46
2.4.4	Histology	52
2.5	Discussion.....	53
2.6	Conclusion.....	57
2.7	Acknowledgment	57
2.8	References	58
Chapter 3	Development of a Drug Delivery System	61
3.1	Abstract.....	62
3.2	Introduction	63
3.3	Materials and Methods.....	64
3.3.1	<i>In vitro</i> Cell Assay.....	64
3.3.2	Hydrogel Preparation	65
3.3.3	Drug Release Study.....	66
3.3.4	<i>In vivo</i> Study.....	66
3.3.5	Histology	67

3.3.6	Statistics.....	68
3.4	Results.....	68
3.4.1	Cell Assay	68
3.4.2	Drug Release Study.....	70
3.4.3	<i>In vivo</i> Study.....	71
3.4.4	Histology	76
3.5	Discussion.....	77
3.6	Conclusion.....	81
3.7	Acknowledgements.....	82
3.8	References	83
Chapter 4	Evaluation of Implant Fixation with Micro-Finite-Element Analysis.....	85
4.1	Abstract.....	86
4.2	Introduction	87
4.3	Materials and Methods.....	88
4.3.1	<i>In vivo</i> MicroCT Study	88
4.3.2	Experimental Pullout Test.....	88
4.3.3	Image Processing	90
4.3.4	MicroFE Analysis	91
4.3.5	Statistical Analysis.....	92
4.4	Results.....	92
4.4.1	Experimental Pullout Test.....	92
4.4.2	Identification of the Failure Criteria for the MicroFE Models	92
4.4.3	Analysis of the <i>In vivo</i> Study	94
4.5	Discussion.....	96
4.6	Conclusion.....	99
4.7	Acknowledgements.....	100
4.8	References	101
Chapter 5	Discussion and Perspectives	103
5.1	Clinical Situation and Specifications for the Drug Delivery System	103
5.2	Hydrogel as Drug Delivery System for Bisphosphonates.....	104

5.3	Applicability of the New Drug Delivery System	105
5.4	Perspectives	107
5.4.1	Testing the Model and Dose Dependency of the Results.....	107
5.4.2	Investigation of the Enhanced Early Bone Formation	107
5.4.3	Investigation of the <i>in vivo</i> Hydrogel Mineralization.....	107
5.4.4	Improvement of Implant Primary Stability.....	108
5.4.5	The Path towards a Clinical Study	108
5.5	References	110
Annex	113
A.1	Chronology of the Project: From Coating to Hydrogel	113
A.1.1	Evaluation of a Drug Delivering Coating	113
A.1.2	Evaluation of a Solid Drug Delivering Bone Plug	114
A.2	Hollow Hydroxyapatite-Polylactide Microspheres	115
A.3	References	115
Curriculum Vitae	117

Chapter 1 Introduction

1.1 Bone

Bone is defined as “any piece of hard whitish tissue making up the skeleton in humans and other vertebrates” in the Oxford Dictionary. Despite its simple appearance, bone is a complex and dynamic living tissue that fulfills many functions in the human body. First, the 206 bones of an adult provide a structural framework for the body and attachment points for tendons and the skeletal muscles. The resulting leverage system allows us to move. Another important function of the bones is to support and protect the sensitive inner organs such as the brain and the heart. Apart from their mechanical and structural functions, bones are also involved in metabolic processes: they store and release important minerals such as calcium and phosphorus (mineral homeostasis). Furthermore, the red marrow of bone produces platelets and red and white blood while the yellow bone marrow is rich in adipose cells and stores triglycerides (Nordin 2012; Tortora 2013).

1.1.1 Bone Structure

Bone is characterized by a very specific structure that varies depending on its position and function. Two main structures can be distinguished: trabecular (cancellous) and cortical (compact) bone (Figure 1.1). Around 80% of the human skeleton is cortical bone and 20% is trabecular bone. **Cortical bone** is the strongest type of bone tissue and forms the shell for all bones. Additionally, it makes up the bulk of the diaphyses of long bones. Cortical bone is very dense and arranged in repeating structural units called osteons or haversian systems. Each osteon contains a longitudinal central haversian channel that houses blood vessels, nerves, or lymphatic vessels surrounded by concentrically arranged lamellae made of hard, calcified extracellular matrix. The tube-shaped osteons are bundled together longitudinally to the bone axis. The osteocytes (mature bone cells) in the cortical bone are interspersed between the osteons in structures called lacunae. These lacunae are connected via tiny fluid-filled canaliculi. This channel system ensures a nutrient supply for the osteocytes.

In contrast to cortical bone, **trabecular bone** does not contain osteons. It is composed of irregular lattices of thin bone columns called trabeculae. The spaces between the trabeculae of most bones are filled with red bone marrow. The trabeculae themselves are composed of concentric lamellae, osteocytes lying in lacunae, and a canaliculi network. Trabecular bone is very light-weight compared to cortical bone and helps to reduce the overall weight of bone to facilitate body movements (Nordin 2012; Tortora 2013). The orientation of the trabeculae in trabecular bone is according to the “form follows function” principle (Stromsoe 2004). A dense fibrous membrane, called periosteum, surrounds all bones. This membrane,

which is highly permeated with nerves and blood vessels, is connected with the haversian channels of the cortex. A thinner membrane, called the endosteum, lines the marrow cavities of yellow fatty bone marrow (Nordin 2012).

On a microscopic level, bone has two distinct states as it matures: woven bone and lamellar bone. Woven bone is immature bone and is found in fetuses, in newborns, in fracture calli, close to the growth plate of bones, and in certain bone diseases. Lamellar bone replaces the woven bone one month after birth, or after the remodeling process of a fracture callus (Nordin 2012).

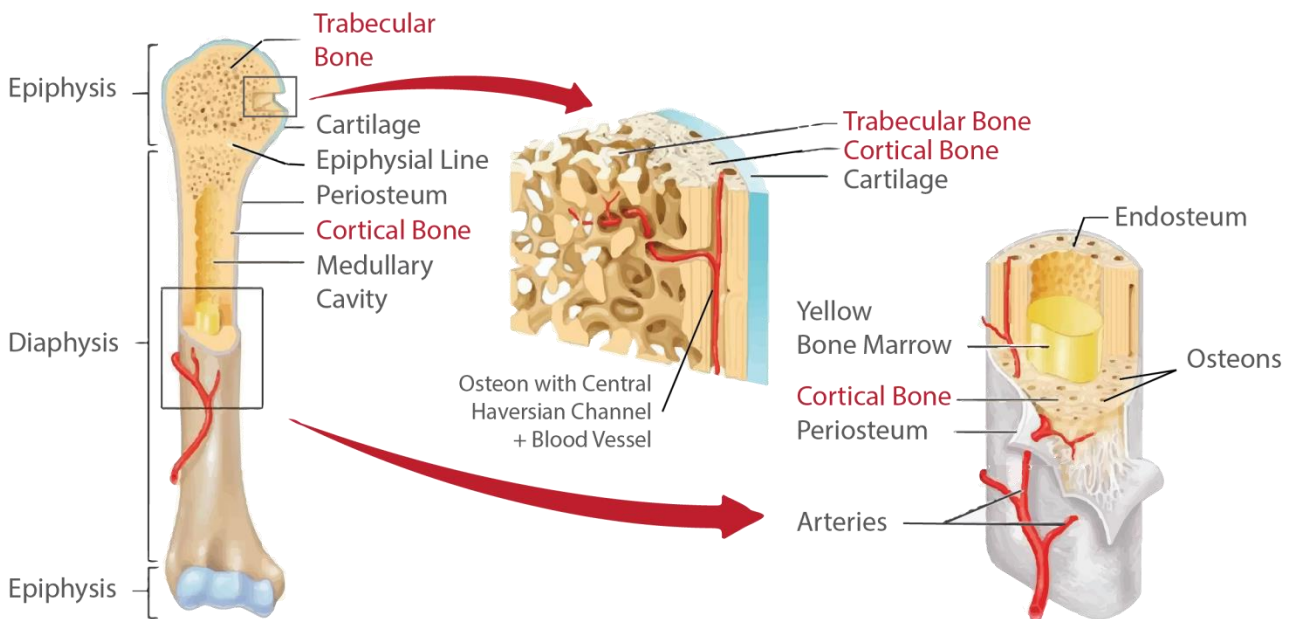


Figure 1.1: Structure and composition of a typical long bone (adapted from <http://classes.midlandstech.edu/carterp/Courses/bio210/chap06/lecture1.html>).

1.1.2 Bone Cells

Bone as a connective tissue is composed from an extracellular matrix that surrounds widely separated cells. This extracellular matrix contains around 25% water, 25% type 1 collagen fibers, and 50% mineral crystallized salts (apatite) (Stromsoe 2004). The collagen is responsible for the tensile strength of bone and the mineral component is responsible for the compressive strength of bone. Four major cell types can be found in bone tissue. The first type is **osteogenic cells**, which are unspecialized mesenchymal stem cells and the only bone cells that undergo cell division. Osteogenic cells develop into **osteoblasts**, the second cell type, and are known to be responsible for bone formation. Osteoblasts are responsible for building the extracellular bone matrix by synthesis and secretion of collagen fibers and other organic components. This initially soft matrix, called osteoid, is later transformed into hard bone matrix via a mineralization process. Once the osteoblasts are surrounded by their matrix and become trapped, they change their form and function and become **osteocytes**, or mature bone cells. Osteocytes are the main cells in bone and they are responsible for metabolic functions such as the exchange of nutrients and waste with blood cells. Osteoblasts can also flatten and become lining cells, which cover and protect the bone surface (Boyce,

Rosenberg et al. 2012). The last group of important bone cells are **osteoclasts**. These huge, multinucleated cells are derived from a fusion of around 50 monocytes. Osteoclasts release lysosomal enzymes and acids that can digest the protein and mineral components of the bone extracellular matrix during the bone resorption process (Tortora 2013).

1.1.3 Bone Modeling and Remodeling

Two important processes, bone modeling and remodeling, ensure the development and maintenance of a vertebrate's skeletal system (Raggatt and Partridge 2010). Bone modeling is required for the growth and adaptation of the skeleton to mechanical loads. Modeling requires the osteoblast-mediated formation and osteoclast-mediated resorption of bone; these two processes occur independently at distinct anatomical sites (Raggatt and Partridge 2010). Bone remodeling, however, is needed for the removal and repair of old and damaged bone as well as for mineral homeostasis (Seeman 2009; Boyce, Rosenberg et al. 2012). For bone remodeling, resorption and formation occur sequentially and well-coordinated at the same location to preserve bone mass as much as possible (Raggatt and Partridge 2010). The bone remodeling process occurs over several weeks and is performed by clusters of osteoclasts and osteoblasts arranged in basic multicellular units (BMUs) (Figure 1.2) (Boyce, Rosenberg et al. 2012). An active BMU contains a leading front of bone-resorbing osteoclast that creates trenches in the bone surface (Raggatt and Partridge 2010; Boyce, Rosenberg et al. 2012). Reversal cells of unclear phenotype then cover the exposed bone surface and prepare it for the deposits of new bone. The tail portion of the BMU is occupied by osteoblasts that secrete osteoid and later on direct the transfer of mineralized lamellar bone (Raggatt and Partridge 2010). Collagen type 1 fibers and other matrix-bound proteins such as growth factors are released during resorption and can influence the osteoblasts and cells in the bone marrow adjacent to the bone remodeling sites (Boyce, Rosenberg et al. 2012).

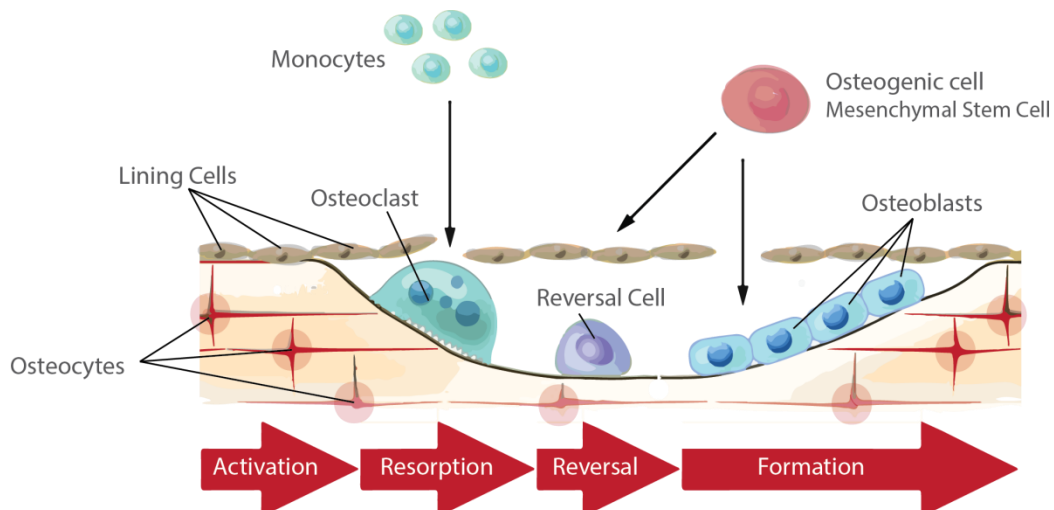


Figure 1.2: Bone remodeling process in a basic multicellular unit (BMU) (adapted from (Raisz 2005)).

1.1.4 Osteoporosis and Bone Loss

An imbalance in bone formation and resorption compromises bone homeostasis and leads to an abnormal bone loss or, less frequently, bone gain. This loss of equilibrium occurs in many common bone diseases such as osteoporosis, osteopetrosis, hyperparathyroidism, renal osteodystrophy, Paget's disease, and bone tumors (Cummings and Melton 2002). Osteoporosis is the most frequent bone metabolic disease and has existed throughout human history, but it has only recently been considered a major clinical problem due to increasing life expectancy in humans. This systemic disease is characterized by a loss of bone mass and a deterioration of the bone microarchitecture, resulting in bone fragility and susceptibility to fractures (Figure 1.3) (Stromsoe 2004). The world health organization (WHO) defined a diagnostic criterion for osteoporosis to be a bone mineral density (BMD) of at least 2.5 standard deviations lower than the average bone peak mass of a 30-year old individual of the same gender (Hernlund, Svedbom et al. 2013). Based on this criterion, approximately 22 million women and 5.5 million men between the ages of 50 to 84 were estimated to have osteoporosis in the EU in 2010. Due to the changes in population demography, the number of men and women with osteoporosis in the EU is expected to rise by 23% from 27.5 million in 2010 to 33.9 million in 2025 (Hernlund, Svedbom et al. 2013).

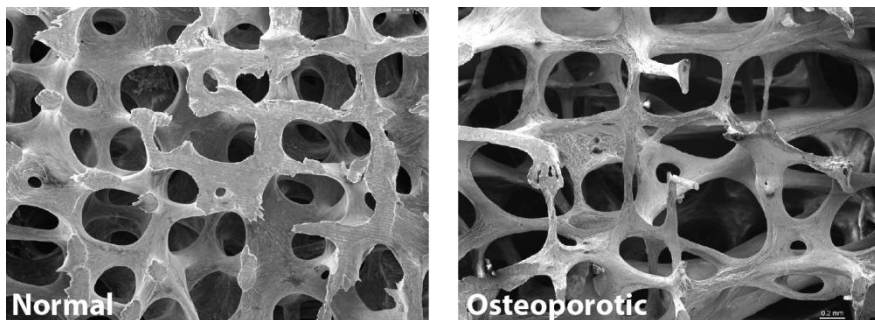


Figure 1.3: Scanning electron microscope images of human 3rd lumbar vertebrae with normal and osteoporotic bone microarchitecture (adapted from: <http://www.brsoc.org.uk/gallery>).

The three main pathogenic mechanisms leading to osteoporosis are failure to achieve a strong skeleton during growth and development, excessive bone resorption, and failure to replace lost bone due to bone formation defects (Raisz 2005). There are numerous causes of these three malfunctions of the bone remodeling process. Estrogen deficiency is known to play a critical role in the development of osteoporosis; this explains why women are very likely to develop osteoporosis after the abrupt cessation of ovarian function during the menopausal transition. Men also show a slight but steady decrease in estradiol and testosterone levels with aging, which can manifest itself in osteoporosis (Pietschmann, Rauner et al. 2009). Idiopathic, postmenopausal osteoporosis in women and senile osteoporosis affecting both genders are grouped as primary osteoporosis. In contrary, bone loss that occurs due to external factors, such as certain types of medication (e.g. corticosteroids), and forms due to endocrine diseases is classified as secondary osteoporosis (Stromsoe 2004).

1.2 Implant Treatment in Low Quality Bone

Osteoporosis does not only increase fracture risk, but also contributes to the severity of fractures and complicates their treatment (Schneider, Goldhahn et al. 2005). The decreased strength of the thinned cortical and trabecular bone dramatically affects the primary stability of osteosynthesis implants (Stromsoe, Kok et al. 1993; Lim, An et al. 1995). Furthermore, experimental and clinical data suggests that osteoporosis negatively influences fracture healing (Kubo, Shiga et al. 1999; Namkung-Matthai, Appleyard et al. 2001; Nikolaou, Efsthopoulos et al. 2009) and osteointegration and therefore also the secondary stability of implants (Blomqvist, Alberius et al. 1996; Schneider, Goldhahn et al. 2005). Osteosynthesis implants, such as typical plate screw constructs or intramedullary nails (Figure 1.4) were initially developed for younger patients with healthy, strong bones and they are often not well adapted to the needs of patients with fragile osteoporotic bones.

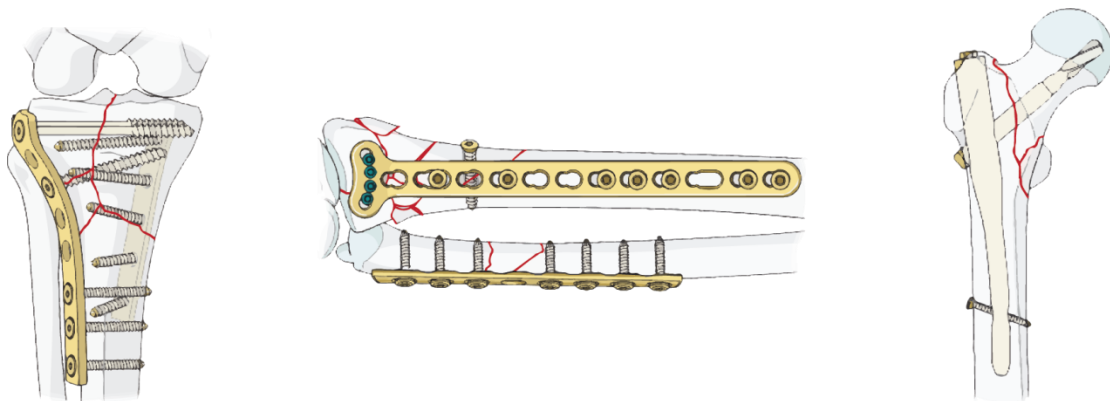


Figure 1.4: Examples for trauma implants, left: proximal tibia plate, middle: distal radius plate, right: intramedullary nail proximal femur (adapted from <https://www2.aofoundation.org/wps/portal/surgery>).

1.2.1 Osteoporotic fractures

Osteoporosis causes more than 8.9 million fractures worldwide per year, this corresponds to around 1000 fractures per hour (Johnell and Kanis 2006). Loss of mechanical strength due to a decreased thickness and increased porosity of the cortical bone can be partially compensated for in the diaphyseal area of long bones by an increase in bone diameter as is typically seen in osteoporotic patients. This mechanism does not work for the rarefaction of the trabecular network in the metaphyseal regions, the reason why osteoporotic bone is more likely to fracture at this sites under heavy mechanical load (Stromsoe 2004). Fractures in trabecular regions such as the vertebrae, distal radius and proximal femur (hip) are therefore regarded as typical osteoporotic fractures (Hernlund, Svedbom et al. 2013). Large prospective studies have shown that the risk for almost all types of fractures are increased in patients suffering from osteoporosis (Cummings and Melton 2002). The fracture risk typically increases with age due to age-related decrease in bone mineral density combined with an increasing number of falls in older patients (Cummings and Melton 2002). The age-dependent rapid rise in incidence of vertebral fractures is shown as an example in Figure 1.5. Osteoporotic fractures are not only painful for the affected patients, but hip fractures especially are

also associated with an increased morbidity. In 2010, the number of deaths causally related to osteoporotic fractures in the EU was estimated to be 43,000 (Hernlund, Svedbom et al. 2013).

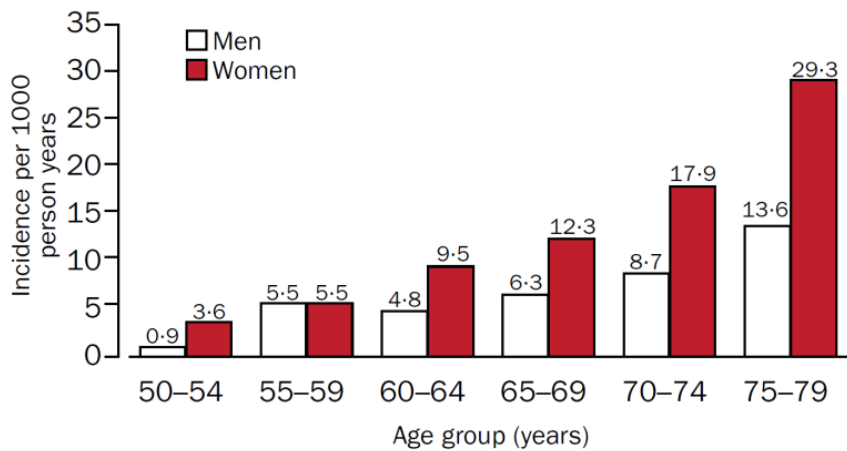


Figure 1.5: Incidence of vertebral fractures in women and men from Europe by age group (Cummings and Melton 2002).

1.2.2 Improving Implant Fixation in Low Quality Bone

The behavior of bone under load can be compared to that of a stiff spring that deforms when loaded and regains its original shape once the load is removed. The phenomenon can be distorted when a typically less elastic metal implant is attached to the bone. Therefore, implants that rely on the holding power of the screws in the bone are more sensitive to the inherent bone material properties than implants that achieve structural stability with locking bolts (Stromsoe 2004). The classical osteosynthesis plate gets its stability from the friction between the cortical bone surface and the plate, and only works if the screws are well anchored in the bone (Figure 1.6 left). As a consequence, the screws create a lot of stress in the surrounding bone structure, especially in sites with low bone density since screw holding power is known to be linearly correlated to loss of bone mass (Stromsoe, Kok et al. 1993). The result can be a cutout of the screws in the bone with resulting implant loosening and instability, a condition that often impairs fracture healing. Currently, the most successful strategy to ameliorate implant fixation problems in low quality bone is the use of angular stable constructs, for example screws that are locked directly to the plate (Figure 1.6 right). These angularly stable implants are much less dependent on screw holding power since no friction between the plate and the cortical bone is required (Sommer, Gautier et al. 2003; Stromsoe 2004; Kammerlander, Erhart et al. 2013).

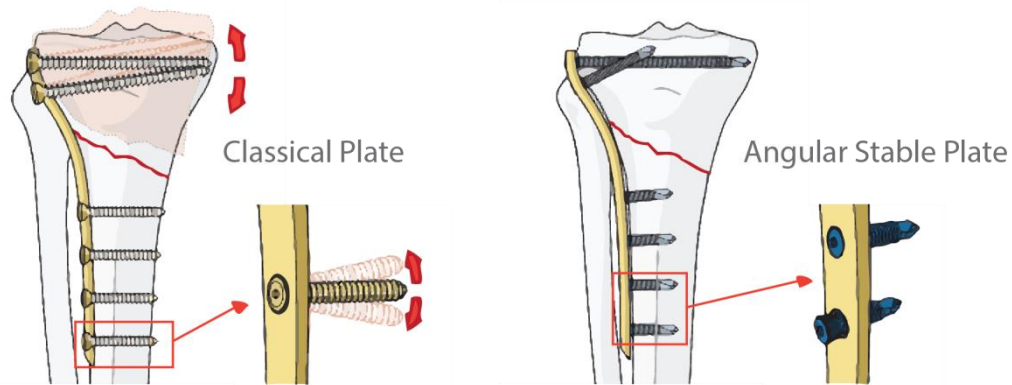


Figure 1.6: Principle of the angular stable plate (right) in comparison with a classical osteosynthesis plate (left) (adapted from <https://www2.aofoundation.org/wps/portal/surgery>).

Another strategy to improve implant fixation, especially in trabecular bone, is the use of cement. Cement typically consists of polymethylmethacrylate (PMMA) or tricalcium phosphate (TCP). Cements can increase the contact area between bone and implant to improve the primary stability of the implant (Lindner, Kanakaris et al. 2009; Dall'Oca, Maluta et al. 2010; Kammerlander, Erhart et al. 2013). Despite improved fixation, the non-resorbable PMMA and the very slowly resorbable TCP cements are nevertheless associated with poor long-term outcome for patients (Lindner, Kanakaris et al. 2009). Even with some improvement of the implantation anchorage in low quality bone due to the above mentioned mechanical solutions, the complication rates after implantation are still high (Broderick, Bruce-Brand et al. 2013). Therefore, new approaches for a fast and sustainable improvement of the bone quality around the implant without negative long-term effects are needed. One of the most promising strategies developed during the last decade is a local delivery of either anabolic or anti-catabolic drugs to the peri-implant bone (Pioletti, Gauthier et al. 2008). The local delivery routine is particularly interesting for drugs with a high affinity to bone, such as bisphosphonates, since those substances stay highly localized after administration and therefore do not require a special release profile (McKenzie, Dennis Bobyn et al. 2011).

1.3 Bisphosphonates

Bisphosphonates (BPs) are today the most important anti-resorptive drugs for the treatment of metabolic bone diseases such as osteoporosis, Paget's disease, hypercalcemia and tumor-associated osteolysis (Rogers, Gordon et al. 2000). They were first synthesized in the 1800's but have been progressively used in clinics only in the past 40 years (Russell 2011). This important group of drugs is characterized by a chemically stable structure made up of P-C-P bonds similar to that of inorganic pyrophosphates (PPi) that act as endogenous "water softeners" in the body (Figure 1.7) (Russell 2011). This P-C-P group makes the molecule resistant to chemical and enzymatic hydrolysis, therefore BPs are not metabolized in the body and are excreted unaltered (Russell, Watts et al. 2008). At the same time, the double phosphate groups chelate with Ca^{2+} ions and thus cause the high affinity of the molecule to bone mineral. This affinity gives BPs the unique property of having a selective uptake by the target organ (Russell, Watts et al. 2008).

Researchers have discovered that both the affinity of BPs to bone as well as the potency of BPs can be altered by changing the R_1 and R_2 side chains of the BP molecule (Rogers, Frith et al. 1999; Russell, Watts et al. 2008).

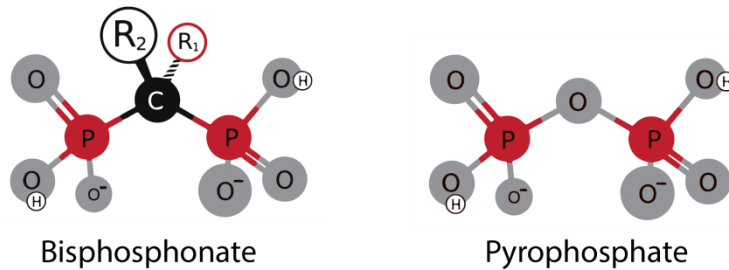


Figure 1.7: Chemical structure of bisphosphonates compared to the naturally occurring pyrophosphate.

Studies using radiolabeled BPs measured the uptake and retention of different BPs in the bone. The resulting data showed that approximately one to two thirds of the administered BP is absorbed into the skeleton while the remainder is expelled in the urine within a few hours of administration (Khan, Kanis et al. 1997; Thompson, Rogers et al. 2006). Nevertheless, small amounts of BPs can be detected in the urine for a long time after administration, this means that BPs are still released from the bone into the blood stream and are ready for a re-uptake into the bone (Khan, Kanis et al. 1997; Russell, Watts et al. 2008). This finding explains the prolonged periods of pharmacological action of BPs.

1.3.1 Molecular Mechanisms and Mode of Action of Bisphosphonates

There are two main groups of BPs, simple BPs and nitrogen-containing BPs, which have significantly different modes of action. Etidronate and Clodronate are typical examples of simple BPs, which were the first generation of this anti-resorptive group of drugs. Simple BPs are known to be converted into methylene-containing analogues of ATP in cells. This substance accumulates to toxic concentrations in the cytosol of all cell types which can incorporate BPs, such as osteoclasts and macrophages, leading to apoptosis of the affected cells (Roelofs, Thompson et al. 2006).

Not only is the mode of action of nitrogen-containing BPs (N-BPs) different, but this difference makes them several orders of magnitude more potent than simple BPs. N-BPs such as Alendronate and Zoledronate act by inhibiting the farnesyl diphosphate synthase in the cell which blocks prenylation of small GTPases. The accumulation of unprenylated GTPases in the cytoplasm of the osteoclasts leads to a disruption of the normal osteoclast function and apoptosis (Green, Muller et al. 1994; Green and Rogers 2002).

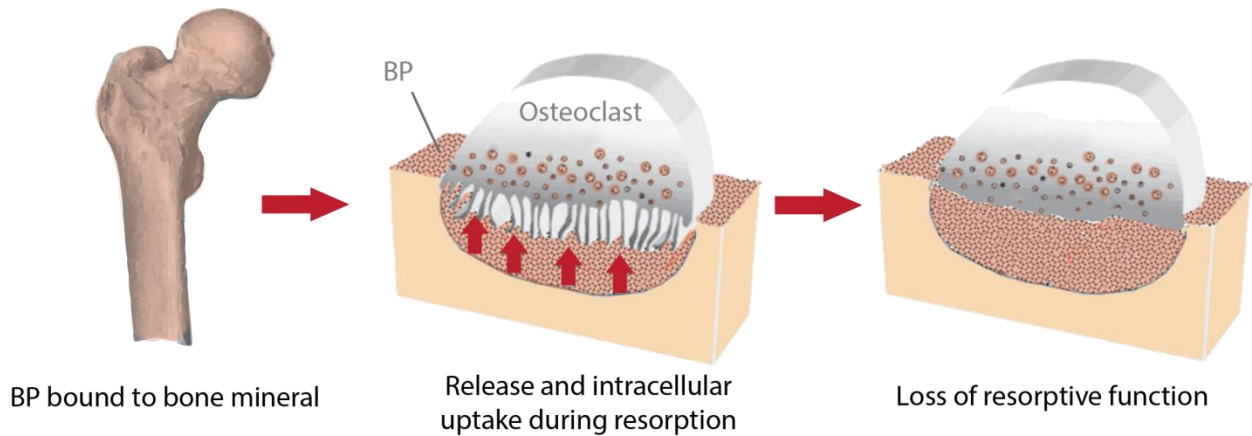


Figure 1.8: Mode of action of bisphosphonates on osteoclasts.

The acidic pH in the resorption lacuna of the osteoclasts causes a dissociation of the BP from the hydroxyapatite (Ebetino, Francis et al. 1998). The dissociated BP can then be taken up by the osteoclast, most likely via fluid-phase endocytosis (Thompson, Rogers et al. 2006) (Figure 1.8).

Besides the known inhibitory effect of BPs on osteoclasts, effects on other bone cells have been described as well, but the exact mechanisms are not clear yet (Roelofs, Thompson et al. 2006; Idris, Rojas et al. 2008). It has been reported that low concentrations of BPs can protect osteoblasts and osteocytes against apoptosis (Plotkin, Weinstein et al. 1999; Plotkin, Manolagas et al. 2006), stimulate the mineralized bone nodule formation *in vitro* (Giuliani, Pedrazzoni et al. 1998), and have a beneficial effect on osteoblast differentiation and protein synthesis (Greiner, Kadow-Romacker et al. 2006). Other studies demonstrated an improved mineralization and proliferation of human osteoblast-like cells exposed to Zoledronate (Pan, To et al. 2004). But also conflicting results can be found showing that especially aminobisphosphonates inhibit mineralization and osteoblast growth, induce osteoblast apoptosis and inhibit protein prenylation in osteoblasts *in vitro* in a dose-dependent manner (Idris, Rojas et al. 2008; Orriss, Key et al. 2009). Those findings show that *in vitro* effects of BPs require a careful interpretation as different experimental designs, BP types and concentrations can drastically influence the results. In contrary to the *in vitro* situation, bone cells would not be exposed to BP solutions over a long time in the body as the drug is absorbed rapidly to the bone mineral surface. Furthermore, the significance of the *in vitro* results for the *in vivo* situation is unclear as the reduced osteoclast activity can have numerous indirect effects on the bone remodeling cycle (Maruotti, Corrado et al. 2012). Published *in vivo* studies are also not conclusive regarding the influence of BPs on other cells than osteoclasts. Depending on the experimental setup used, a positive, negative or no influence on bone formation were reported (Tobias, Chow et al. 1993; Brouwers, Lambers et al. 2008; Gasser, Ingold et al. 2008; Recker, Delmas et al. 2008; Belfrage, Isaksson et al. 2012).

1.3.2 Local Release of Bisphosphonates

After the big success of systemically administered BPs in clinics, researchers focused also on the local delivery of this drug. The local administration routine became of particular interest for cases where existing bone needs to be preserved and augmented in specific regions of the body, e.g. around an implant, while avoiding side effects related to a systemic administration such as atypical fractures (Pazianas, Cooper et al. 2010; Watts and Diab 2010). This is an important aspect as many of the today used drugs for osteoporosis treatment have been shown to not affect all parts of the skeleton the same way (Hernlund, Svedbom et al. 2013) and to cause adverse effects (Ott 2005; Watts and Diab 2010; Reginster, Pelousse et al. 2013; Verron and Bouler 2014). The delivery of BPs was demonstrated to be very efficient in enhancing bone mass locally. Numerous studies showed that a local release of BPs can enhance peri-implant bone density (Roshan-Ghias, Arnoldi et al. 2011; Bobyn, Thompson et al. 2014), implant fixation (Åstrand and Aspenberg 2004; Tengvall, Skoglund et al. 2004; Peter, Gauthier et al. 2006; Hilding and Aspenberg 2007) and the repair of bony defects (Srisubut, Teerakapong et al. 2007; Cottrell, Vales et al. 2010) in animal models and humans. Furthermore it was shown to preserve bone allografts (Åstrand, Harding et al. 2006; Jakobsen, Baas et al. 2010) as well as bone sites affected by osteonecrosis (Cheng, Murphy et al. 2013). Despite the promising results, there are still no products for a local delivery of bisphosphonates on the market available.

1.3.3 Delivery Systems for Bisphosphonates

As a local delivery requires a direct access to bone, which is the target site of BPs, it is usually indicated during a surgical intervention such as a fracture treatment. In this context, it is a logical approach to link the drug directly to commonly used implants or biomaterials. Due to the high affinity of BPs to bone mineral, the easiest way to combine BP and implant is a simple absorption of the drug to either a commercially available hydroxyapatite coating for metal implants or to mineral containing biomaterials. Both strategies have already been shown to be successful. Peter et al. demonstrated that a Zoledronate-loaded hydroxyapatite coating could enhance the implant fixation in osteoporotic rats (Peter, Gauthier et al. 2006). Others improved bone formation with Alendronate coated bioactive glass (Srisubut, Teerakapong et al. 2007) or Zoledronate-loaded tricalcium phosphate bone cement (Sørensen, Arnoldi et al. 2013) in rat models. But not only ceramic materials were used for the delivery of BPs. Greiner et al. incorporated Zoledronate in a polylactide (PLLA) coating and showed an accelerated fracture healing in a rat model (Greiner, Wildemann et al. 2008). Abtahi et al. were the first to perform a clinical trial with BP coated implants. They implanted dental implants coated with Zoledronate that was immobilized via a fibrinogen layer on the metal surface in 16 patients. After 2 and 6 months they were able to show a decreased peri-implant bone resorption and an increased implant stability (Abtahi, Tengvall et al. 2012).

1.4 Evaluation of Implant Outcome

Whenever new techniques intended to improve implant fixation are introduced, it is important to prove an enhanced efficiency compared to existing systems. Implant stability is usually characterized with two terms: the primary stability that describes the initial fixation of the implant directly after insertion and the secondary stability characterizing the long-term fixation after the remodeling of the peri-implant bone. A good primary stability is associated with a stable mechanical engagement between implant and surrounding bone, which helps to avoid instabilities and micro-movements. This stable situation is a prerequisite for a successful peri-implant bone regeneration resulting in a good secondary stability afterwards (Javed, Ahmed et al. 2013).

The primary stability of implants is usually tested with artificial bone substitutes or cadaveric human or animal bones (Steeves, Stone et al. 2005; Poukalova, Yakacki et al. 2010). The evaluation of the secondary stability however requires the performance of *in vivo* studies in suitable animal models or clinical studies in humans as the peri-implant bone remodeling cannot be simulated *in vitro* (Peter, Gauthier et al. 2006; Gao, Zou et al. 2009; Abtahi, Tengvall et al. 2012).

1.4.1 Mechanical Testing of the Implant Stability

The traditional way of testing the anchorage of implants and especially screws in bone are biomechanical tests such as pullout-, pushout- or torque-tests (Cho and Park 2003; Gao, Luo et al. 2009; Qi, Hu et al. 2012; Stadlinger, Korn et al. 2012). Those tests can be used to evaluate both primary and secondary stabilities. The test parameters are usually adapted to the type and size of the implant so that it is often difficult to compare results. Therefore, ASTM standards were set (e.g. ASTM F543-13E1 "Standard Specification and Test Methods for metallic medical Bone Screws") that should be followed if applicable. The main disadvantage of most mechanical tests is their destructive character that does not allow a re-use of the samples. There are only a few methods such as the resonance frequency analysis/vibration analysis or the cutting torque resistance analysis that allow a non-destructive mechanical testing and can therefore be used also *in vivo* (Atsumi, Park et al. 2007; Degidi, Daprile et al. 2013). As those techniques require a direct access to the implant, they are almost exclusively used for dental implants (Abtahi, Tengvall et al. 2010).

1.4.2 Numerical Evaluation of the Implant Stability

Due to the destructive character of most mechanical tests (section 1.4.1) the *in vivo* monitoring of the fixation of orthopedic implants was always a challenge. A big step forward was done when the first studies show that a simulation of the implant stability can be done by means of micro-finite-element (microFE) analysis (Wirth, Mueller et al. 2010; Wirth, Muller et al. 2010). This rather new technique is based on the microCT images that can be performed multiple times *in vivo* due to their non-invasive character. The high-resolution three-dimensional scans are in a second step transformed into a numerical model with the typical bone parameters assigned to its elements (Pistoia, Van Rietbergen et al. 2002). The models can then be used to simulate mechanical experiments such as pullout tests (Figure 1.9). Wirth et al. demonstrated

excellent correlations between the pullout strength predicted with microFE and the experimentally measured pullout strength in an ovine vertebra model (Wirth, Mueller et al. 2010). Stadelmann et al. were the first that used *in vivo* microCT data from a rat study for their microFE models and monitored this way the time course of the failure load and the bone-screw stiffness of bone screws implanted in rat tibiae (Stadelmann, Conway et al. 2013). Using *in vivo* data has the huge advantage over destructive mechanical tests that it allows a close and direct monitoring of the time course of implant stability with a significantly reduced number of animals. At the same time the important parameters affecting the implant fixation can be identified easily due to the direct link between bone structure (microCT based bone analysis) and implant stability (microCT based microFE) (Wirth, Goldhahn et al. 2011).

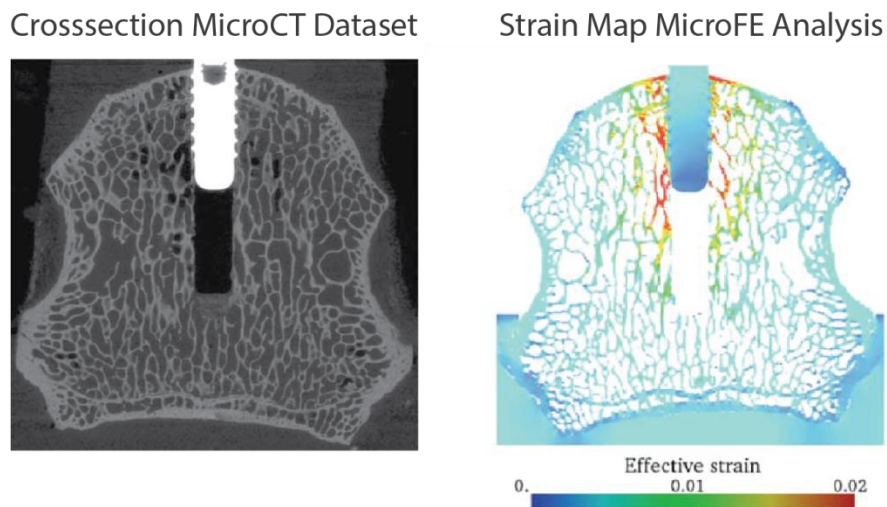


Figure 1.9: Principle of the microCT-based microFE analysis: microCT scans (left) are transferred into detailed finite element models (right) that can predict the implant fixation in a non-destructive way (images taken from (Wirth, Mueller et al. 2010)).

1.4.3 Bone Analysis with CT-Based Dynamic Bone Histomorphometry

When investigating the effect of bone-active drugs, there is a great interest in monitoring the bone changes *in vivo* without having to sacrifice the experimental animals. The only technique that allows today to do so over longer time periods is the so-called dynamic histomorphometry, a technique that is based on the comparison of time-lapsed CT scans (Waarsing, Day et al. 2004; Schulte, Lambers et al. 2011). The non-destructive character of the dynamic histomorphometry is a big advantage against the traditional two-dimensional histology-based histomorphometry as it is for the microFE compared to mechanical testing. Another decisive benefit of the microCT-based technique compared to histology is that bone resorption can be quantified in a direct manner, this is very useful when studying the effect of anti-resorptive drugs such as BPs (Schulte, Lambers et al. 2011). One inherent limitation of this technique is the limited resolution of research *in vivo* microCT scanners that is typically around several μm and around 1 mm for clinical CTs. So far the CT-based dynamic histomorphometry was used to study bone changes in mouse vertebrae following ovariectomy (Lambers, Kuhn et al. 2012) and mechanical stimulation (Schulte, Lambers et al. 2011). Others investigated with this technique changes in of the rat tibia in aged and ovariectomized rats (Waarsing, Day

et al. 2006) and the bone ingrowth in a scaffold implanted in the femoral condyles of rats (Roshan-Ghias, Lambers et al. 2011).

The CT-based dynamic histomorphometry requires a series of microCT scans taken sequentially from the same bone site in the same animal. Then, in a first step, all scans are superimposed with a registration algorithm, as it is not possible to perform the CT scans always in an identical position. The second step of this technique is a voxel-wise comparison of two consecutive image datasets (Figure 1.10). Bone volume that is present only on the first microCT scan is considered as being resorbed, the one present only on the second scan is considered as formed. This way it is possible to monitor bone remodeling in 3 dimensions over long time periods.

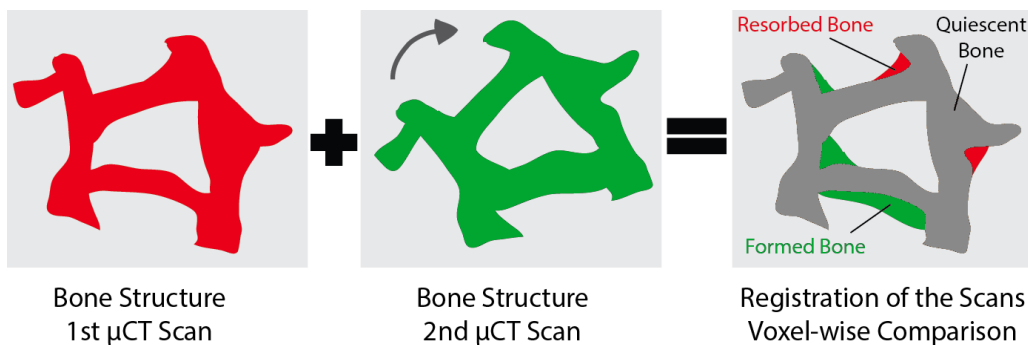


Figure 1.10: Principle of the μ CT based dynamic histomorphometry.

Static and dynamic bone parameters can then be assessed with the CT-based dynamic histomorphometry. Static parameters are measured for a specific time point separately on each of the performed microCT scans, their time-dependent changes (dynamic parameters) can be investigated by comparing the values of different time points. Examples for static bone parameters are the often-used bone volume fraction (BV/TB), trabecular thickness (Tb.Th) or structure model index (SMI). The dynamic bone parameters can be the volume based bone formation rate (BFR) or bone resorption rate (BRR) that were measured in this study by dividing the formed/resorbed bone by the quiescent bone and by the number of days between the two scans. It is important to choose an adequate time interval between two scans (typically several days up to 2 weeks for small rodents) which is long enough to be able to see changes but at the same time short enough so that clear changes (e.g. bone formation followed by bone resorption at the same site) are not missed.

1.5 Scope of the Thesis

This thesis was prepared in the framework of a Commission for Technology and Innovation Switzerland (CTI)-funded project in collaboration with two industrial partners. Therefore, the industrial background is mentioned as this aspect influenced significantly the performed work.

1.5.1 Industrial Background

The total costs caused by osteoporosis in the EU in 2010 was estimated at €37 billion – out of which 66% were spent for treating incident fractures, 29% for long-term fracture care and only 5% for the pharmacological prevention (Hernlund, Svedbom et al. 2013). Especially the €10.7 billion spend for the long-term treatment of fractures show that there is still a high demand for new implants that are adapted to the special needs of osteoporotic patients and can significantly improve the patient's outcomes. As shown above, effort has been made to improve the existing mechanical solutions and implant designs but they have inherent limitations. One very promising approach that came up during the last years and might help to overcome those limitations is the use of drug-implant combination products. For this strategy, implants that are already well adapted for osteoporotic bone can be combined with local drug delivery which can additionally enhance their performance.

The annual number of osteoporotic fractures in the EU is expected rise from 3.5 million in 2010 to 4.5 million in 2025, corresponding to an increase of 28% (Hernlund, Svedbom et al. 2013). Those numbers cause a significant growth in all trauma device segments with a continuing shift towards premium price devices. Surgeons that are facing more and more patients with insufficient bone quality demand new solutions and are motivated to adopt new technologies. Manufactured in Switzerland, a BP releasing drug delivery system with a high clinical performance is expected to have a great market potential in Europe, the US and Japan.

1.5.2 Objectives of the Thesis

The overall goal of this thesis is the development of a Zoledronate delivery system that can locally enhance peri-implant bone quality and as a result implant fixation. An overview about the specific aims is shown in Figure 1.11.

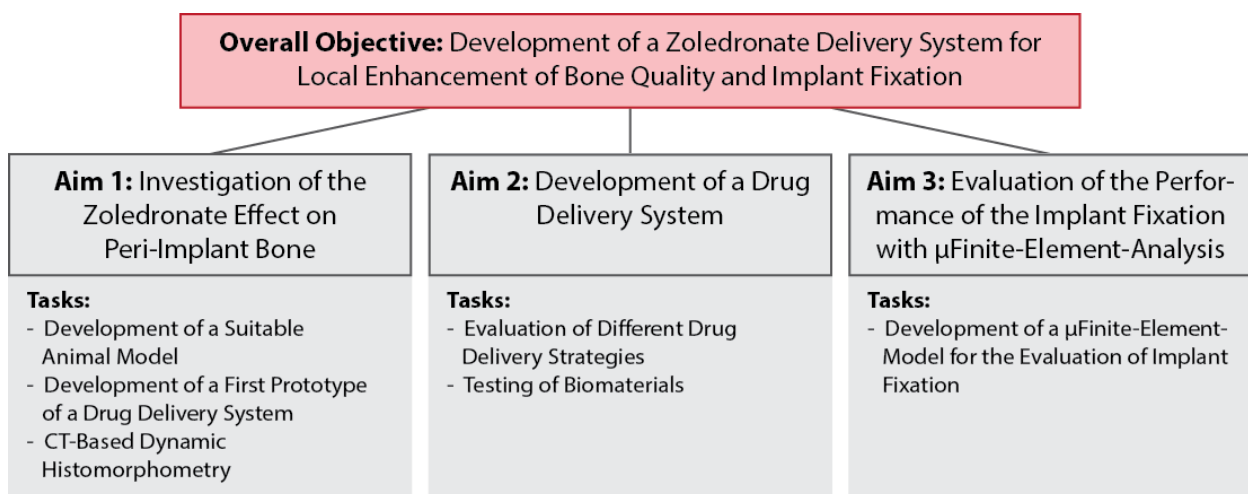


Figure 1.11: Overall objective and specific aims of this thesis.

1.5.3 Aim 1: Investigation of the Zoledronate Effect on Peri-Implant Bone

Based on a literature survey, it is clear that many research projects have already tested and evaluated the local delivery of BPs to peri-implant bone. Most of those studies revealed an improved bone density and bone-implant contact after several weeks. However, as those results were mostly gained with terminal measurements like histology or ex vivo microCT scans, so there is no information available about the exact drug range and mode of action that leads to the increased bone density. We are therefore the first ones using the microCT based dynamic histomorphometry to study the peri-implant bone remodeling and how it is altered by the presence of locally delivered Zoledronate in an ovariectomized rat model of postmenopausal osteoporosis. The study design and results of aim 1 can be found in chapter 2.

1.5.4 Aim 2: Development of a Drug Delivery System

The second aim of this thesis is the development of a suitable drug delivery system based on the information gained from aim 1. We started with a Zoledronate-loaded polylactide (PDLLA) coating that was directly applied to the surface of the implant. However, due to insoluble problems with the mechanical abrasion resistance and difficulties with a precise drug dosing, we had to switch concepts and started working on a stand-alone system that is applied to the prepared implant bed before implant insertion. After working on different scaffold solutions, we tried for the first time the use of a Zoledronate-loaded hydrogel that came out to be very suitable during the *in vivo* studies for aim 1. We then evaluated other functionalities to the hydrogel like the possibility to improve the primary stability of the implant by adding different materials. The development process of the drug delivery system and the results are described in chapter 3 and in the annex.

1.5.5 Aim 3: Evaluation of the Implant Fixation with μ Finite-Element-Analysis

The third and last goal of this thesis is the evaluation of the implant stability induced by the developed drug delivery system. We were able to demonstrate *in vivo* in a rat model that locally delivered Zoledronate can significantly enhance the bone density around implants. The proof that a higher peri-implant bone density is resulting in a better implant fixation was still missing. A numerical simulation of the pullout test was performed based on the microCT datasets that were acquired for the dynamic histomorphometry. This technique has been shown in literature to correlate well with the actual implant fixation (Wirth, Goldhahn et al. 2011; Wirth, Müller et al. 2012; Stadelmann, Conway et al. 2013). Furthermore, it offers the possibility to evaluate the evolution of the implant fixation over time, which is not possible with a destructive, experimental pullout test.

1.6 References

- Abtahi, J., P. Tengvall, et al. (2010). "Bisphosphonate coating might improve fixation of dental implants in the maxilla: A pilot study." *Int J Oral Maxillofac Surg* **39**: 673-677.
- Abtahi, J., P. Tengvall, et al. (2012). "A bisphosphonate-coating improves the fixation of metal implants in human bone. A randomized trial of dental implants." *Bone* **50**(5): 1148-1151.
- Astrand, J. and P. Aspenberg (2004). "Topical, single dose bisphosphonate treatment reduced bone resorption in a rat model for prosthetic loosening." *J Orthop Res* **22**(2): 244-249.
- Åstrand, J., A. K. Harding, et al. (2006). "Systemic zoledronate treatment both prevents resorption of allograft bone and increases the retention of new formed bone during revascularization and remodelling. A bone chamber study in rats." *BMC Musculoskeletal Disorders* **7**.
- Atsumi, M., S. H. Park, et al. (2007). "Methods used to assess implant stability: Current status." *International Journal of Oral and Maxillofacial Implants* **22**(5): 743-754.
- Belfrage, O., H. Isaksson, et al. (2012). "Local treatment of a bone graft by soaking in zoledronic acid inhibits bone resorption and bone formation. A bone chamber study in rats." *BMC Musculoskeletal Disorders* **13**.
- Blomqvist, J. E., P. Alberius, et al. (1996). "Factors in implant integration failure after bone grafting: An osteometric and endocrinologic matched analysis." *International Journal of Oral and Maxillofacial Surgery* **25**(1): 63-68.
- Bobyn, J. D., R. Thompson, et al. (2014). "Local alendronic acid elution increases net periimplant bone formation: A micro-CT analysis." *Clin Orthop Relat Res* **472**(2): 687-694.
- Boyce, B. F., E. Rosenberg, et al. (2012). "The osteoclast, bone remodelling and treatment of metabolic bone disease." *European Journal of Clinical Investigation* **42**(12): 1332-1341.
- Broderick, J. M., R. Bruce-Brand, et al. (2013). "Osteoporotic Hip fractures: The burden of fixation failure." *The Scientific World Journal* **2013**(515197).
- Brouwers, J. E. M., F. M. Lambers, et al. (2008). "Bone degeneration and recovery after early and late bisphosphonate treatment of ovariectomized wistar rats assessed by in vivo micro-computed tomography." *Calcif Tissue Int* **82**(3): 202-211.
- Cheng, T. L., C. M. Murphy, et al. (2013). "Local delivery of recombinant human bone morphogenetic proteins and bisphosphonate via sucrose acetate isobutyrate can prevent femoral head collapse in Legg-Calve-Perthes disease: a pilot study in pigs." *Int Orthop* **38**(7): 1527-1533.
- Cho, S. A. and K. T. Park (2003). "The removal torque of titanium screw inserted in rabbit tibia treated by dual acid etching." *Biomaterials* **24**(20): 3611-3617.
- Cottrell, J. A., F. M. Vales, et al. (2010). "Osteogenic activity of locally applied small molecule drugs in a rat femur defect model." *J Biomed Biotechnol* **2010**: 597641.
- Cummings, S. R. and L. J. Melton (2002). "Osteoporosis I: Epidemiology and outcomes of osteoporotic fractures." *Lancet* **359**(9319): 1761-1767.
- Dall'Oca, C., T. Maluta, et al. (2010). "Cement augmentation of intertrochanteric fractures stabilised with intramedullary nailing." *Injury* **41**(11): 1150-1155.
- Degidi, M., G. Daprile, et al. (2013). "Development of a New Implant Primary Stability Parameter: Insertion Torque Revisited." *Clinical Implant Dentistry and Related Research* **15**(5): 637-644.
- Ebetino, F. H., M. D. Francis, et al. (1998). "Mechanisms of action of etidronate and other bisphosphonates." *Reviews in Contemporary Pharmacotherapy* **9**(4): 233-243.
- Gao, Y., E. Luo, et al. (2009). "Effect of combined local treatment with zoledronic acid and basic fibroblast growth factor on implant fixation in ovariectomized rats." *Bone* **44**(2): 225-232.
- Gao, Y., S. Zou, et al. (2009). "The effect of surface immobilized bisphosphonates on the fixation of hydroxyapatite-coated titanium implants in ovariectomized rats." *Biomaterials* **30**(9): 1790-1796.
- Gasser, J. A., P. Ingold, et al. (2008). "Long-term protective effects of zoledronic acid on cancellous and cortical bone in the ovariectomized rat." *J Bone Miner Res* **23**(4): 544-551.
- Giuliani, N., M. Pedrazzoni, et al. (1998). "Bisphosphonates stimulate formation of osteoblast precursors and mineralized nodules in murine and human bone marrow cultures in vitro and promote early osteoblastogenesis in young and aged mice in vivo." *Bone* **22**(5): 455-461.
- Green, J. R., K. Muller, et al. (1994). "Preclinical pharmacology of CGP 42'446, a new, potent, heterocyclic bisphosphonate compound." *J Bone Miner Res* **9**(5): 745-751.
- Green, J. R. and M. J. Rogers (2002). "Pharmacologic Profile of Zoledronic Acid: A Highly Potent Inhibitor of Bone Resorption." *Drug Dev Res* **55**: 210-224.
- Greiner, S., A. Kadow-Romacker, et al. (2006). "The effect of zoledronic acid incorporated in a poly(D,L-lactide) implant coating on osteoblasts in vitro." *J Biomed Mater Res A* **80**(4): 769-775.

- Greiner, S. H., B. Wildemann, et al. (2008). "Local application of zoledronic acid incorporated in a poly(D,L-lactide)-coated implant accelerates fracture healing in rats." *Acta Orthop* **79**(5): 717-725.
- Hernlund, E., A. Svedbom, et al. (2013). "Osteoporosis in the European Union: Medical management, epidemiology and economic burden: A report prepared in collaboration with the International Osteoporosis Foundation (IOF) and the European Federation of Pharmaceutical Industry Associations (EFPIA)." *Archives of Osteoporosis* **8**(1-2).
- Hilding, M. and P. Aspenberg (2007). "Local peroperative treatment with a bisphosphonate improves the fixation of total knee prostheses: a randomized, double-blind radiostereometric study of 50 patients." *Acta Orthop* **78**(6): 795-799.
- Idris, A. I., J. Rojas, et al. (2008). "Aminobisphosphonates cause osteoblast apoptosis and inhibit bone nodule formation in vitro." *Calcif Tissue Int* **82**(3): 191-201.
- Jakobsen, T., J. Baas, et al. (2010). "The effect of soaking allograft in bisphosphonate: a pilot dose-response study." *Clin Orthop Relat Res* **468**(3): 867-874.
- Javed, F., H. Ahmed, et al. (2013). "Role of primary stability for successful osseointegration of dental implants: Factors of influence and evaluation." *Interventional Medicine and Applied Science* **5**(4): 162-167.
- Johnell, O. and J. A. Kanis (2006). "An estimate of the worldwide prevalence and disability associated with osteoporotic fractures." *Osteoporosis International* **17**(12): 1726-1733.
- Kammerlander, C., S. Erhart, et al. (2013). "Principles of osteoporotic fracture treatment." *Best Practice and Research: Clinical Rheumatology* **27**(6): 757-769.
- Khan, S. A., J. A. Kanis, et al. (1997). "Elimination and biochemical responses to intravenous alendronate in postmenopausal osteoporosis." *Journal of Bone and Mineral Research* **12**(10): 1700-1707.
- Kubo, T., T. Shiga, et al. (1999). "Osteoporosis influences the late period of fracture healing in a rat model prepared by ovariectomy and low calcium diet." *J Steroid Biochem Mol Biol* **68**(5-6): 197-202.
- Lambers, F. M., G. Kuhn, et al. (2012). "Longitudinal assessment of in vivo bone dynamics in a mouse tail model of postmenopausal osteoporosis." *Calcif Tissue Int* **90**(2): 108-119.
- Lim, T. H., H. S. An, et al. (1995). "Strength of anterior vertebral screw fixation in relationship to bone mineral density." *Journal of Spinal Disorders* **8**(2): 121-125.
- Lindner, T., N. K. Kanakaris, et al. (2009). "Fractures of the hip and osteoporosis: The role of bone substitutes." *Journal of Bone and Joint Surgery - Series B* **91**(3): 294-303.
- Maruotti, N., A. Corrado, et al. (2012). "Bisphosphonates: Effects on osteoblast." *European Journal of Clinical Pharmacology* **68**(7): 1013-1018.
- McKenzie, K., J. Dennis Bobyne, et al. (2011). "Bisphosphonate Remains Highly Localized After Elution From Porous Implants." *Clin Orthop Relat Res* **469**(2): 514-522.
- Namkung-Matthai, H., R. Appleyard, et al. (2001). "Osteoporosis influences the early period of fracture healing in a rat osteoporotic model." *Bone* **28**(1): 80-86.
- Nikolaou, V. S., N. Efstathiopoulos, et al. (2009). "The influence of osteoporosis in femoral fracture healing time." *Injury* **40**(6): 663-668.
- Nordin, M. F., V.H. (2012). *Basic Biomechanics of the Musculoskeletal System*, Lippincott Williams & Wilkins, a Wolters Kluwer business.
- Orriss, I. R., M. L. Key, et al. (2009). "Inhibition of osteoblast function in vitro by aminobisphosphonates." *J Cell Biochem* **106**(1): 109-118.
- Ott, S. M. (2005). "Long-term safety of bisphosphonates." *J Clin Endocrinol Metab* **90**(3): 1897-1899.
- Pan, B., L. B. To, et al. (2004). "The nitrogen-containing bisphosphonate, zoledronic acid, increases mineralisation of human bone-derived cells in vitro." *Bone* **34**(1): 112-123.
- Pazianas, M., C. Cooper, et al. (2010). "Long-term treatment with bisphosphonates and their safety in postmenopausal osteoporosis." *Ther Clin Risk Manag* **6**: 325-343.
- Peter, B., O. Gauthier, et al. (2006). "Local delivery of bisphosphonate from coated orthopedic implants increases implants mechanical stability in osteoporotic rats." *J Biomed Mater Res A* **76**(1): 133-143.
- Pietschmann, P., M. Rauner, et al. (2009). "Osteoporosis: an age-related and gender-specific disease--a mini-review." *Gerontology* **55**(1): 3-12.
- Pioletti, D. P., O. Gauthier, et al. (2008). "Orthopedic implant used as drug delivery system: clinical situation and state of the research." *Curr Drug Deliv* **5**(1): 59-63.
- Pistoia, W., B. Van Rietbergen, et al. (2002). "Estimation of distal radius failure load with micro-finite element analysis models based on three-dimensional peripheral quantitative computed tomography images." *Bone* **30**(6): 842-848.

- Plotkin, L. I., S. C. Manolagas, et al. (2006). "Dissociation of the pro-apoptotic effects of bisphosphonates on osteoclasts from their anti-apoptotic effects on osteoblasts/osteocytes with novel analogs." *Bone* **39**(3): 443-452.
- Plotkin, L. I., R. S. Weinstein, et al. (1999). "Prevention of osteocyte and osteoblast apoptosis by bisphosphonates and calcitonin." *Journal of Clinical Investigation* **104**(10): 1363-1374.
- Poukalova, M., C. M. Yakacki, et al. (2010). "Pullout strength of suture anchors: Effect of mechanical properties of trabecular bone." *J Biomech* **43**(6): 1138-1145.
- Qi, M., J. Hu, et al. (2012). "Effect of zoledronate acid treatment on osseointegration and fixation of implants in autologous iliac bone grafts in ovariectomized rabbits." *Bone* **50**(1): 119-127.
- Raggatt, L. J. and N. C. Partridge (2010). "Cellular and molecular mechanisms of bone remodeling." *Journal of Biological Chemistry* **285**(33): 25103-25108.
- Raisz, L. G. (2005). "Pathogenesis of osteoporosis: Concepts, conflicts, and prospects." *Journal of Clinical Investigation* **115**(12): 3318-3325.
- Recker, R. R., P. D. Delmas, et al. (2008). "Effects of intravenous zoledronic acid once yearly on bone remodeling and bone structure." *Journal of Bone and Mineral Research* **23**(1): 6-16.
- Reginster, J. Y., F. Pelousse, et al. (2013). "Safety concerns with the long-term management of osteoporosis." *Expert Opinion on Drug Safety* **12**(4): 507-522.
- Roelofs, A. J., K. Thompson, et al. (2006). "Molecular mechanisms of action of bisphosphonates: Current status." *Clinical Cancer Research* **12**(20 PART 2): 6222s-6230s.
- Rogers, M. J., J. C. Frith, et al. (1999). "Molecular mechanisms of action of bisphosphonates." *Bone* **24**(5 Suppl): 73S-79S.
- Rogers, M. J., S. Gordon, et al. (2000). "Cellular and molecular mechanisms of action of bisphosphonates." *Cancer* **88**(12 Suppl): 2961-2978.
- Roshan-Ghias, A., J. Arnoldi, et al. (2011). "In vivo assessment of local effects after application of bone screws delivering bisphosphonates into a compromised cancellous bone site." *Clin Biomech* **26**(10): 1039-1043.
- Roshan-Ghias, A., F. M. Lambers, et al. (2011). "In vivo loading increases mechanical properties of scaffold by affecting bone formation and bone resorption rates." *Bone* **49**(6): 1357-1364.
- Russell, R. G. (2011). "Bisphosphonates: The first 40 years." *Bone* **49**(1): 2-19.
- Russell, R. G., N. B. Watts, et al. (2008). "Mechanisms of action of bisphosphonates: similarities and differences and their potential influence on clinical efficacy." *Osteoporos Int* **19**(6): 733-759.
- Schneider, E., J. Goldhahn, et al. (2005). "The challenge: fracture treatment in osteoporotic bone." *Osteoporos Int* **16** Suppl 2: S1-2.
- Schulte, F. A., F. M. Lambers, et al. (2011). "In vivo micro-computed tomography allows direct three-dimensional quantification of both bone formation and bone resorption parameters using time-lapsed imaging." *Bone* **48**(3): 433-442.
- Seeman, E. (2009). "Bone modeling and remodeling." *Critical Reviews in Eukaryotic Gene Expression* **19**(3): 219-233.
- Sommer, C., E. Gautier, et al. (2003). "First clinical results of the Locking Compression Plate (LCP)." *Injury* **34**(SUPPL. 2): SB43-SB54+SB81+SB85+SB89.
- Sörensen, T. C., J. Arnoldi, et al. (2013). "Locally enhanced early bone formation of zoledronic acid incorporated into a bone cement plug in vivo." *Journal of Pharmacy and Pharmacology* **65**(2): 201-212.
- Srisubut, S., A. Teerakapong, et al. (2007). "Effect of local delivery of alendronate on bone formation in bioactive glass grafting in rats." *Oral Surgery, Oral Medicine, Oral Pathology, Oral Radiology and Endodontology* **104**(4): e11-e16.
- Stadelmann, V. A., C. M. Conway, et al. (2013). "In vivo monitoring of bone-implant bond strength by microCT and finite element modelling." *Computer Methods in Biomechanics and Biomedical Engineering* **16**(9): 993-1001.
- Stadlinger, B., P. Korn, et al. (2012). "Osseointegration of biochemically modified implants in an osteoporosis rodent model." *European Cells and Materials* **25**: 326-340.
- Steeves, M., C. Stone, et al. (2005). "How pilot-hole size affects bone-screw pullout strength in human cadaveric cancellous bone." *Can J Surg* **48**(3): 207-212.
- Stromsoe, K. (2004). "Fracture fixation problems in osteoporosis." *Injury* **35**(2): 107-113.
- Stromsoe, K., W. L. Kok, et al. (1993). "Holding power of the 4.5 mm AO/ASIF cortex screw in cortical bone in relation to bone mineral." *Injury* **24**(10): 656-659.
- Tengvall, P., B. Skoglund, et al. (2004). "Surface immobilized bisphosphonate improves stainless-steel screw fixation in rats." *Biomaterials* **25**(11): 2133-2138.
- Thompson, K., M. J. Rogers, et al. (2006). "Cytosolic entry of bisphosphonate drugs requires acidification of vesicles after fluid-phase endocytosis." *Molecular Pharmacology* **69**(5): 1624-1632.

- Tobias, J. H., J. W. M. Chow, et al. (1993). "3-Amino-1-hydroxypropylidene-1-bisphosphonate (AHPPrBP) suppresses not only the induction of new, but also the persistence of existing bone-forming surfaces in rat cancellous bone." Bone **14**(4): 619-623.
- Tortora, G. J. D. B. (2013). Essentials of anatomy and physiology. Hoboken, N.J., Wiley.
- Verron, E. and J. M. Bouler (2014). "Is bisphosphonate therapy compromised by the emergence of adverse bone disorders?" Drug Discovery Today **19**(3): 312-319.
- Waarsing, J. H., J. S. Day, et al. (2004). "Detecting and tracking local changes in the tibiae of individual rats: A novel method to analyse longitudinal in vivo micro-CT data." Bone **34**(1): 163-169.
- Waarsing, J. H., J. S. Day, et al. (2006). "Bone loss dynamics result in trabecular alignment in aging and ovariectomized rats." Journal of Orthopaedic Research **24**(5): 926-935.
- Watts, N. B. and D. L. Diab (2010). "Long-term use of bisphosphonates in osteoporosis." J Clin Endocrinol Metab **95**(4): 1555-1565.
- Wirth, A. J., J. Goldhahn, et al. (2011). "Implant stability is affected by local bone microstructural quality." Bone **49**(3): 473-478.
- Wirth, A. J., T. L. Mueller, et al. (2010). "Mechanical competence of bone-implant systems can accurately be determined by image-based micro-finite element analyses." Archive of Applied Mechanics **80**(5): 513-525.
- Wirth, A. J., R. Müller, et al. (2010). "Computational analyses of small endosseous implants in osteoporotic bone." Eur Cell Mater **20**: 58-71.
- Wirth, A. J., R. Müller, et al. (2012). "Augmentation of peri-implant bone improves implant stability: Quantification using simulated bone loss." Journal of Orthopaedic Research **30**(2): 178-184.

Chapter 2 Investigation of the Effect of Locally Delivered Zoledronate on Peri-Implant Bone

*Paper 1 Does Locally Delivered Zoledronate Influence Peri-implant
Bone Formation? – Spatio-temporal Monitoring of Bone Remodeling in
vivo
(published in Biomaterials)*

2.1 Abstract

Bisphosphonates are known for their strong inhibitory effect on bone resorption. Their influence on bone formation however is less clear. In this study we investigated the spatio-temporal effect of locally delivered Zoledronate on peri-implant bone formation and resorption in an ovariectomized rat femoral model. A cross-linked hyaluronic acid hydrogel was loaded with the drug and applied bilaterally in predrilled holes before inserting polymer screws. Static and dynamic bone parameters were analyzed based on *in vivo* microCT scans performed first weekly and then biweekly. The results showed that the locally released Zoledronate boosted bone formation rate up to 100% during the first 17 days after implantation and reduced the bone resorption rate up to 1000% later on. This shift in bone remodeling resulted in an increase in bone volume fraction (BV/TV) by 300% close to the screw and 100% further away. The double effect on bone formation and resorption indicates a great potential of Zoledronate-loaded hydrogel for enhancement of peri-implant bone volume which is directly linked to improved implant fixation.

Keywords: Drug delivery; hydrogel; bisphosphonate; implant; dynamic histomorphometry; microCT

2.2 Introduction

The human skeleton is constantly renewed and repaired by the bone remodeling process, a well-coordinated sequence of osteoclast-mediated bone resorption and osteoblast-mediated bone formation (Seeman 2009; Boyce, Rosenberg et al. 2012). Anti-catabolic drugs, such as bisphosphonates (BPs), can slow down this process and shift the balance between bone formation and resorption activity by selectively affecting osteoclast function (Riggs and Parfitt 2005). Osteoclasts are considered to be the main target for BPs as only this cell type can liberate and internalize mineral bound BPs during the resorption process (Rogers, Gordon et al. 2000; Russell, Watts et al. 2008). However, effects of BPs on cells of the osteoblast lineage have also been described, which raises the question if BPs can also enhance bone formation activity (Roelofs, Thompson et al. 2006; Idris, Rojas et al. 2008). In vitro experiments have shown that low concentrations of BPs can protect osteoblasts and osteocytes against apoptosis (Plotkin, Weinstein et al. 1999; Plotkin, Manolagas et al. 2006), stimulate mineralized bone nodule formation (Giuliani, Pedrazzoni et al. 1998), and have a beneficial effect on osteoblast differentiation and protein synthesis (Greiner, Kadow-Romacker et al. 2006). Specifically for Zoledronate, the most potent bisphosphonate used in clinics today, an improved mineralization and proliferation of human osteoblast-like cells has been demonstrated (Pan, To et al. 2004). However, conflicting results can also be found showing that BPs might inhibit mineralization and osteoblast growth, induce osteoblast apoptosis, and inhibit protein prenylation in osteoblasts in a dose-dependent manner (Idris, Rojas et al. 2008; Orriss, Key et al. 2009). Taken together, these findings suggest that BPs might, in addition to their known anti-resorptive effect, also have the ability to stimulate bone formation.

BPs are usually administered orally or intravenously. Local application is of particular interest in cases where existing bone needs to be preserved and augmented whilst avoiding the known side effects related to systemic administration (Pazianas, Cooper et al. 2010; Watts and Diab 2010). Several in vivo studies have shown that a local delivery of BPs can enhance peri-implant bone density (Roshan-Ghias, Arnoldi et al. 2011; Bobyn, Thompson et al. 2014), implant fixation (Åstrand and Aspenberg 2004; Tengvall, Skoglund et al. 2004; Peter, Gauthier et al. 2006; Hilding and Aspenberg 2007; Andersson, Agholme et al. 2010), and the repair of bony defects (Srisubut, Teerakapong et al. 2007; Cottrell, Vales et al. 2010) in animal models and humans. Furthermore BPs have been shown to preserve bone allografts (Åstrand, Harding et al. 2006; Jakobsen, Baas et al. 2010) as well as bone sites affected by osteonecrosis (Cheng, Murphy et al. 2013).

Currently published studies are mostly based on static analysis techniques like single CT/microCT scans, histology or pullout/pushout tests performed after euthanasia of the animals (Peter, Gauthier et al. 2006; Andersson, Agholme et al. 2010; Back, Pauly et al. 2012). These techniques do not allow a separate investigation of the dynamic bone formation and bone resorption processes. Few studies can be found that looked at dynamic bone parameters after a systemic administration of BPs, but they did not show enhanced bone formation activity in humans nor in animals (Gasser, Ingold et al. 2008; Recker, Delmas et al. 2008). Some studies even demonstrated reduced bone formation and a suppressed activity of pre-

existing bone-forming surfaces at medium to high doses of BPs (Tobias, Chow et al. 1993; Allen, Follet et al. 2006; Brouwers, Lambers et al. 2008; Fuchs, Phipps et al. 2008; Belfrage, Isaksson et al. 2012).

Therefore, the aim of the present study is to investigate the spatio-temporal effect of locally delivered Zoledronate on peri-implant bone remodeling using the so-called dynamic histomorphometry. This previously developed microCT-based technique enables us to quantitatively measure the average outcome of bone formation and resorption over long time periods (Waarsing, Day et al. 2004; Schulte, Lambers et al. 2011), allowing an investigation of the so far unclear effect of locally applied BPs on the dynamic bone formation processes. Understanding the effects of Zoledronate and how it interacts with normal bone healing is important when it comes to designing drug delivering implants and materials. The active range, the time delay, and duration of the BPs' effects (very local versus widespread, fast versus slow, long term versus short term effects) are crucial for targeting specific bone sites, as well as certain phases of bone healing.

2.3 Materials and Methods

2.3.1 General Study Design

Custom-made polymeric miniature screws were implanted bilaterally in the femoral condyles of ovariectomized (OVX) rats. Unlike metal implants, these screws are visible on microCT scans without creating image disturbing artifacts. A hydrogel based drug delivery system was used to release Zoledronate into the peri-implant bone stock. During surgery, the hydrogel was inserted into the predrilled screw-hole before screw implantation. The study included 3 experimental groups with 4 animals assigned to each group. In the first group, the hydrogel was loaded with 5 μg Zoledronate (Zol-Gel-group); in the second group, unloaded hydrogel was used (Gel-group); and in the third group, no hydrogel was inserted (Control-group) before screw implantation. Time-lapsed *in vivo* microCT scans of the animals were performed for close monitoring of the bone response to the implantation and how it is altered by the bisphosphonates delivery. A time line of the study is shown in Figure 2.1.

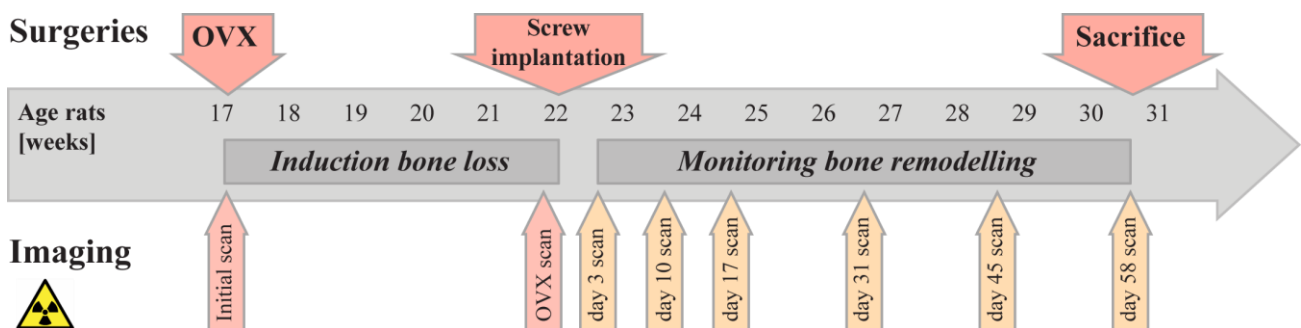


Figure 2.1: Timeline of the study; the rats are ovariectomized at an age of 17 weeks followed by the bilateral implantation of miniature screws at an age of 22 weeks. Two microCT scans were performed to confirm the bone loss after OVX, 6 more were performed after the screw implantation to monitor bone remodeling.

2.3.2 Hydrogel Preparation

A commercially available cross-linked hyaluronic acid (Termira Auxigel™, Stockholm, Sweden) was used as the drug delivery system for the BPs because this gel had already been shown to be a suitable material for delivering drugs such as growth factors to bone (Bergman, Engstrand et al. 2009; Martínez-Sanz, Varghese et al. 2012; Kisiel, Klar et al. 2013; Martínez-Álvarez, González-Meli et al. 2013). The crosslinking of the hydrogel is achieved by mixing a hyaluronan derivative (component A) with a PVA cross-linker (component B). First, an aqueous solution containing 2 mg/ml Zoledronate (Art.-Nr. ALX-430-153-0000, Enzo Life Sciences, Farmingdale, USA) was prepared. The exact drug dose was ensured by mixing precisely weighed and measured amounts of Zoledronate and distilled water. All solutions were sterile filtered and the mixing of the gels was performed under sterile conditions. Five parts of the Zoledronate solution were mixed with 3 parts of component A and 2 parts of component B for the Zol-Gel-group. The Zoledronate solution was replaced by bi-distilled water for the Gel-group. The resulting gels were allowed to settle for 1 h before filling the capillary pistons of a positive displacement pipette (Microman®, Gilson, Middleton, USA) with 5 µl gel each. The capillaries were pulled off the pipette with the gel inside and left 1 h for settling. Then they were sterile packed in plastic tubes and frozen at -20°C.

2.3.3 Animal Model

All animal procedures were approved by the local animal care and use committee (license no. 2508.1, EXPANIM, SCAV, Epalinges, Switzerland). Twelve 14 week old virgin female rats were received from Janvier Labs (Saint-Berthevin, France) and acclimatized in the animal facilities for 3 weeks. All rats were housed 4 per cage under 12 h light to 12 h dark cycles at 22°C room temperature with 55% humidity. They were fed with a standard rodent diet (KLIBA NAFAG 3436, Provimi Kliba AG, Switzerland) and tap water *ad libitum*. After ovariectomy (OVX), food intake was limited to 50 g per kg body weight per day. Sterilized hay, paper tunnels and wooden sticks were offered as cage environment enrichment. The animals were fed in groups and equal nutrition of all animals was ensured by close monitoring and regular weighing.

2.3.4 Surgical Procedures

Ovariectomy

The rats were ovariectomized bilaterally at an age of 17 weeks and a weight of 293 ± 11 g to induce an estrogen deficiency related bone loss (Hogan, Ruhmann et al. 2000). We used a dorsal approach similar to the procedure described by Alghamdi et al (Alghamdi, Bosco et al. 2013). Buprenorphine (Temgesic®, Reckitt Benckiser AG, Wallisellen, Switzerland) was administered subcutaneously before surgery and every 8 h for the first 48 h after surgery for pain relief. Paracetamol (Dafalgan 500 mg effervescent tablet, UPSA Bristol-Myers Squibb SA, Baar, Switzerland) was added to the drinking water of the rats for 5 days. The skin incisions were closed with running subcuticular sutures (Vinyl 5.0, Ethicon, Somerville NJ, USA) so that the rats did not have to be kept in separate cages after the surgery. No antibiotics were given.

Screw Implantation

Screws were implanted when the rats were aged 22 weeks and weighed 338 ± 18 g. One miniature screw was implanted in each femoral condyle under Isoflurane anesthesia with Buprenorphine to avoid intraoperative pain. The surgery was done under aseptic conditions. The rat was prepared for surgery and the first leg was fixed on a special table with the knee in a flexed position. A skin incision of 1-2 cm was made on the lateral side of the distal femoral end and the muscles were bluntly dissected in order to expose the condyle. One hole with a diameter of 1.2 mm and 3.5 mm length was drilled unicortically in the condyle with a motorized dentist's drill (DEC 100, Nobelcare, Sweden). The cortex was pre-tapped to avoid deformation and damage to the polymer screws. The drilled hole was rinsed with saline solution and surgical vacuum was used to remove bone particles. As a next step, the hydrogel was inserted in the predrilled hole with a positive displacement pipette before implanting a miniature screw (Figure 2.2). The screws with a thread length of 3 mm and a diameter of 1.4 mm were custom made from radiopaque polyetheretherketone (RISystem, Davos, Switzerland) with a 100 nm titanium coating to mimic the interface with a standard orthopedic screw. After implanting the screw, the fascia of the muscle was closed with resorbable sutures (Vinyl 5.0). The skin was closed with interrupted subcuticular sutures (Vicryl 5.0) before performing the same procedure at the contralateral femur. The rat was placed in a heated incubator for post-surgical recovery. The post-OP medication and care was similar to the procedure after ovariectomy described above.

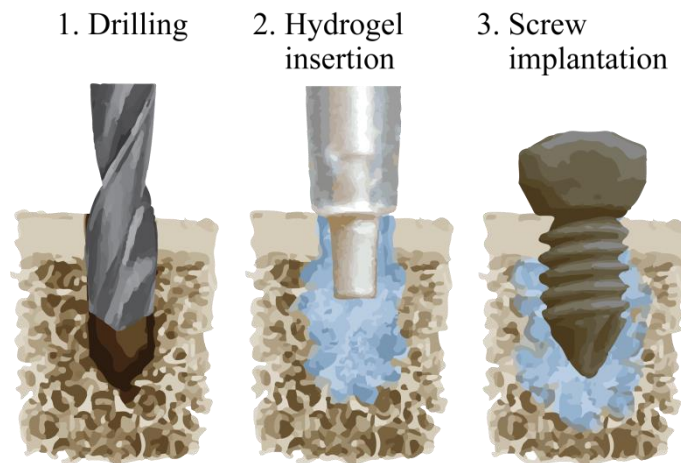


Figure 2.2: Hydrogel insertion in the predrilled bone hole located in the femoral condyle of the rat; the gel is inserted in the hole via a positive displacement pipette before implanting the screw.

2.3.5 MicroCT Imaging, Data Processing and Analysis

In vivo MicroCT Imaging

In vivo microCT scans (Skyscan 1076, Bruker microCT, Kontich, Belgium) of only the right femur were performed one day before OVX and one day before screw implantation in order to confirm the bone loss caused by the estrogen deficiency. Both femurs were then scanned at day 3, 10, 17, 31, 45, and 58 after

screw implantation for the dynamic histomorphometry. According to literature, no bone damage due to radiation can be expected after 8 consecutive microCT scans (Brouwers, Van Rietbergen et al. 2007). The animals were kept under Isoflurane anesthesia during the scans to avoid motion artifacts. The rats were euthanized at the time of the last microCT scan with an intraperitoneal injection of Pentobarbital (Esconarkon, Streuli Pharma SA, Uznach) while under anesthesia.

Data Acquisition and Reconstruction

The parameters for the scans assessing the bone loss before screw implantation were the following: 0.5 mm aluminum filter, voltage 60 kV, current 167 μ A, exposure time 480 ms, rotation step 0.4°. The peri-implant bone after screw insertion was scanned with different parameters adapted to the density of the screw: 0.5 mm aluminum filter, voltage 80 kV, current 120 μ A, exposure time 400 ms, rotation step 0.5°. The spatial resolution of all scans was 18.4 μ m. Two polymer-hydroxyapatite phantoms with known mineral density were scanned under the same conditions as the rats and served for a calibration of the bone mineral density (BMD) and tissue mineral density (TMD) measurement histograms. The reconstruction of the projection images was done with NRecon and GPURecon Server (Bruker microCT, Kontich, Belgium). A ring artifact correction of 4 and a beam hardening correction of 20% for the scans assessing bone loss and 30% for the peri-implant bone scans were set to improve the image quality. The reconstruction output was stacks of cross-sections in 8-bit bitmap format.

Assessment of the Estrogen Deficiency Introduced Bone Loss

The scans taken before OVX and before screw implantation were analyzed with the software CTan (Bruker microCT) to confirm the induced bone loss. A volume of interest (VOI) with a length of 4 mm was defined proximal to the growth plate located in the femoral condyle. Cortical and trabecular regions were selected automatically with a customized algorithm before analyzing the morphometric parameters as well as the BMD of the trabecular region and the TMD of the cortical region.

MicroCT-based Dynamic Histomorphometry

The microCT datasets were used to perform dynamic histomorphometry, a technique that is based on the registration and comparison of two consecutive microCT scans (Waarsing, Day et al. 2004; Schulte, Lambers et al. 2011). Bone was considered to be resorbed if it was present on the first microCT scan and not on the second, whereas bone was considered to be formed if it was present on the second scan and did not appear on the first. Bone which appeared in both scans was considered to be quiescent. In this way, bone remodeling can be monitored in three dimensions over long periods of time without the need to euthanize the animals.

Image processing for the dynamic histomorphometry was done with Amira® (FEI Visualization Sciences Group, Burlington, USA) and CTan. In the femoral condyle, a VOI of 4.5 mm in height around the screw was manually defined with CTan for all animals. Using an automated algorithm, the background and the patella

were removed and the dataset size was reduced to facilitate image processing. Then all datasets were loaded into Amira® for further processing with a custom script. The script first super positioned all original grey value images using the built-in registration function and their correlations as a similarity measure. Each dataset was registered with the image from the previous time step. All images were transformed into the coordinate system of the first image using the built-in standard interpolation method and the datasets were filtered with a median-based 3D noise-reduction filter. Next, a VOI containing only trabecular bone was automatically defined on the first dataset and adapted manually so that it would also fit consecutive scans which are slightly different due to ongoing bone remodeling. Then, for all datasets, the VOI was binarized with a threshold of 80. By comparing consecutive scans voxel by voxel, resorbed, formed, and quiescent bone regions were identified and assigned one of three grey values. Two additional grey values were assigned to the screw and the bone marrow. These images were saved and loaded into CTan. The static and dynamic bone parameters around the screw were measured in four layers of 368 μm (20 voxels) (Figure 2.3). The static bone parameters bone volume fraction (BV/TV), trabecular thickness (Tb.Th), trabecular number (Tb.N), trabecular separation (Tb.Sp), and structure model index (SMI) were analyzed for a complete assessment of the bone structure changes. The volume-based bone formation rate (BFR) and bone resorption rate (BRR) were chosen as representative parameters as their calculation is robust and not as sensitive to registration inaccuracies as the surface-based parameters. The bone formation rate is given in percent per day (%/d) and calculated as the ratio of formed bone volume to quiescent bone volume divided by the number of days between the two scans. The bone resorption rate is calculated as the ratio of resorbed bone volume to quiescent bone volume divided by the days between the scans.

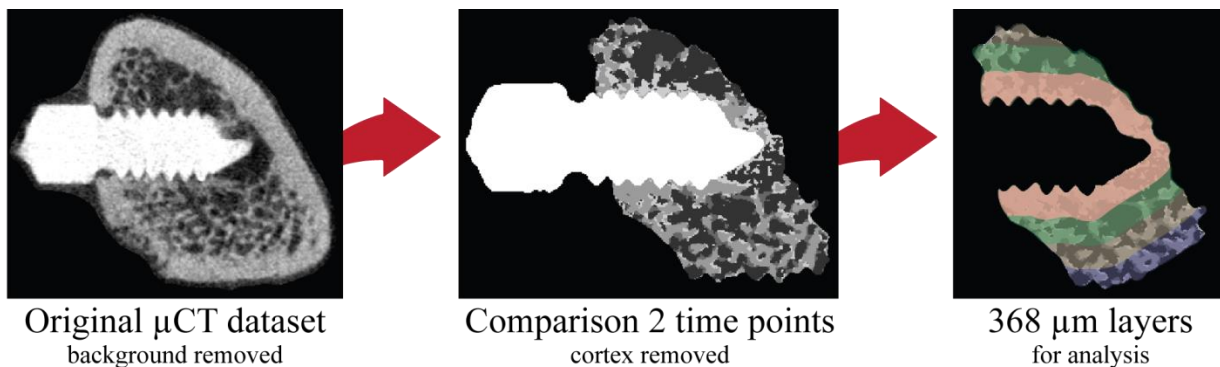


Figure 2.3: Main steps of the dynamic histomorphometry. First, pairs of microCT scans from consecutive time points are registered and segmented. The cortex is removed with an automated algorithm and the time points are compared voxel by voxel by assigning different grey values to bone present only on the first, only on the second or on both datasets. In a last step, 4 layered VOIs of 368 μm each are created and analyzed separately for static and dynamic bone parameters.

2.3.6 Histology

The rat femurs were dissected just after euthanasia and fixed in 4% paraformaldehyde solution before dehydrating them in a series of ethanol solutions with ascending concentration (70%, 80%, 90%, 95% and 100%). After clearing the samples in toluol, they were embedded by infiltration with methylmethacrylate 99% (MMA), Bis(tert-butylcyclohexyl) peroxydicarbonate (Perkadox 16) and dibutylphtalate (DBP). All

agents were purchased from Sigma-Aldrich (St. Louis, US). After polymerization during 3 weeks at room temperature, the samples were cut with a diamond-coated inner diameter saw (Leica SP 1600, Leica Microsystems, Wetzlar, Germany) to slices of around 200 μm thickness. Those slices were glued with acrylic glue (Loctite 401, Henkel, Düsseldorf, Germany) to custom-made opaque PMMA microscope slides (Semadeni, Ostermündingen, Switzerland) and ground to around 60 μm thickness with a grinding machine (Pedemax-2, Struers, Willich, Germany). Finally, the surface of the slides was etched with 0.7 % formic acid (Applichem, Gatersleben, Germany) before staining it with toluidine blue (VWR, Dietikon, Switzerland). Images were taken with an upright light microscope (DM 5500, Leica Microsystems, Wetzlar, Germany).

2.3.7 Statistics

Statistical testing was done with Matlab (Mathworks, Natick MA, USA). Values lying outside an interval of 1.5 times the quartile range were identified as outliers and excluded. The results of the OVX scans were analyzed with a paired t-test after performing a Lilliefors test for a normal distribution. In case the normal distribution could not be confirmed, a Wilcoxon signed rank test was used. The static and dynamic bone parameters were tested for significance with a non-parametric Kruskal Wallis ANOVA followed by a Tukey's HSD (Honestly Significant Difference) test since not all groups followed a normal distribution and nor did they all have equal variance.

2.4 Results

2.4.1 Clinical Observations

All rats tolerated both surgeries well and returned to normal activity post-surgery. One rat from the Zol-Gel-group had to be euthanized 4 weeks after screw implantation due to a cholangiocarcinoma that was unrelated to the study. The results from this animal were still included in the analysis as the statistical tests did not identify them as outliers when compared with the other animals of the same group. The limited food intake allowed a controlled weight gain in the animals; their final mean weight was 372 ± 21 g.

2.4.2 Assessment of the Estrogen Deficiency Induced Bone Loss

The *in vivo* microCT scans confirmed that the rats had a diminished BMD, enlarged marrow cavities, and a significantly lower trabecular bone volume only 35 days after OVX (Table 2.1). This was shown by the decreasing BV/TV and Tb.N, and the increasing Tb.Sp. No significant changes could be detected for the Tb.Th. The rising SMI showed that the trabecular bone had shifted from a mainly plate-like structure to a more rod-like structure that is typical of osteoporotic bone (Hildebrand and Rüegsegger 1997). However, the estrogen deficiency had no short-term influence on the cortical bone. No changes could be detected in the cortical thickness (C.Th); the TMD of the cortex increased slightly by 2%.

	Cancellous Bone Parameters						Cortical Bone Parameters	
	BMD [g/mm ³]	BV/TV [%]	SMI [μ]	Tb.Th [mm]	Tb.Sp [mm]	Tb.N [1/mm]	TMD [g/mm ³]	C.Th [mm]
before OVX	0.32 ± 0.03	33.4 ± 3.9	1.19 ± 0.25	0.14 ± 0.01	0.32 ± 0.09	2.39 ± 0.32	1.09 ± 0.03	0.55 ± 0.01
35 d after OVX	0.23 ± 0.04	20.8 ± 4.9	1.79 ± 0.27	0.15 ± 0.02	0.92 ± 0.25	1.39 ± 0.31	1.11 ± 0.03	0.56 ± 0.02
mean change	-28%	-38%	50%	7%	191%	-42%	2%	0%
p-value	0.000	0.000	0.001	0.126	0.000	0.000	0.008	0.133

Table 2.1: Changes in bone parameters following OVX. Bone within the first 4 mm proximal to the femoral growth plate was analyzed. The mean changes were calculated as ratio of the difference between the mean values before and after OVX to the mean value before OVX.

2.4.3 MicroCT-based Dynamic Histomorphometry

A total of 138 microCT scans were analyzed for the dynamic histomorphometry, of which 2 had to be excluded due to motion artifacts. The sample size of the analyzed groups varied from 5 to 8 after removal of the outliers. The hyaluronic acid hydrogel used as a drug delivery system did not show any effect on the analyzed bone parameters. No significant differences were found between the Control-group and the Gel-group at any time. Volume rendered comparisons of two time points for one femur from the Gel-group and one from the Zol-Gel-group are shown in Figure 2.4.

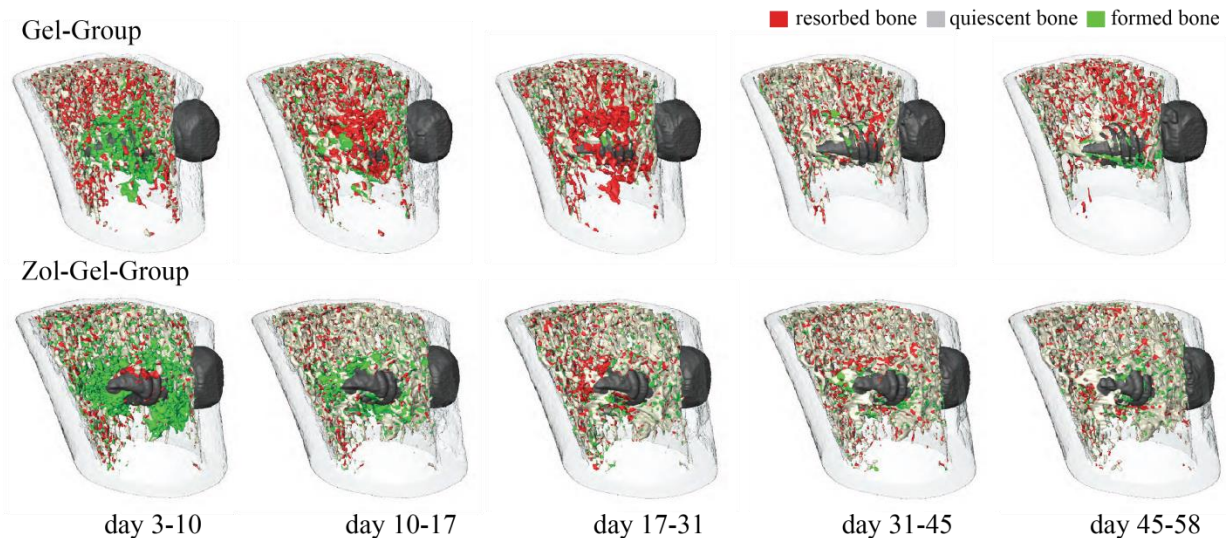


Figure 2.4: Three-dimensional visualization of the peri-implant bone indicating bone formation and resorption sites of two samples, one from the Gel-group (top), one from the Zol-Gel-group (bottom). The data were acquired by a comparison of pairs of consecutive microCT scans as described in section 2.5.4. The analyzed trabecular region of the bone is shown in light grey, red and green, the screw in dark grey and the cortex in transparent.

Static Bone Parameters

Two main bone regions can be distinguished in the results: the inner layer (0-368 μ m from screw surface) and part of the second layer (368-736 μ m) reflect the bone reaction to the screw implantation. The two outer layers (736-1472 μ m) are not affected by the implant and show stable bone parameters.

All experimental groups showed a clear gain in BV/TV, Tb.Th, and Tb.N in direct proximity to the screw between day 3 and day 10 after screw implantation (Figure 2.5, 2.6, 2.7). The Tb.Sp and the SMI decreased in accordance with the other bone parameters, which indicates a more compact bone structure (Figure 2.8, 2.9). This gain in bone mass continued for the Zol-Gel-group until day 17 and plateaued at a BV/TV of around 55% until the end of the study. In the Control- and the Gel-groups, the initial bone gain was followed first by a rapid and then later by a moderate bone loss. The final BV/TV in those two groups was around 13%. The effect of Zoledronate diminished with increasing distance from the screw surface. The trabecular parameters of the Zol-Gel-group show that the gain in bone volume further from the screw is mainly caused by an increasing Tb.N and a decreasing Tb.Sp (Figure 2.6, 2.7). The Tb.Th in the outer two layers was identical for all groups and constant throughout the whole study (Figure 2.8).

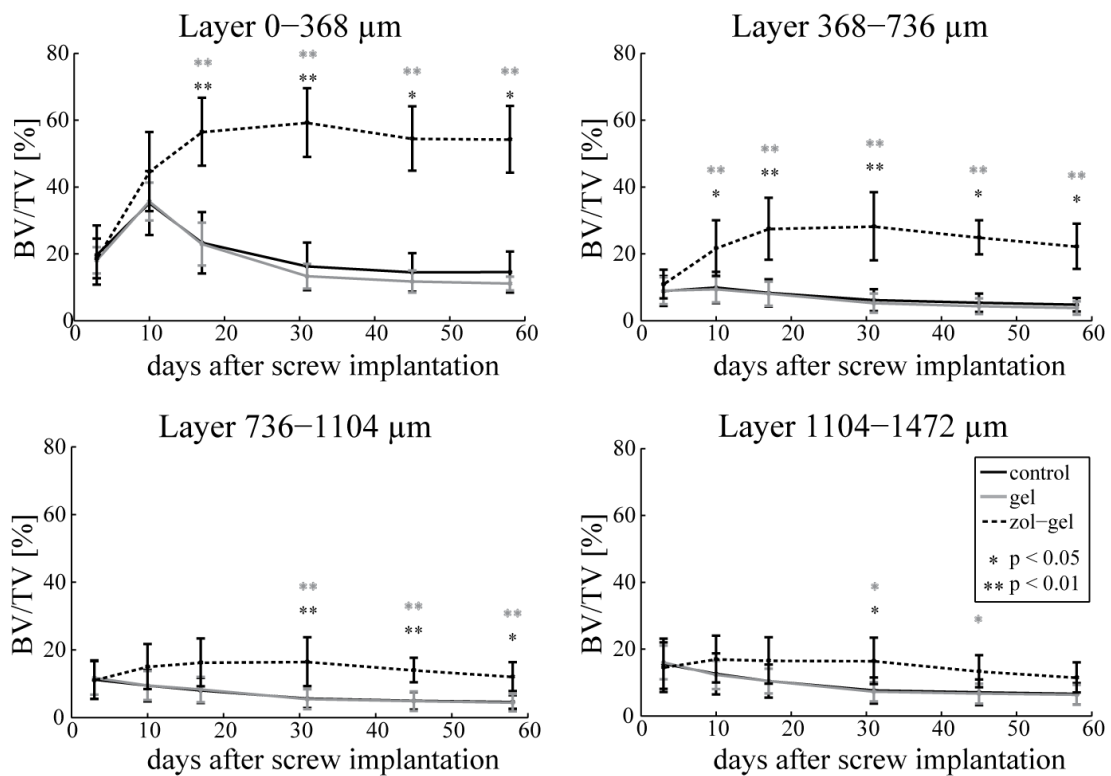


Figure 2.5: Bone volume/ tissue volume measured in 4 layers around the screw, the grey asterisks indicate the significant differences between Zol-Gel-group and Gel-group, the black ones between Control-group and Zol-Gel-group.

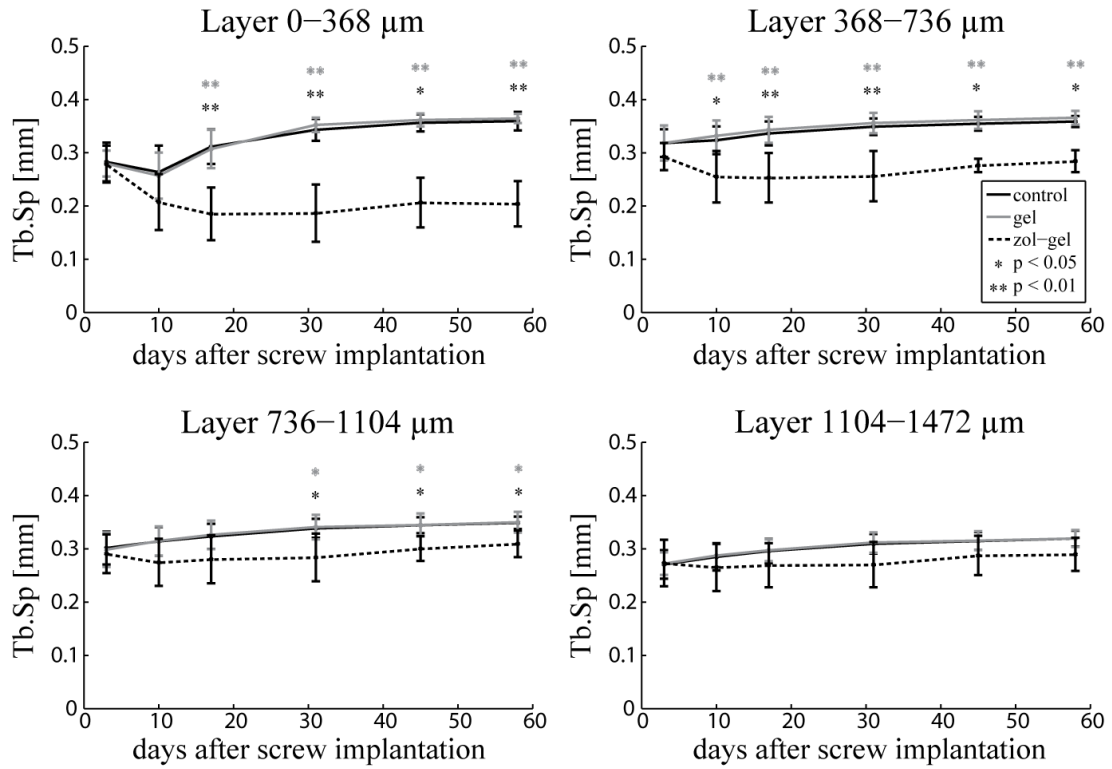


Figure 2.6: Trabecular separation measured in 4 layers around the screw, the grey asterisks indicate the significant differences between Zol-Gel-group and Gel-group, the black ones between Control-group and Zol-Gel-group.

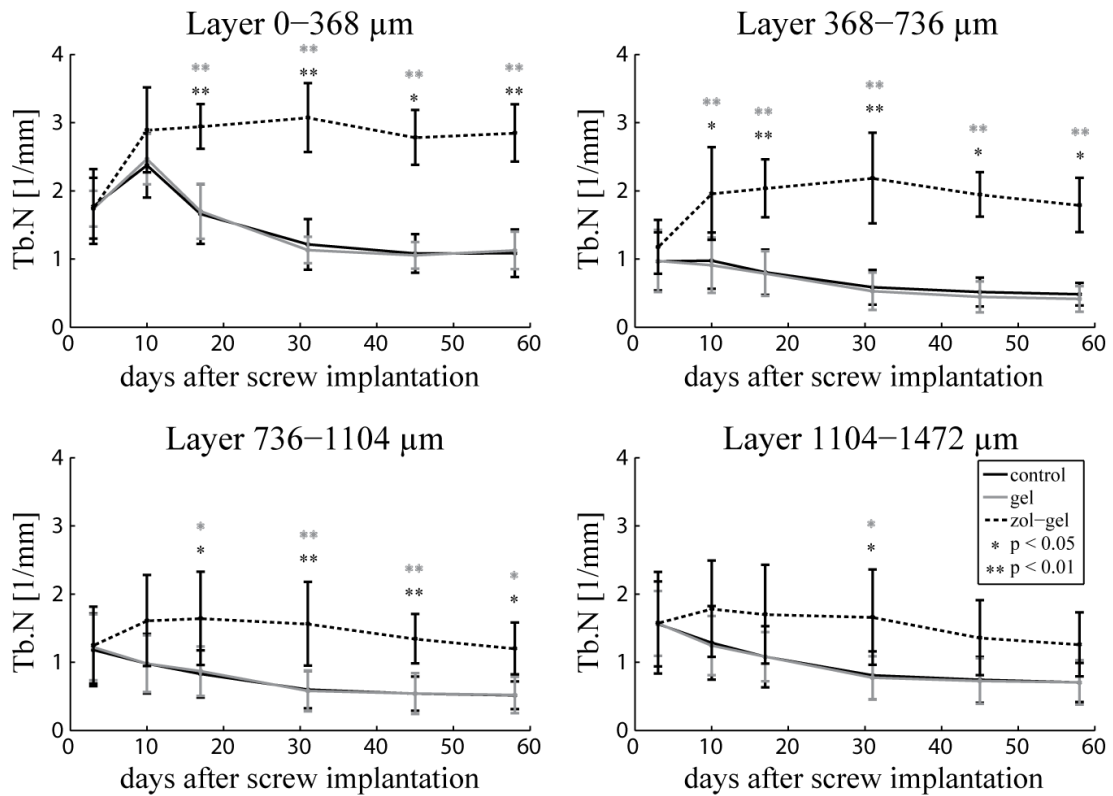


Figure 2.7: Trabecular number measured in 4 layers around the screw, the grey asterisks indicate the significant differences between Zol-Gel-group and Gel-group, the black ones between Control-group and Zol-Gel-group.

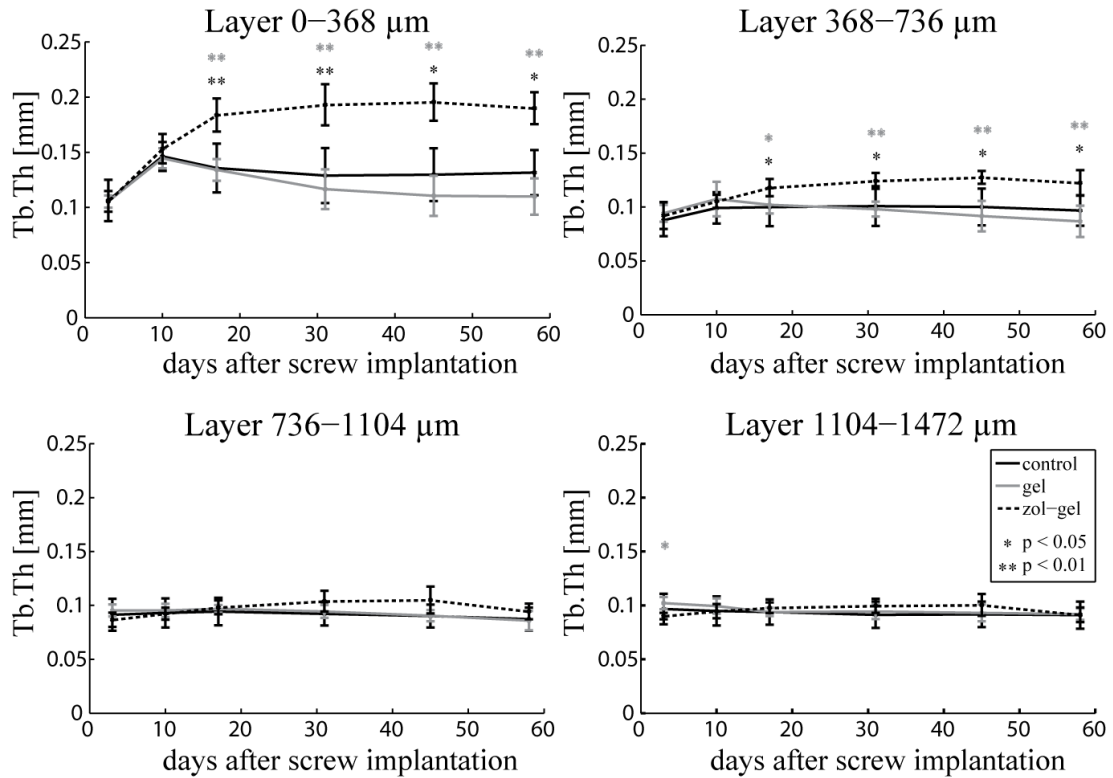


Figure 2.8: Trabecular thickness measured in 4 layers around the screw, the grey asterisks indicate the significant differences between Zol-Gel-group and Gel-group, the black ones between Control-group and Zol-Gel-group.

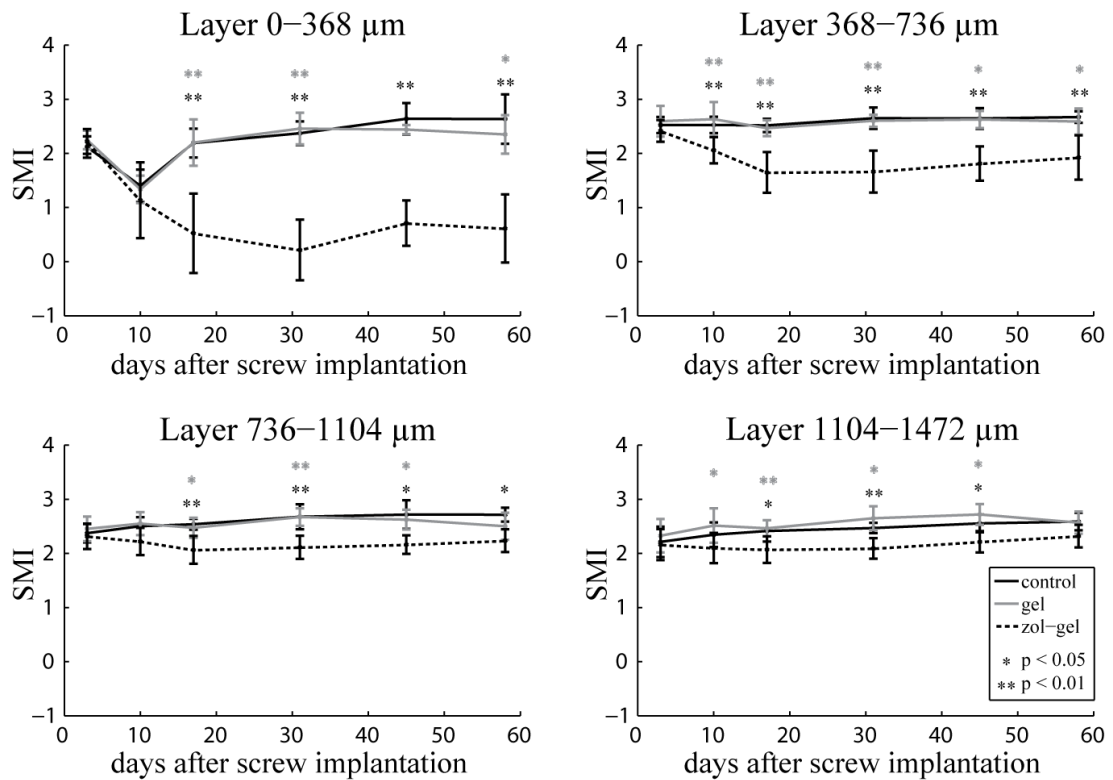


Figure 2.9: Structure model index measured in 4 layers around the screw, the grey asterisks indicate the significant differences between Zol-Gel-group and Gel-group, the black ones between Control-group and Zol-Gel-group.

Dynamic Bone Parameters

In direct proximity to the screw, a constant low BRR of around 2-3 %/d was seen for the Zol-Gel-group throughout the whole study (Figure 2.10). The Control- and Gel-groups initially showed (day 3-10) an equally low BRR followed by a high peak of around 12 %/d from day 10-17. From then onward, the BRR diminished until the study end point and reached a value equal to the Zol-Gel-group for the last period analyzed, which was 45-58 days after screw implantation. In the outer three layers, the BRR in the Control- and Gel-groups was initially very high (8-10 %/day) compared to the Zol-Gel-group (3-5 %/day). This difference evened out over time and was no longer significant from day 31-58.

Unlike the effect of Zoledronate on bone resorption, its influence on bone formation was small. The results of the BFR showed that the implantation of the screw induced an early peak in bone formation in the inner two layers in all groups (Figure 2.11). The BFR in the Control- and Gel-groups was characterized by a peak of around 20 %/d from day 3 to 10, followed by an almost constant low BFR of 1-2 %/d during the rest of the study. This phenomenon was also found to a lesser degree in the second layer from 368 – 736 μm where the initial BFR reached 10 %/d and then decreased to 2-3 %/d. The BFR in the two outer layers was unaffected by the screw implantation and showed a constant value of 3-4 %/d. The initial peak was enhanced for the Zol-Gel-group compared to the two other groups, a significant difference was found from days 10-17 in the inner layer and from days 3-17 in the second layer. The outer two layers of the Control- and the Gel-groups were not affected by the screw implantation and showed a constant BFR of around 5 %/d. The Zol-Gel-group differed in this region only from day 3-10, where it showed a small but significant bone formation peak of 9 %/d in the region from 736-1104 μm respective 6 %/d from 1104-1472 μm .

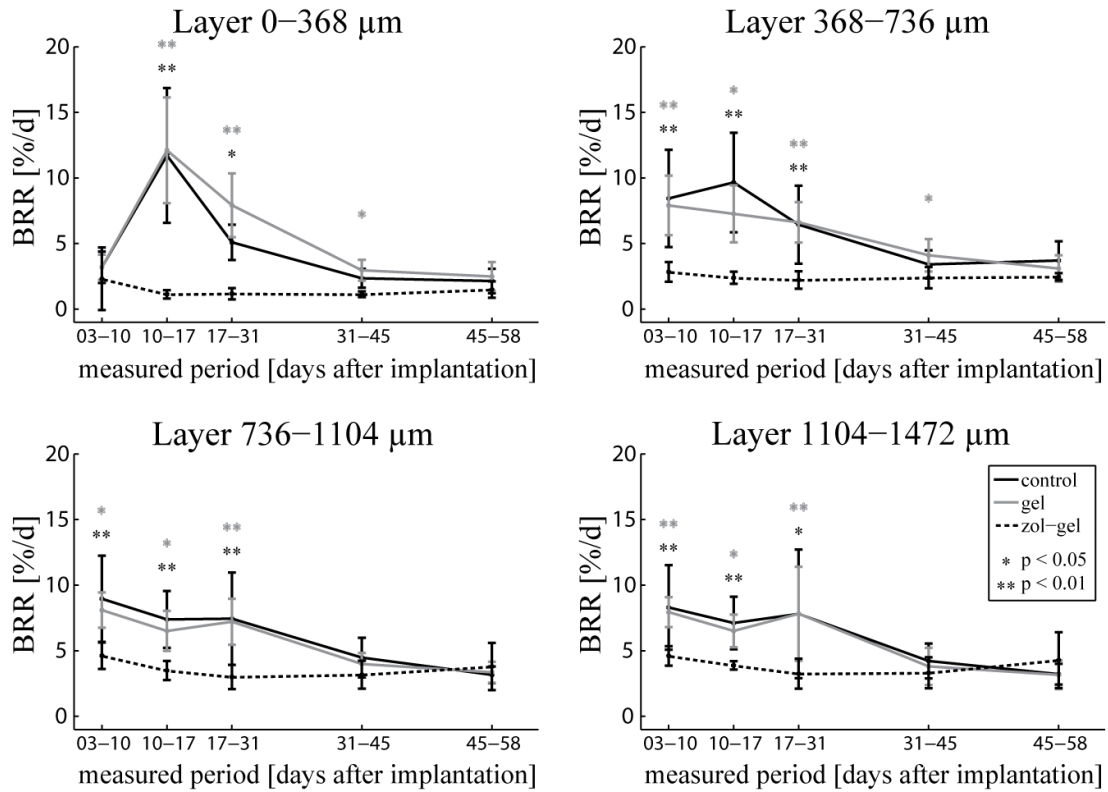


Figure 2.10: Bone resorption rate measured in 4 layers around the screw, the grey asterisks indicate the significant differences between Zol-Gel-group and Gel-group, the black ones between Control-group and Zol-Gel-group.

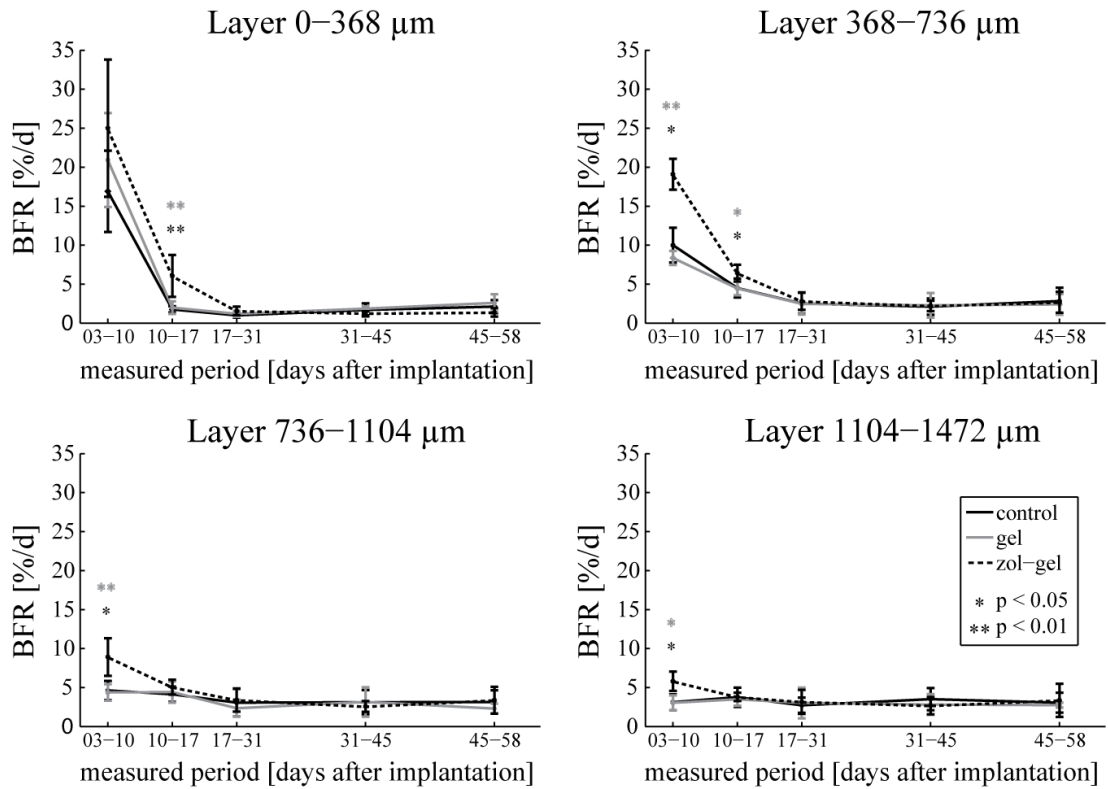


Figure 2.11: Bone formation rate measured in 4 layers around the screw, the grey asterisks indicate the significant differences between Zol-Gel-group and Gel-group, the black ones between Control-group and Zol-Gel-group.

2.4.4 Histology

Histology results showed that the hyaluronic acid hydrogel was fully degraded after 58 days of implantation since hydrogel residues could no longer be detected in neither the Gel- nor the Zol-Gel-groups (Figure 2.12). The screws were well osteointegrated in all groups; no significant amounts of fibrotic tissue could be detected close to the screw surfaces. In the Control- and the Gel-groups, new bone matrix was deposited only in direct proximity to the screws; no new bone formation could be detected further away. In the Zol-Gel-group, significant periosteal callus formation was found even far from the implantation site.

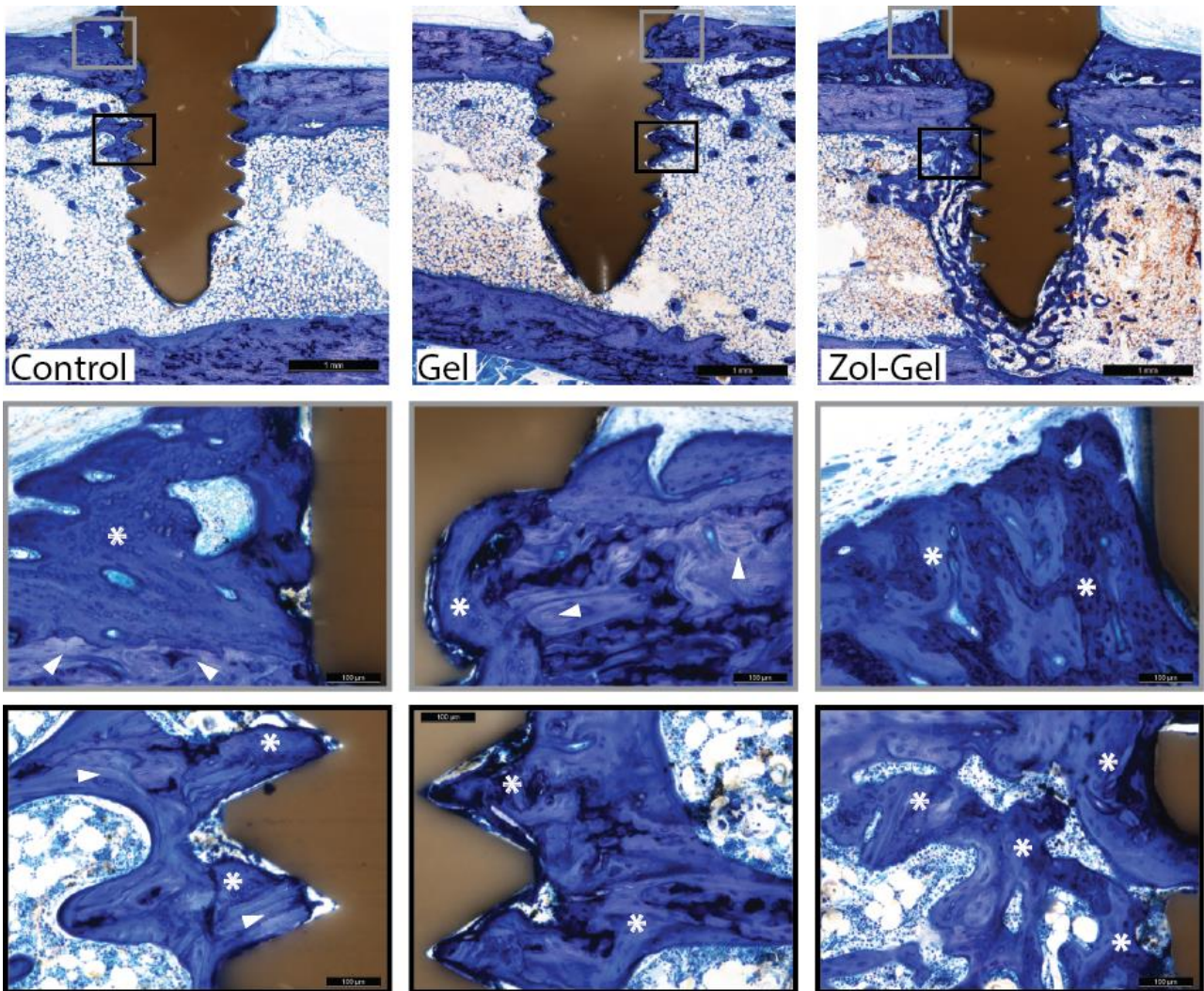


Figure 2.12: Toluidine blue stained ground sections from the Control-group (left), the Gel-group (middle) and the Zol-Gel-group (right). The white asterisks in the darker blue regions indicate immature, non-remodeled bone with an irregular structure and large amounts of cells, the white arrows on brighter blue regions show mature trabecular bone with less cells and a regular structure.

Only small periosteal callus formation was visible around the screw heads of the Control- and Gel-groups, the bone structure within those calli was still immature. In contrast, a large amount of newly formed bone trabeculae were detected close to and further away from the screw surface in the Zol-Gel-group. This newly formed bone also showed a woven structure typical of immature bone with an irregular arrangement of the collagen fibers, a large cell number and reduced mineral content. In the Zol-Gel-group, significant periosteal callus formation was found even far from the implantation site. Normal-shaped

osteoclasts and foreign body giant cells were present in all three groups, but to a much lower extent in the Zol-Gel-group than in the other two groups. The bone lining osteoblasts seemed to be more activated in the Zol-Gel-group compared to Control- and Gel-groups. The histology showed a significantly enhanced peri-implant bone density in the Zol-Gel-group. The newly formed bone was not fully remodeled in all groups, whereas the bone remodeling in the Zol-Gel-group seemed to be less advanced than in the other two groups.

2.5 Discussion

The main goal of the present study is to investigate the spatio-temporal effect of locally delivered Zoledronate on peri-implant bone remodeling based on time-lapsed microCT scans. In this context, a cross-linked hyaluronic acid hydrogel was used as drug delivery material.

The significant new result of this study is an up to 100% increase of the early bone formation rate caused by locally delivered Zoledronate that accompanies an efficient inhibition of peri-implant bone resorption. In this way, Zoledronate initially boosts bone formation and later on helps to preserve the newly formed bone. It is the first *in vivo* study unambiguously demonstrating the positive effect of Zoledronate on bone formation. This result opens new possibilities for local delivery of this drug as well as for the understanding of its global effect on bone remodeling.

MicroCT-based histomorphometry was chosen for this study as it has been shown to be a very suitable technique for the quantitative analysis of three-dimensional bone formation and bone resorption rates over long *in vivo* time periods (Schulte, Lambers et al. 2011). Obtaining data from multiple time points without having to euthanize the animals is a key advantage of a longitudinal study compared to the traditional two-dimensional histology-based histomorphometry. The second benefit of the microCT-based technique compared to histology is that bone resorption rate can be quantified in a direct manner that is very useful when studying the effect of anti-resorptive drugs such as BPs (Schulte, Lambers et al. 2011). Metal induced artifact issues that are typically related to CT scans and complicate the analysis of peri-implant bone were overcome in the present study by using radiopaque PEEK screws.

In order to understand the influence of the BPs on the peri-implant bone remodeling, it is important to have a look at the normal bone healing as it was found in the Control-group. First, the changes in bone structure caused by the estrogen deficiency are consistent with those reported in the literature and confirm the success of the OVX (Brouwers, Lambers et al. 2008). The results from the histomorphometry performed after screw implantation showed that the bone reaction to the trauma caused by the screw implantation took place principally in the two innermost layers (the “bone-healing-zone”, 0-736 μm from the screw surface). This zone was characterized by a large increase in bone formation rate during the first 17 days after the surgery up to a distance of 736 μm from the screw surface. This early peri-implant bone formation is in accordance with literature where it was shown to be the result of the so-called static osteogenesis (Ferretti, Palumbo et al. 2002; Marco, Milena et al. 2005). Osteogenic cells and a new calcified

matrix are therefore deposited after only a few days on the cement line created on the implant surface (Meyer, Joos et al. 2004). This rapid deposition of calcified matrix restores the continuity of the bone structure, even if the mechanical competence of the woven bone is lower than that of mature remodeled bone due to the random orientation of the collagen fibers (Probst and Spiegel 1997). No microCT-based studies could be found confirming bone formation this early next to an implant.

The woven structure of the newly formed bone in the Control-group was confirmed in the present study by a decrease in SMI and an increase in Tb.N and Tb.Th that accompanied the gain in BV/TV in the bone-healing-zone from day 3-10. Woven bone is reported to be progressively remodeled and substituted by mature bone with a trabecular structure and delimiting marrow spaces later on (Franchi, Orsini et al. 2004), a process that also removes bone debris and necrotized bone caused by the implant bed preparation (Futami, Fujii et al. 2000). In the present study, the remodeling was initiated by a significant loss in bone volume in the bone-healing-zone that started 10 days after screw implantation in the Control-group.

Another interesting finding from the Control-group is the initially high, and then progressively decreasing, BRR in the outer two layers that are not in contact with the screw (the “bone-remodeling-zone”). This phenomenon can be explained by the initial rapid bone loss phase induced by the estrogen deficiency of the animals that terminates 3-4 months after OVX (Hogan, Ruhmann et al. 2000). The bone loss is even enhanced in this study by the growth of the animals that results in a “flow” of the screw and the surrounding volume of interest towards the less trabecularized diaphyseal region. Normally, the growth of rats slows down and ceases around 26 weeks of age (Walker and Kember 1972), this corresponds in this study with day 31 after screw implantation. When comparing bone resorption with formation in the Control-group, it can be seen that, beside the early bone formation peak, the BRR clearly exceeded the BFR in all bone regions most of the time and leveled out only towards the end of the study. This imbalance resulted in a steady bone loss in the bone-remodeling-zone as can be seen in the diminishing BV/TV in the control animals.

The Gel-group did not show any statistically different results compared to the Control-group, therefore the chosen hydrogel can be considered not to have any influence on peri-implant bone remodeling. It was resorbed completely during the study without leaving any visible residuals, as confirmed by histology.

The locally delivered Zoledronate interfered with the normal healing and remodeling process at a very early stage as demonstrated in the Zol-Gel-group. An increase of up to 100 % of the BFR was seen from days 3 to 17 in the bone-healing-zone and from days 3 to 10 in the bone-remodeling-zone. Later on during the study, no more differences could be detected between the groups. This result suggests that Zoledronate is only influencing bone formation during the first “flush” with the drug where bone forming cells are either in contact with the gel or exposed to Zoledronate in solution. The direct contact could allow them to incorporate the drug via fluid phase endocytosis, an uptake mechanism for Zoledronate that has been described by Thompson et al. (Thompson, Rogers et al. 2006). BPs are known to be rapidly cleared from the circulation and absorbed to bone mineral surface (Lin 1996). The fast uptake in the bone can explain why

no further Zoledronate effect on bone formation could be detected later on in the study. This is because osteoclasts are the only cells that can liberate and incorporate BPs once they are bound to bone mineral (Rogers, Gordon et al. 2000). It remains unclear if the initial boost in bone formation is caused by a direct stimulation of the osteoblast activity, or by unknown indirect coupling effects. Arnoldi et al. recently found a higher level of cellular proliferation and osseous differentiation at an early time point around implants coated with fibrinogen and loaded with a very low dose of Zoledronate (Arnoldi, Alves et al. 2014). This finding supports the theory that Zoledronate can have a direct anabolic effect on bone formation. Published *in vitro* studies are not conclusive as they demonstrate that Zoledronate can have positive as well as negative results on osteoblasts, depending on the dose and study design (Pan, To et al. 2004; Greiner, Kadow-Romacker et al. 2006; Walter, Klein et al. 2010). Orriss et al. showed that the Zoledronate dose has to be increased 10- to 100-fold to achieve the same inhibitory effect on osteoblasts when those are cultured on dentin slides, a finding that supports the theory that absorbed BPs are significantly less effective on osteoblasts (Orriss, Key et al. 2009).

Since Zoledronate is an anti-resorptive agent, the drug is expected to mainly influence bone resorption. In the present study, this was shown by the significantly reduced BRR in the drug treated animals. The strong resorption peak seen in the Control-group was not at all present in the bone-healing-zone of the Zol-Gel-group in which the BRR remained at a constant low level. A slightly higher but still constant BRR level could be found in the bone-remodeling-zone of the Zol-Gel-group. The investigated time period was too short to detect a clear end of the drug effect on bone resorption. However, static and dynamic bone parameters of the last analyzed time points and periods suggested a diminishing drug effect with a slightly increasing BRR and decreasing differences between the groups, particularly in the bone-remodeling-zone.

Looking at the spatial effect of the locally delivered Zoledronate, this study revealed that the majority of the effects of BPs occur at a distance of up to 736 μm around the screw, which corresponds to the earlier defined bone-healing-zone. Tests with hydrogel loaded with hydroxyapatite-particles (size 200 nm) that give the gel a light radiopacity (data not shown) revealed that the gel is located within a range of 0 - 600 μm around the screw. Therefore, it can be assumed that bone is in direct contact with the Zoledronate-loaded gel within the region that shows the strong drug effect. These results suggest that it may be possible to control the range of action of the Zoledronate-loaded gel via its penetration depth in bone. This is a promising approach as the penetration depth can be adapted by altering the mechanical properties of the gel or the volume of gel inserted into the implant bed. However, a significantly weaker drug effect was also shown for the bone-remodeling-zone that is not in contact with the gel. This finding suggests that a small part of the released Zoledronate diffuses through the bone despite its high affinity to mineral and its fast absorption in bone surfaces.

The boost in initial bone formation, the effective inhibition of the bone resorption in the bone-healing-zone, and the stabilization of the bone loss in the bone-remodeling-zone resulted in a BV/TV that was up to 300 % higher compared to the Control-group in the bone-healing-zone and up to 100 % higher in the bone remodeling-zone. The reduction of SMI and Tb.Sp as well as the increase Tb.N confirmed a shift from

osteoporotic towards a more normal bone structure. This is a very positive finding as an augmented microstructure of peri-implant bone is linked to improved implant anchorage (Yakacki, Poukalova et al. 2010; Wirth, Goldhahn et al. 2011; Wirth, Müller et al. 2012). The gain in bone volume and therefore in mechanical resistance might nevertheless be partly compensated for by the less mature bone structure that was present 2 months after screw implantation, as confirmed by histology in the present study. The SMI of 0.6 that characterized the bone in the bone-healing zone of the Zol-Gel-group at day 58 compared to an SMI of 2.6 in the Control-group confirmed that the very compact woven bone had not yet remodeled. Findings in similar studies provide enough evidence to show that Zoledronate treated bone can enhance implant fixation despite the reduced mechanical competence of the immature bone structure (Tengvall, Skoglund et al. 2004; Peter, Gauthier et al. 2006; Andersson, Agholme et al. 2010). Furthermore, Amanat et al. showed with an indentation study that Zoledronate has no influence on the intrinsic mechanical properties of healing bone (Amanat, He et al. 2008).

The present study has inherent limitations. The microCT-based dynamic histomorphometry averages bone formation and resorption rate over the time period between two scans which makes the results sensitive to the chosen time points for the scans (Schulte, Lambers et al. 2011). In this study bone formation and bone resorption have to be interpreted as gain and loss of mineralized bone tissue since the microCT cannot analyze the bone on a cellular level. Furthermore, the age of the rats was not ideal due to the fact that the end of the initial OVX related bone loss phase and the cessation of bone length growth occurred during the experimental phase. Furthermore, in future studies, histology should be performed at early time points for a better understanding of how Zoledronate enhances very early peri-implant bone formation. It might also be useful to prolong the experimental phase in order to assess when bone maturity is reached in the Zol-Gel-group. In this study, only one drug dose of 5 µg per implant was tested. A future dose-response study could help to investigate the dose-dependency of the present findings.

In summary, the quickly degradable hydrogel used in this study appeared to be a very suitable drug delivery system for BPs. The texture and material properties of the gel allowed for an easy and precise application, combined with a deep penetration of the bone tissue that significantly increased the range of action of the drug. Numerous studies have shown that BPs released from coatings stay highly localized and result in a very thin layer of dense bone around implants which is not ideal for implant fixation (Stadelmann, Gauthier et al. 2008; McKenzie, Dennis Bobyne et al. 2011). This is not the case in the present study where an increased bone volume could be shown all over the analyzed trabecular region. The present study also demonstrated a positive influence of Zoledronate on early bone formation in addition to its known anti-resorptive action. This effect seems to be supported by a fast release of the small BP molecules from the highly porous hydrogel, another point in favor of the use of hydrogels as drug-delivery systems for BPs.

2.6 Conclusion

The present study was able to show that Zoledronate delivered from a quickly degrading hydrogel can boost early bone formation and later on efficiently inhibit peri-implant bone resorption close to an implant. It can also stabilize bone loss away from an implant in an OVX rat model. This process significantly enhanced bone mass and improved bone micro-structure in the treated peri-implant bone during the two months post-implantation that were studied. A reinforced bone structure is directly linked to improved implant fixation. The presented approach using Zoledronate-loaded hydrogel for implant bed preparation is highly promising, especially for patients suffering from low quality bone, though more studies are needed.

2.7 Acknowledgment

Special thanks to Sandra Jaccoud at the LBO for her assistance during surgeries and for the preparation of the histology slides. Thanks to Caroline Sieger Fernandes for the English proofreading of the manuscript. We benefited from the help of Prof. Brigitte von Rechenberg, Dr. Karina Klein and Dr. Salim Darwiche at the University of Zurich for the interpretation of the histology slides. This study was partially supported by a KTI grant (Project no. 11098.1).

2.8 References

- Alghamdi, H. S., R. Bosco, et al. (2013). "Osteogenicity of titanium implants coated with calcium phosphate or collagen type-I in osteoporotic rats." *Biomaterials* **34**(15): 3747-3757.
- Allen, M. R., H. Follet, et al. (2006). "Antiremodeling agents influence osteoblast activity differently in modeling and remodeling sites of canine rib." *Calcif Tissue Int* **79**(4): 255-261.
- Amanat, N., L. H. He, et al. (2008). "The effect of zoledronic acid on the intrinsic material properties of healing bone: an indentation study." *Med Eng Phys* **30**(7): 843-847.
- Andersson, T., F. Agholme, et al. (2010). "Surface immobilized zoledronate improves screw fixation in rat bone: a new method for the coating of metal implants." *J Mater Sci Mater Med* **21**(11): 3029-3037.
- Arnoldi, J., A. Alves, et al. (2014). "Early tissue responses to zoledronate, locally delivered by bone screw, into a compromised cancellous bone site: A pilot study." *BMC Musculoskeletal Disorders* **15**(1).
- Astrand, J. and P. Aspenberg (2004). "Topical, single dose bisphosphonate treatment reduced bone resorption in a rat model for prosthetic loosening." *J Orthop Res* **22**(2): 244-249.
- Åstrand, J., A. K. Harding, et al. (2006). "Systemic zoledronate treatment both prevents resorption of allograft bone and increases the retention of new formed bone during revascularization and remodelling. A bone chamber study in rats." *BMC Musculoskeletal Disorders* **7**.
- Back, D. A., S. Pauly, et al. (2012). "Effect of local zoledronate on implant osseointegration in a rat model." *BMC Musculoskeletal Disorders* **13**.
- Belfrage, O., H. Isaksson, et al. (2012). "Local treatment of a bone graft by soaking in zoledronic acid inhibits bone resorption and bone formation. A bone chamber study in rats." *BMC Musculoskeletal Disorders* **13**.
- Bergman, K., T. Engstrand, et al. (2009). "Injectable cell-free template for bone-tissue formation." *Journal of Biomedical Materials Research - Part A* **91**(4): 1111-1118.
- Bobyn, J. D., R. Thompson, et al. (2014). "Local alendronic acid elution increases net periimplant bone formation: A micro-CT analysis." *Clin Orthop Relat Res* **472**(2): 687-694.
- Boyce, B. F., E. Rosenberg, et al. (2012). "The osteoclast, bone remodelling and treatment of metabolic bone disease." *European Journal of Clinical Investigation* **42**(12): 1332-1341.
- Brouwers, J. E. M., F. M. Lambers, et al. (2008). "Bone degeneration and recovery after early and late bisphosphonate treatment of ovariectomized wistar rats assessed by in vivo micro-computed tomography." *Calcif Tissue Int* **82**(3): 202-211.
- Brouwers, J. E. M., B. Van Rietbergen, et al. (2007). "No effects of in vivo micro-CT radiation on structural parameters and bone marrow cells in proximal tibia of wistar rats detected after eight weekly scans." *Journal of Orthopaedic Research* **25**(10): 1325-1332.
- Cheng, T. L., C. M. Murphy, et al. (2013). "Local delivery of recombinant human bone morphogenetic proteins and bisphosphonate via sucrose acetate isobutyrate can prevent femoral head collapse in Legg-Calve-Perthes disease: a pilot study in pigs." *Int Orthop* **38**(7): 1527-1533.
- Cottrell, J. A., F. M. Vales, et al. (2010). "Osteogenic activity of locally applied small molecule drugs in a rat femur defect model." *J Biomed Biotechnol* **2010**: 597641.
- Ferretti, M., C. Palumbo, et al. (2002). "Static and dynamic osteogenesis: Two different types of bone formation." *Anatomy and Embryology* **206**(1-2): 21-29.
- Franchi, M., E. Orsini, et al. (2004). "Osteogenesis and morphology of the peri-implant bone facing dental implants." *TheScientificWorldJournal [electronic resource]*. **4**: 1083-1095.
- Fuchs, R. K., R. J. Phipps, et al. (2008). "Recovery of trabecular and cortical bone turnover after discontinuation of risedronate and alendronate therapy in ovariectomized rats." *Journal of Bone and Mineral Research* **23**(10): 1689-1697.
- Futami, T., N. Fujii, et al. (2000). "Tissue response to titanium implants in the rat maxilla: Ultra structural and histochemical observations of the bone-titanium interface." *Journal of Periodontology* **71**(2): 287-298.
- Gasser, J. A., P. Ingold, et al. (2008). "Long-term protective effects of zoledronic acid on cancellous and cortical bone in the ovariectomized rat." *J Bone Miner Res* **23**(4): 544-551.
- Giuliani, N., M. Pedrazzoni, et al. (1998). "Bisphosphonates stimulate formation of osteoblast precursors and mineralized nodules in murine and human bone marrow cultures in vitro and promote early osteoblastogenesis in young and aged mice in vivo." *Bone* **22**(5): 455-461.
- Greiner, S., A. Kadow-Romacker, et al. (2006). "The effect of zoledronic acid incorporated in a poly(D,L-lactide) implant coating on osteoblasts in vitro." *J Biomed Mater Res A* **80**(4): 769-775.
- Hildebrand, T. and P. Rüeggsegger (1997). "Quantification of bone microarchitecture with the structure model index." *Computer Methods in Biomechanics and Biomedical Engineering* **1**(1): 15-23.

- Hilding, M. and P. Aspenberg (2007). "Local peroperative treatment with a bisphosphonate improves the fixation of total knee prostheses: a randomized, double-blind radiostereometric study of 50 patients." Acta Orthop **78**(6): 795-799.
- Hogan, H. A., S. P. Ruhmann, et al. (2000). "The mechanical properties of cancellous bone in the proximal tibia of ovariectomized rats." Journal of Bone and Mineral Research **15**(2): 284-292.
- Idris, A. I., J. Rojas, et al. (2008). "Aminobisphosphonates cause osteoblast apoptosis and inhibit bone nodule formation in vitro." Calcif Tissue Int **82**(3): 191-201.
- Jakobsen, T., J. Baas, et al. (2010). "The effect of soaking allograft in bisphosphonate: a pilot dose-response study." Clin Orthop Relat Res **468**(3): 867-874.
- Kisiel, M., A. S. Klar, et al. (2013). "Evaluation of Injectable Constructs for Bone Repair with a Subperiosteal Cranial Model in the Rat." PLoS ONE **8**(8).
- Lin, J. H. (1996). "Bisphosphonates: a review of their pharmacokinetic properties." Bone **18**(2): 75-85.
- Marco, F., F. Milena, et al. (2005). "Peri-implant osteogenesis in health and osteoporosis." Micron **36**(7-8): 630-644.
- Martínez-Álvarez, C., B. González-Meli, et al. (2013). "Injection and adhesion palatoplasty: a preliminary study in a canine model." Journal of Surgical Research **183**(2): 654-662.
- Martínez-Sanz, E., O. P. Varghese, et al. (2012). "Minimally invasive mandibular bone augmentation using injectable hydrogels." Journal of Tissue Engineering and Regenerative Medicine **6**(SUPPL. 3): s15-s23.
- McKenzie, K., J. Dennis Bobyn, et al. (2011). "Bisphosphonate Remains Highly Localized After Elution From Porous Implants." Clin Orthop Relat Res **469**(2): 514-522.
- Meyer, U., U. Joos, et al. (2004). "Ultrastructural characterization of the implant/bone interface of immediately loaded dental implants." Biomaterials **25**(10): 1959-1967.
- Orriss, I. R., M. L. Key, et al. (2009). "Inhibition of osteoblast function in vitro by aminobisphosphonates." J Cell Biochem **106**(1): 109-118.
- Pan, B., L. B. To, et al. (2004). "The nitrogen-containing bisphosphonate, zoledronic acid, increases mineralisation of human bone-derived cells in vitro." Bone **34**(1): 112-123.
- Pazianas, M., C. Cooper, et al. (2010). "Long-term treatment with bisphosphonates and their safety in postmenopausal osteoporosis." Ther Clin Risk Manag **6**: 325-343.
- Peter, B., O. Gauthier, et al. (2006). "Local delivery of bisphosphonate from coated orthopedic implants increases implants mechanical stability in osteoporotic rats." J Biomed Mater Res A **76**(1): 133-143.
- Plotkin, L. I., S. C. Manolagas, et al. (2006). "Dissociation of the pro-apoptotic effects of bisphosphonates on osteoclasts from their anti-apoptotic effects on osteoblasts/osteocytes with novel analogs." Bone **39**(3): 443-452.
- Plotkin, L. I., R. S. Weinstein, et al. (1999). "Prevention of osteocyte and osteoblast apoptosis by bisphosphonates and calcitonin." Journal of Clinical Investigation **104**(10): 1363-1374.
- Probst, A. and H. U. Spiegel (1997). "Cellular mechanisms of bone repair." Journal of Investigative Surgery **10**(3): 77-86.
- Recker, R. R., P. D. Delmas, et al. (2008). "Effects of intravenous zoledronic acid once yearly on bone remodeling and bone structure." Journal of Bone and Mineral Research **23**(1): 6-16.
- Riggs, B. L. and A. M. Parfitt (2005). "Drugs used to treat osteoporosis: The critical need for a uniform nomenclature based on their action on bone remodeling." Journal of Bone and Mineral Research **20**(2): 177-184.
- Roelofs, A. J., K. Thompson, et al. (2006). "Molecular mechanisms of action of bisphosphonates: Current status." Clinical Cancer Research **12**(20 PART 2): 6222s-6230s.
- Rogers, M. J., S. Gordon, et al. (2000). "Cellular and molecular mechanisms of action of bisphosphonates." Cancer **88**(12 Suppl): 2961-2978.
- Roshan-Ghias, A., J. Arnoldi, et al. (2011). "In vivo assessment of local effects after application of bone screws delivering bisphosphonates into a compromised cancellous bone site." Clin Biomech **26**(10): 1039-1043.
- Russell, R. G., N. B. Watts, et al. (2008). "Mechanisms of action of bisphosphonates: similarities and differences and their potential influence on clinical efficacy." Osteoporos Int **19**(6): 733-759.
- Schulte, F. A., F. M. Lambers, et al. (2011). "In vivo micro-computed tomography allows direct three-dimensional quantification of both bone formation and bone resorption parameters using time-lapsed imaging." Bone **48**(3): 433-442.
- Seeman, E. (2009). "Bone modeling and remodeling." Critical Reviews in Eukaryotic Gene Expression **19**(3): 219-233.
- Srisubut, S., A. Teerakapong, et al. (2007). "Effect of local delivery of alendronate on bone formation in bioactive glass grafting in rats." Oral Surgery, Oral Medicine, Oral Pathology, Oral Radiology and Endodontology **104**(4): e11-e16.
- Stadelmann, V. A., O. Gauthier, et al. (2008). "Implants delivering bisphosphonate locally increase periprosthetic bone density in an osteoporotic sheep model. A pilot study." Eur Cell Mater **16**: 10-16.

- Tengvall, P., B. Skoglund, et al. (2004). "Surface immobilized bisphosphonate improves stainless-steel screw fixation in rats." *Biomaterials* **25**(11): 2133-2138.
- Thompson, K., M. J. Rogers, et al. (2006). "Cytosolic entry of bisphosphonate drugs requires acidification of vesicles after fluid-phase endocytosis." *Molecular Pharmacology* **69**(5): 1624-1632.
- Tobias, J. H., J. W. M. Chow, et al. (1993). "3-Amino-1-hydroxypropylidene-1-bisphosphonate (AHPrBP) suppresses not only the induction of new, but also the persistence of existing bone-forming surfaces in rat cancellous bone." *Bone* **14**(4): 619-623.
- Waarsing, J. H., J. S. Day, et al. (2004). "Detecting and tracking local changes in the tibiae of individual rats: A novel method to analyse longitudinal in vivo micro-CT data." *Bone* **34**(1): 163-169.
- Walker, K. V. and N. F. Kember (1972). "Cell kinetics of growth cartilage in the rat tibia. II. Measurements during ageing." *Cell and Tissue Kinetics* **5**(5): 409-419.
- Walter, C., M. O. Klein, et al. (2010). "Influence of bisphosphonates on endothelial cells, fibroblasts, and osteogenic cells." *Clin Oral Investig* **14**(1): 35-41.
- Watts, N. B. and D. L. Diab (2010). "Long-term use of bisphosphonates in osteoporosis." *J Clin Endocrinol Metab* **95**(4): 1555-1565.
- Wirth, A. J., J. Goldhahn, et al. (2011). "Implant stability is affected by local bone microstructural quality." *Bone* **49**(3): 473-478.
- Wirth, A. J., R. Müller, et al. (2012). "Augmentation of peri-implant bone improves implant stability: Quantification using simulated bone loss." *Journal of Orthopaedic Research* **30**(2): 178-184.
- Yakacki, C. M., M. Poukalova, et al. (2010). "The effect of the trabecular microstructure on the pullout strength of suture anchors." *J Biomech* **43**(10): 1953-1959.

Chapter 3 Development of a Drug Delivery System

Paper 2 Combining a Locally Delivered Bisphosphonate with Hydroxyapatite Particles – Can We Achieve Synergistic Effects?

3.1 Abstract

Locally applied Zoledronate has been shown in several studies to inhibit peri-implant bone resorption and recently also to enhance bone formation. Other studies have demonstrated positive effects of hydroxyapatite particles on peri-implant bone regeneration and an enhancement of the anti-resorptive effect of bisphosphonates by the presence of calcium. Therefore an increase of the positive Zoledronate effect on early bone formation was assumed for a combined release of Zoledronate and hydroxyapatite nanoparticles (nHA). Possible synergistic effects were first investigated *in vitro* in a RAW 264.7 cell assay and then *in vivo* in a rat model of postmenopausal osteoporosis. The *in vitro* study confirmed that the inhibitory effect of Zoledronate on murine macrophages was enhanced by loading the drug on nHA. For the *in vivo* investigation, Zoledronate-loaded nHA or nHA were integrated in hyaluronic acid hydrogel and applied in the screw holes in rat femoral condyles before insertion of miniature screws. MicroCT based dynamic histomorphometry and histology revealed an unexpected rapid mineralization of the hydrogel *in vivo* through formation of granules which served as scaffold for new bone formation. The delivery of Zoledronate-loaded nHA further inhibited a degradation of the mineralized hydrogel as well as a resorption of the peri-implant bone to a similar extent than Zoledronate without nHA. The rapid *in vivo* mineralization combined with the inhibitory effect of Zoledronate on bone resorption and biomaterial degradation is highly interesting. However, the microCT based study did not allow us to distinguish between forming/resorbing bone and mineralizing/degrading biomaterial, preventing a possibility to evaluate *in vivo* synergistic effects on bone remodeling. Hyaluronic acid with Zoledronate-loaded nHA, thanks to its dual effect on inducing mineralization and preventing resorption, is nevertheless a very promising and versatile material for bone repair and augmentation.

Keywords: Drug delivery; hydrogel; hydroxyapatite; bisphosphonate; microCT; biomaterial mineralization

3.2 Introduction

Zoledronate-loaded hyaluronic acid hydrogel has recently been shown to efficiently improve early bone formation and inhibit bone resorption around an implant in a rat model of postmenopausal osteoporosis (chapter 2). This is an important finding as a sufficient peri-implant bone density is directly linked to a successful implant fixation (Stromsoe, Kok et al. 1993; Wilmes, Rademacher et al. 2006; Wirth, Goldhahn et al. 2011). A reliable implant anchorage is however often difficult to achieve in patients suffering from bone diseases that are characterized by a reduced bone density, such as osteoporosis. Implant migration and revision surgeries are often the consequence in those cases (Lobo-Escolar, Joven et al. 2010). Therefore the local delivery of a bisphosphonate (BP) to the peri-implant bone stock, as demonstrated with the drug-loaded hydrogel (chapter 2), is a very promising approach to improve the outcome of implant fixation in patients presenting low bone quality.

In parallel, other strategies have been proven to be able to successfully improve implant anchorage. One of them is the application of hydroxyapatite (HA) particles to the implant bed. Tami et al. demonstrated that HA-particles that are filled in a screw hole are able to induce and maintain a denser bone mantle in osteoporotic bone (Tami, Leitner et al. 2009). HA is chemically similar to the inorganic components of the bone matrix and therefore exhibits an excellent biocompatibility with soft and hard tissues (Zhou and Lee 2011). It is known to be bioactive, osteoconductive and biodegradable and therefore it is widely used as biomaterial for dental and orthopedic applications (LeGeros 2008). Considering also the fact that Ca^{2+} ions have been shown to enhance the inhibitory effect of nitrogen-containing BPs on macrophages by enhancing their endocytic internalization *in vitro* (Monkkonen, Taskinen et al. 1994; Thompson, Rogers et al. 2006), it can be assumed that a combination of BPs and calcium phosphate particles may induce synergetic effect on bone remodeling.

So far BPs have mainly been absorbed on HA bulk implants or coatings using the high affinity of the drug to mineral (Yoshinari, Oda et al. 2002; Peter, Gauthier et al. 2006; Suratwala, Cho et al. 2008; Faucheux, Verron et al. 2009; Sörensen, Arnoldi et al. 2013). Binding BPs to bulk hydroxyapatite is associated with a slow release of the drug as a low pH is required for a spontaneous release of the drug from a mineral surface (Rogers, Gordon et al. 2000; Nancollas, Tang et al. 2006). However, as shown in our previous work, a fast availability of the BP seems to be important for a positive effect on early bone formation (chapter 2). Therefore it would be favorable to combine the BP with small enough HA-particles that could be distributed easily in bone and be uptaken by osteoclasts.

Several studies have investigated the applicability of bisphosphonate-loaded nanoparticles for antitumor drug delivery properties (Palazzo, Iafisco et al. 2007) and for intravenous drug delivery systems (Ong, Loo et al. 2008). Boanini et al. showed that Zoledronate-HA nano-composites promote osteoclast formation and osteoclast apoptosis *in vitro*, but they did not publish comparative results with pure Zoledronate (Boanini, Torricelli et al. 2012). Nejadnik et al. demonstrated recently that bisphosphonate-functionalized hyaluronic acid containing calcium phosphate particles is stable *in vivo* and attracts bone ingrowth (Nejadnik, Yang et

al. 2014). This study however used Pamidronate as chemical link between calcium phosphate particles and the hydrogel matrix (Wang, Zhang et al. 2006). Contrary to the present work, a release of the drug to the bone was not intended and expected to be minimal (Nejadnik, Yang et al. 2014).

In present study we investigate *in vitro* in cell assays and *in vivo* in an osteoporotic rat model if we can achieve synergistic effects on peri-implant bone remodeling by adding osteoconductive hydroxyapatite nano-sized particles loaded with Zoledronate to hyaluronic acid hydrogel.

3.3 Materials and Methods

Zoledronate used for this study was bought from Enzo Life Sciences (Art.-Nr. ALX-430-153-0000, Enzo Life Sciences, Farmingdale, USA). Hydroxyapatite powder (nHA) with a particle size around 200 nm was bought from Sigma (art.-nr. 677418, Sigma-Aldrich, St. Louis, MO, USA). Those particles have a round shape (Figure 3.1). The nHA-particles were heat sterilized before use. Cell culture medium (CCM) for the *in vitro* studies was prepared by mixing Dulbecco's Modified Eagle Medium (DMEM, art.-nr. 41966-029, Gibco, Life Technologies, Carlsbad, CA, USA) with 10% fetal bovine serum (Sigma-Aldrich, art.-nr. F7524-500ML) and 1% penicillin/streptomycin (art.-nr. 15140122, Gibco) and 1% L-glutamine (art.-nr. 25030024, Gibco).

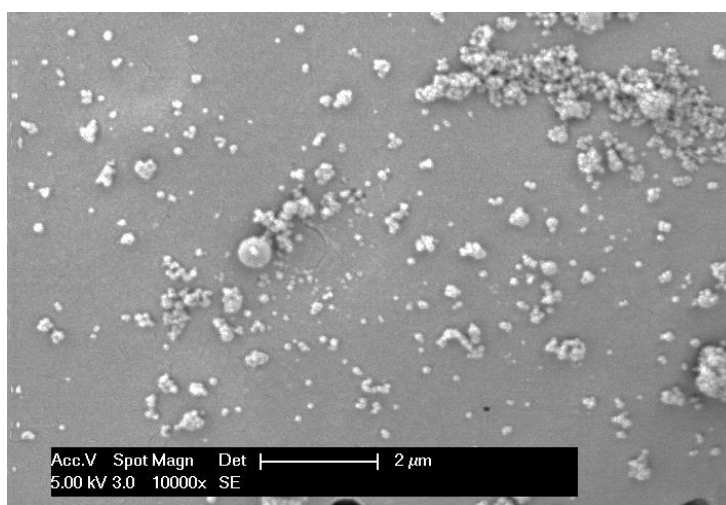


Figure 3.1: Scanning electron microscope image of the hydroxyapatite nanoparticles used for the present study.

3.3.1 *In vitro* Cell Assay

Murine macrophages (RAW 264.7, passage 13-16) were used for the present study as those cells have been shown to react *in vitro* to bisphosphonate exposure in a similar way than osteoclasts and to tolerate well the presence of HA-particles (Scheel, Weimans et al. 2009; Abe, Yoshimura et al. 2012).

An aqueous Zoledronate solution with a concentration of 2 mg/ml was prepared and sterile filtered. The drug solution was diluted with CCM to a final concentration of 80 μ M of Zoledronate. A dilution series with CCM resulted in Zoledronate supplemented medium (Zol-CCM) with concentrations from 80 μ M to 0.625

μM . The dilution procedure was repeated with an aqueous dispersion containing 2 mg/ml Zoledronate and 20 mg/ml nHA (nHA-Zol-CCM), and a dispersion containing only 20 mg/ml nHA (nHA-CCM).

Macrophages were seeded with a density of 2500 cells per well in 96-well plates (Microtest™ 96, Becton Dickinson Labware, NJ, USA) using 6 wells per group and incubated with 100 μl CCM at standard incubation conditions (37°C, 5% CO₂). After 24 h of incubation, 100 μl of CCM, Zol-CCM, nHA-Zol-CCM or nHA-CCM were added to the cells. The experimental groups of the three assays are listed in Table 3.1. A cell proliferation test (CellTiter 96® AQueous One Solution, Promega, Fitchburg, WI, USA) was performed after 24, 48 and 72 hours of cell exposure to the modified CCM. The absorbance was measured with a plate reader (Wallac 1420 Victor 2, Perkin Elmer, Waltham, MA, USA). Background plates with modified media only were measured at all time points to avoid a bias caused by nHA-particles in the dispersions. Untreated cells served as control for a normalization of the absorbance results.

Group	1	2	3	4	5	6	7	8	9	
Zoledronate - Assay	0.16	0.31	0.63	1.25	2.5	5	10	20	40	Zol-concentration [μM]
	-	-	-	-	-	-	-	-	-	nHA-concentration [$\mu\text{g/ml}$]
nHA-Zoledronate-Assay	0.16	0.31	0.63	1.25	2.5	5	10	20	40	Zol-concentration [μM]
	0.04	0.09	0.17	0.34	0.68	1.36	2.72	5.44	10.88	nHA-concentration [$\mu\text{g/ml}$]
nHA-Assay	-	-	-	-	-	-	-	-	-	Zol-concentration [μM]
	0.04	0.09	0.17	0.34	0.68	1.36	2.72	5.44	10.88	nHA-concentration [$\mu\text{g/ml}$]

Table 3.1: Experimental groups of the 3 cell assays: Zoledronate and nHA concentration in the CCM are given for each group, each assay was complemented with a control group that is not mentioned in the table.

3.3.2 Hydrogel Preparation

Commercially available cross-linked hyaluronic acid (Termira AuxiGel™, Stockholm, Sweden) was used as the drug delivery system for the BP. This gel has already been shown to be a suitable drug delivery system for bisphosphonates (chapter 2). The preparation of the hydrogel was done under sterile conditions in a laminar flow chapel. An aqueous solution containing 2 mg/ml Zoledronate was prepared and sterile filtered. nHA-particles were added to the solution with a nHA/Zoledronate ratio of 100:1. The exact drug dose was ensured by mixing precisely weighed and measured amounts of Zoledronate, nHA, and distilled water. Crosslinking of the hydrogel was achieved by mixing a hyaluronan derivative (component A) with a PVA cross-linker (component B). Five parts of the Zoledronate/nHA solution were mixed with 3 parts component A and 2 parts component B for the nHA-Zol-Gel-group. The Zoledronate-nHA dispersion was replaced by bi-distilled water with nHA for the nHA-Gel-group. The resulting gels were allowed to settle for 1 h before filling the capillary pistons of a positive displacement pipette (Microman®, Gilson, Middleton, USA) with 5 μl gel each. The capillaries were pulled off the pipette with the gel inside and left 1 h for settling. Then they were sterile packed in plastic tubes and frozen at -20°C.

3.3.3 Drug Release Study

The release of Zoledronate from hydrogel containing nHA-particles and pure hydrogel was assessed indirectly with a cell assay. Zoledronate-loaded hydrogel was prepared with and without nHA following the technique described in 4.2. The gels were incubated for 1 h in bi-distilled water at room temperature. The ratio of water and gel was 3:1 to reach a total concentration of 250 μg per 1 ml liquid/gel volume. For comparison, an aqueous Zoledronate solution with a concentration of 250 $\mu\text{l/l}$ was also prepared (Figure 3.2). The Zoledronate solution was sterile filtered and diluted in CCM to reach final concentrations of 10 μM , 5 μM , and 0.625 μM . The supernatant received from the hydrogel incubation was diluted similarly. RAW 264.7 cells were prepared as described in 4.1. After 24 h of incubation in CCM, 100 μl of the prepared media were added, the final concentrations of Zoledronate were therefore 5 μM , 2.5 μM and 0.3125 μM . A cell proliferation assay was performed after 24, 48 and 72 hours of incubation with Zoledronate.

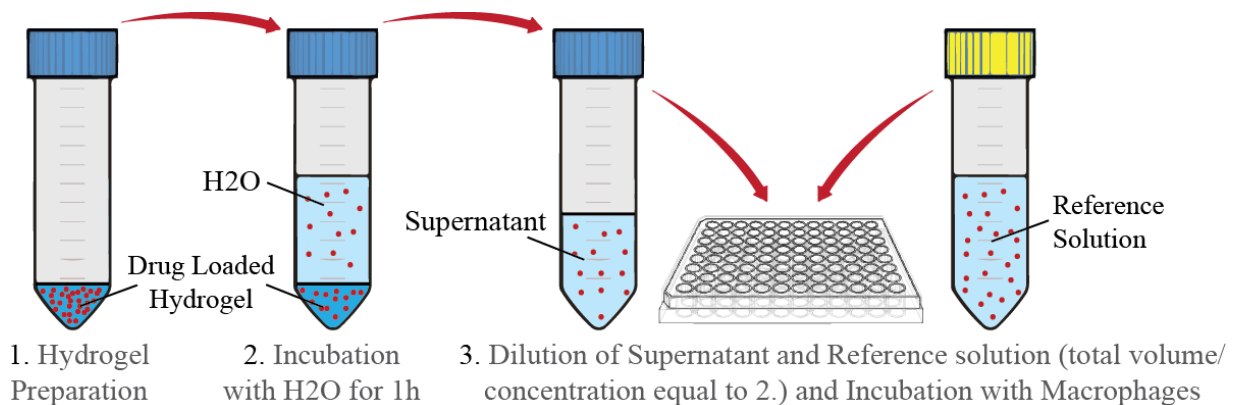


Figure 3.2: Preparation of the indirect release study using a RAW 264.7 macrophages cell assay. The drug-loaded hydrogel with and without nHA was incubated in H₂O during 1 h to investigate if a burst release of the drug occurs. Macrophages were later exposed to the supernatants of the hydrogels that were highly diluted with cell culture medium.

3.3.4 *In vivo* Study

An *in vivo* study in a rat femoral model of postmenopausal osteoporosis was performed following a protocol that was established and published earlier by our group (chapter 2). All animal procedures were approved by the local animal care and use committee (license no. 2508.1, EXPANIM, SCAV, Epalinges, Switzerland).

Surgical Procedures

Eight virgin female Wistar rats (Janvier Labs, Saint-Berthevin, France) were ovariectomized bilaterally with a dorsal approach (Alghamdi, Bosco et al. 2013) at an age of 17 weeks and a weight of 295 \pm 18 g to induce an estrogen deficiency related bone loss (Hogan, Ruhmann et al. 2000). The rats were housed 4 per cage under 12 h light to 12 h dark cycles at 22°C room temperature with 55% humidity. They were fed a standard rodent diet (KLIBA NAFAG 3436, Provimi Kliba AG, Switzerland) and tap water at libitum. After ovariectomy (OVX) of the rats, food intake was limited to 50 g per kg body weight per day. Sterilized hay,

paper tunnels and wooden sticks were offered as cage environment enrichment. Animals were fed in groups, therefore an equal nutrition of all animals was ensured by a close monitoring and regular weighing.

Miniature screws were implanted bilaterally into the femoral condyles of 22 weeks old rats with a mean weight of 350 ± 20 g. The screws with a thread length of 3 mm and a diameter of 1.4 mm were custom made from radiopaque polyetheretherketone (PEEK) (RISystem, Davos, Switzerland) and coated with a 100 nm titanium layer to mimic the interface with a standard orthopedic screw. Before screw insertion, the pre-drilled unicortical screw holes (diameter 1.2 mm, depth 3.5 mm) were filled with 5 μ l of the prepared hydrogel containing only nHA (nHA-Gel-group) or nHA and 5 μ g of Zoledronate (nHA-Zol-Gel-group) with a positive displacement pipette. Both legs of each animal were treated with the same hydrogel to avoid an unwanted drug effect on the contralateral side.

In vivo microCT Image and Image Processing

In vivo microCT scans (Skyscan 1076, Bruker microCT, Kontich, Belgium) of the right femur only were performed one day before OVX and one day before screw implantation in order to confirm the bone loss caused by the estrogen deficiency. Both femurs were then scanned at day 3, 10, 17, 31, 45, and 58 after screw implantation for the dynamic histomorphometry. The parameters for data acquisition and reconstruction were chosen according to our published protocol (chapter 2). The animals were kept under Isoflurane anesthesia during the scanning time to avoid motion artifacts. All rats were sacrificed at the time of the last microCT scan with Pentobarbital (Esconarkon, Streuli Pharma SA, Uznach) while being under anesthesia.

The image taken for the evaluation of the bone loss and for dynamic histomorphometry were processed and analyzed using the software Amira® (FEI Visualization Sciences Group, Burlington, USA) and CTan (Bruker microCT) as published earlier (chapter 2). Dynamic histomorphometry is an image processing technique based on a registration and comparison of consecutive microCT scans (Waarsing, Day et al. 2004; Roshan-Ghias, Lambers et al. 2011; Schulte, Lambers et al. 2011). Mineralized tissue volume that is present only on the first microCT scan is considered as being resorbed/degraded, whilst that present only on the second scan is considered as newly mineralized tissue/formed bone. For an analysis of the spatio-temporal effect, the static and dynamic bone parameters were analyzed in concentric 4 layers of 368 μ m each around the screw. This partition has been shown to furnish useful information of the peri-implant bone remodeling (chapter 2).

3.3.5 Histology

The rat femurs were dissected just after sacrifice at week 58 after screw implantation and fixed, dehydrated and embedded in PMMA following a protocol that we published elsewhere (chapter 2). After polymerization, the sections were cut, glued to PMMA slides and polished before etching their surface with 0.7 % formic acid (Applichem, Gatersleben, Germany) and staining them with Giemsa (VWR, Dietikon, Switzerland) or Toluidine Blue (Promega, Fitchburg, WI, USA). Microscopy images for evaluation were taken

using an upright microscope (DM 5500, Leica Microsystems, Wetzlar, Germany). The ground sections were finally X-rayed (Skyscan 1076, Bruker microCT) for a mapping of the tissue density.

3.3.6 Statistics

Statistical testing was done with Matlab (Mathworks, Natick MA, USA). The Mann-Whitney U-test was used to test for statistical differences in the cell culture results as normal distribution was not always given. The static and dynamic mineralized tissue parameters were tested for significance with a non-parametric Kruskal Wallis ANOVA followed by a Tukey's HSD (Honestly Significant Difference) test as normal distribution and equal variance were not given for all groups. Values lying outside an interval of 1.5 times the quartile range were identified as outliers and excluded.

3.4 Results

3.4.1 Cell Assay

A visual inspection of the RAW 264.7 murine macrophages via microscopy revealed that those cells are capable of incorporating large amounts of the nanoparticles that were used for the present study (Figure 3.3). This way, they were able to remove all particles in their direct surrounding.

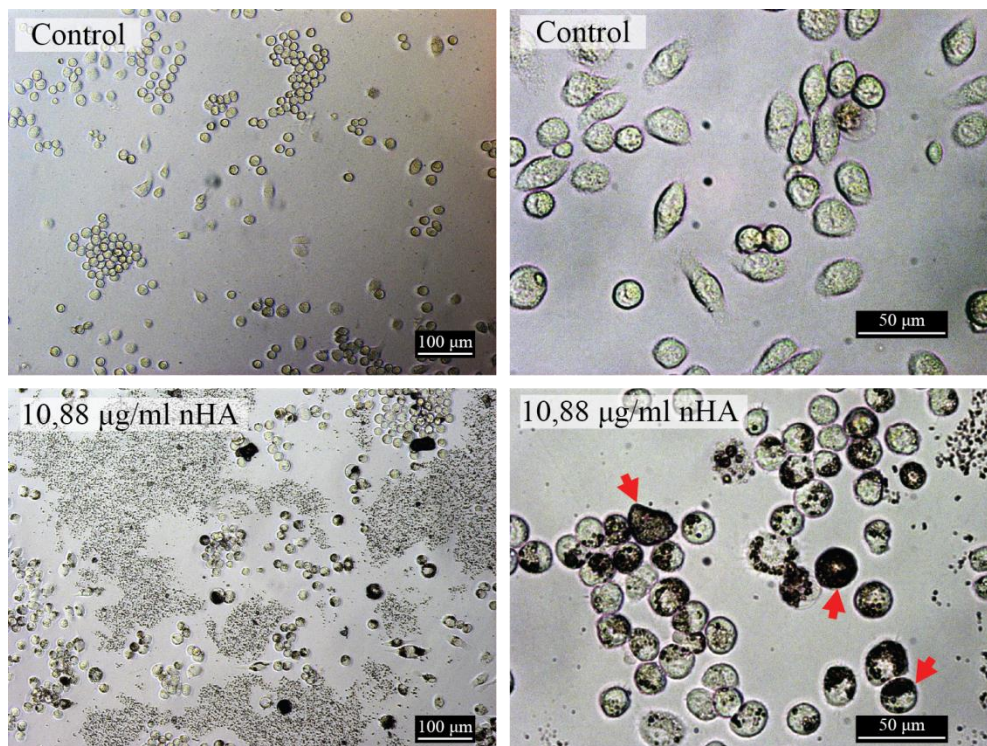


Figure 3.3: Light microscopy images of RAW 264.7 murine macrophages after 72 h of incubation with (bottom) and without (top) nHA, the macrophages are able to incorporate large amounts of particles (red arrows), this way they “clean up” all the particles in their direct surrounding (image bottom left).

When looking on the proliferation of the macrophages incubated with different concentrations of nHA-particles dispersed in the CCM, it could be seen that the HA is well tolerated by the cells as no significant drop of the proliferation can be detected at any time and concentration (Figure 3.4). This results is in good agreement with published data demonstrating that RAW 264.7 macrophages tolerate HA-particles with different sizes and shapes up to a concentration of 500 $\mu\text{g/ml}$ (Scheel, Weimans et al. 2009).

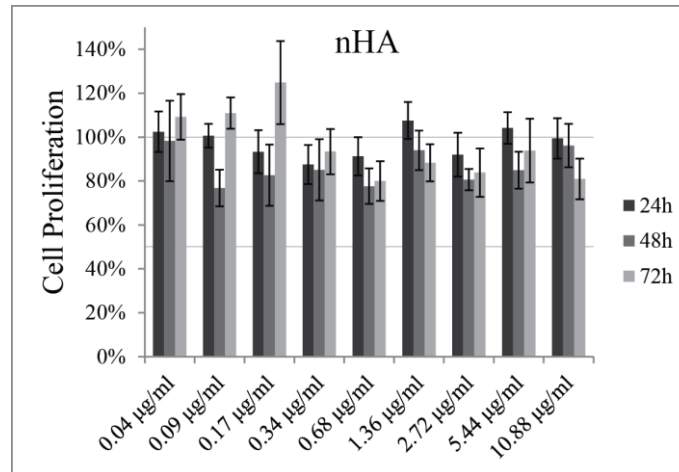


Figure 3.4: Proliferation study with RAW 264.7 macrophages incubated with various concentrations of nHA-particles in the cell culture medium. The proliferation was measured after 24, 48 and 72 hours. The results from the nHA treated cells are displayed normalized by the results from untreated cells that served as control.

When cultivated with different concentrations of Zoledronate, the RAW 264.7 macrophages showed a typical dose- and time- dependent proliferation decrease (Figure 3.5). This result confirms the findings of Abe et al. who showed earlier that nitrogen-containing bisphosphonates are cytotoxic for RAW 264.7 cells (Abe, Yoshimura et al. 2012).

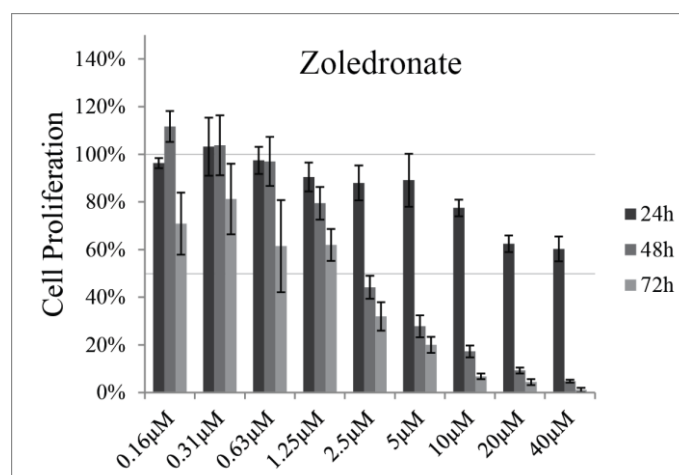


Figure 3.5: Proliferation study with RAW 264.7 macrophages incubated with various concentrations Zoledronate in the cell culture medium. The proliferation was measured after 24, 48 and 72 hours. The results from the nHA treated cells are displayed normalized by the results from untreated cells that served as control.

In a third cell assay, the RAW 264.7 macrophages were incubated with Zoledronate-loaded nHA-particles. Again, a dose- and time-dependent decrease in the cell proliferation was seen (Figure 3.6). Interestingly, this decrease occurred significantly faster than in the cells treated pure Zoledronate (Figure 3.5). This finding indicates that the inhibitory effect of the bisphosphonate on macrophages *in vitro* is significantly more efficient when the Zoledronate is administered bound to hydroxyapatite nanoparticles.

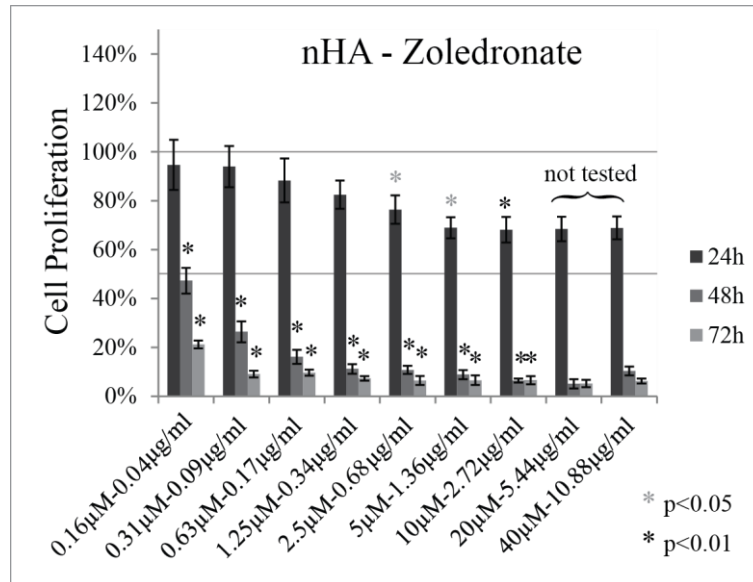


Figure 3.6: Proliferation study with RAW 264.7 macrophages incubated with various concentrations Zoledronate-loaded nHA-particles in the cell culture medium. The proliferation was measured after 24, 48 and 72 hours. The results from the Zoledronate-nHA treated cells are displayed normalized by the results achieved from untreated cells that served as control. Statistical significant differences to the cell assay with equal amounts of pure Zoledronate (Figure 3.5) are indicated. The two highest concentrations were not considered as the measured results did not correlate with the visual inspection of the cells (only dead cells visible after 48/72 h). The absorbance readings might have been biased by the presence of large quantities of nHA-particles.

3.4.2 Drug Release Study

The cell proliferation test with murine macrophages only allowed a functional estimation of the early passive release from the hyaluronic acid hydrogel. The drug concentration in the medium of the two release groups (Zol-Gel, nHA-Zol-Gel) was estimated by comparing their cell proliferation with the reference group (Zol) where a known Zoledronate concentration had been used. When comparing the Zol-Gel-group with the nHA-Zol-Gel group, we saw a clear difference between the cell proliferations (Figure 3.7). By comparing the curves, it could be estimated that the final concentration of Zoledronate in the CCM of the Zol-Gel-group must have been around 75% (50%-100%) of the maximum possible concentrations that would have been seen if the drug would not at all have been retained by the hydrogel (Zol-group). This result confirms the assumption that the highly porous hydrogel delivers the small Zoledronate molecules via a burst release. In contrary, the cells exposed to diluted nHA-Zol-Gel-supernatant did not show a significant difference to untreated cells at any time and any concentration. This result suggests that no significant amount of drug was released during the first hour of incubation in water. However, as the supernatant was filtered before adding it to the CCM, it can only be concluded that no Zoledronate was in

solution after 1 hour of incubation in H₂O. It is still possible that nHA-particles loaded with the drug have been released and were later on removed during the sterile filtering.

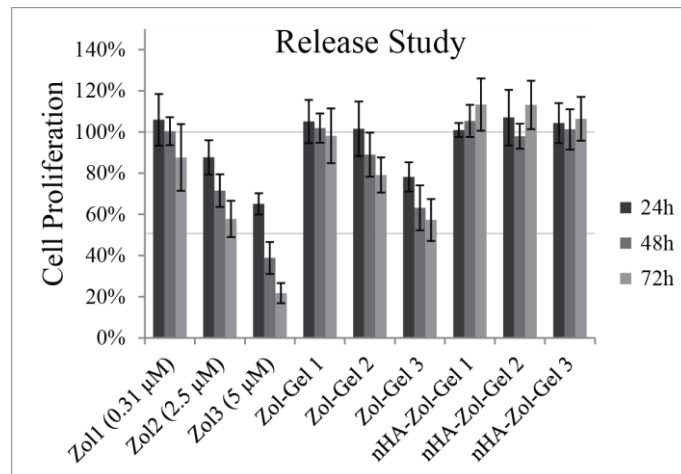


Figure 3.7: Results for the RAW 264.7 cell assay investigating the Zoledronate release from hydrogels during 1 h of incubation in water. RAW 264.7 cells were cultivated for 24-72 hours. The results from the Zoledronate-treated cells are displayed normalized by the results achieved from untreated cells that served as control. Zol1-3 marks the cells that were exposed to a known concentration of Zoledronate (in brackets). Zol-Gel 1-3 and nHA-Zol-Gel 1-3 mark cells that were exposed to the supernatant with unknown Zoledronate concentration received from the hydrogel incubation.

3.4.3 *In vivo* Study

All rats tolerated both surgeries well and returned to normal activity right after surgery. The limited food intake allowed a controlled weight gain of the animals; their final mean weight was 384 ± 24 g. Analysis of the bone parameters based on the microCT scans performed before and after ovariectomy confirmed a successful ovariectomy by showing a bone loss in all animals similar to the results found before in this model (chapter 2).

MicroCT-based Dynamic Histomorphometry

A total of 87 microCT scans were analyzed for the dynamic histomorphometry as 3 had to be excluded due to motion artefacts. One leg of one animal from the nHA-Zol-Gel-group showed an excessive bone formation that was identified as outlier and therefore excluded. Five to eight samples were left in each group after removal of the outliers. The rapidity of the appearance and the structure of the mineralizing tissue that became visible on the microCT scans suggested that not only be formed bone was involved (Figure 3.8). Histology confirmed later that the hydrogel-nHA composite mineralized *in vivo*. As it is not possible to distinguish on the microCT scans between bone and hydroxyapatite, we analyzed mineralization rate (MR) and demineralization rate (DR) instead of bone formation and bone resorption rates and mineralized tissue volume (MV) instead of bone volume (BV).

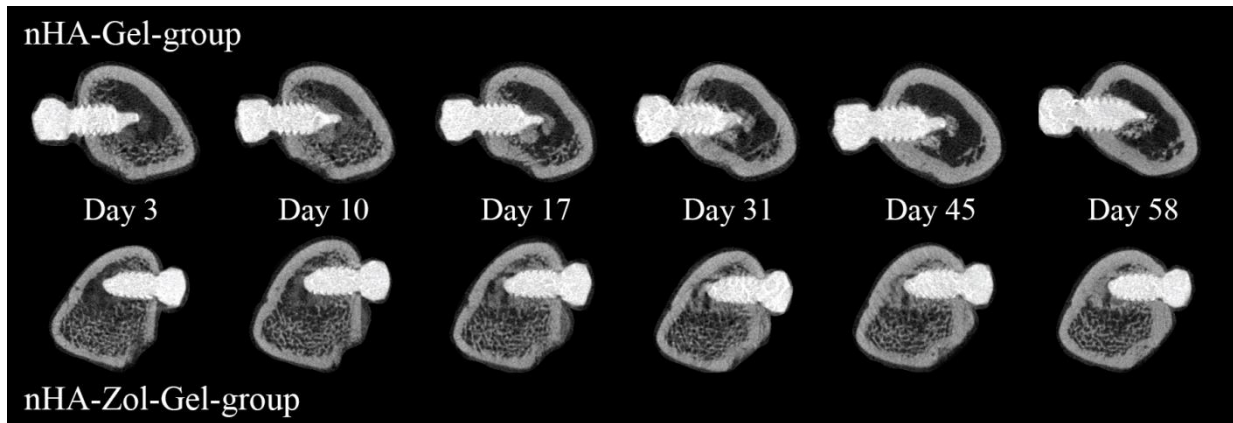


Figure 3.8: MicroCT scans taken at 6 time points after surgery from the nHA-Gel-group (top), and the nHA-Zol-Gel-group (bottom). The images show a rapid mineralization of the tissue around the screws in both groups that is resorbed and remodeled quickly in the nHA-Gel-group and persists in the nHA-Zol-Gel-group.

Static Parameters

Only one static parameter, mineralized tissue fraction (MV/TV) was analyzed for this study as all other typical bone parameters would be misleading when looking at mixture of bone and mineralizing biomaterial. The results from this study were compared to the BV/TV of animals that were treated with Zoledronate-loaded hydrogel and pure hydrogel obtained in a previous study (chapter 2). This comparison was used to investigate synergistic effects between locally delivered nHA and Zoledronate as well as between hyaluronic acid hydrogel and nHA. The MV/TV values were normalized to the first microCT scan (day 3 after screw implantation) to rule out a bias caused by the nHA that was visible already on the scan of day 3 in the nHA-Gel-group and the nHA-Zol-Gel-group. The analysis of the MV/TV in the layer next to the screw surface (0-368 μm) showed no difference at any time between the nHA-Zol-Gel-group and the group that released the drug from pure hydrogel (Zol-Gel-group) (Figure 3.9). In the second layer (368-736 μm) the MV/TV gain was around 50% higher in the nHA-Zol-Gel-group than in the Zol-Gel-group starting from day 17. A large standard deviation however prevented a statistical significance of the results. This difference diminished to around 30% in the third layer (736-1104 μm), a significant difference could again not be shown due to a high variability of the results. No difference at all was visible in the fourth layer (1104-1472 μm).

The results from the nHA-Gel-group were compared to the results of the Gel-group from the previous study (chapter 2). Close to the screw (0-368 μm), the nHA in the hydrogel caused a mineralized tissue fraction gain that was around 30% higher than in the Gel-group during the full experimental period. This difference was however not statistically significant. In the second layer (368-736 μm), the MV/TV doubled between day 3 and day 10, a development comparable to the Zoledronate-treated groups and significantly higher than in the Gel-group which showed a constant MV/TV. Later on, the difference between the two groups diminished and was only marginal at the end of the experimental period. A similar development was observed in the third layer, where the initial gain in MV/TV was only 50% and the difference between nHA-

Gel-group and Gel-group equaled out by day 17. No difference between nHA-Gel-group and the Gel-group was found in the outermost layer (1104-1472 μm).

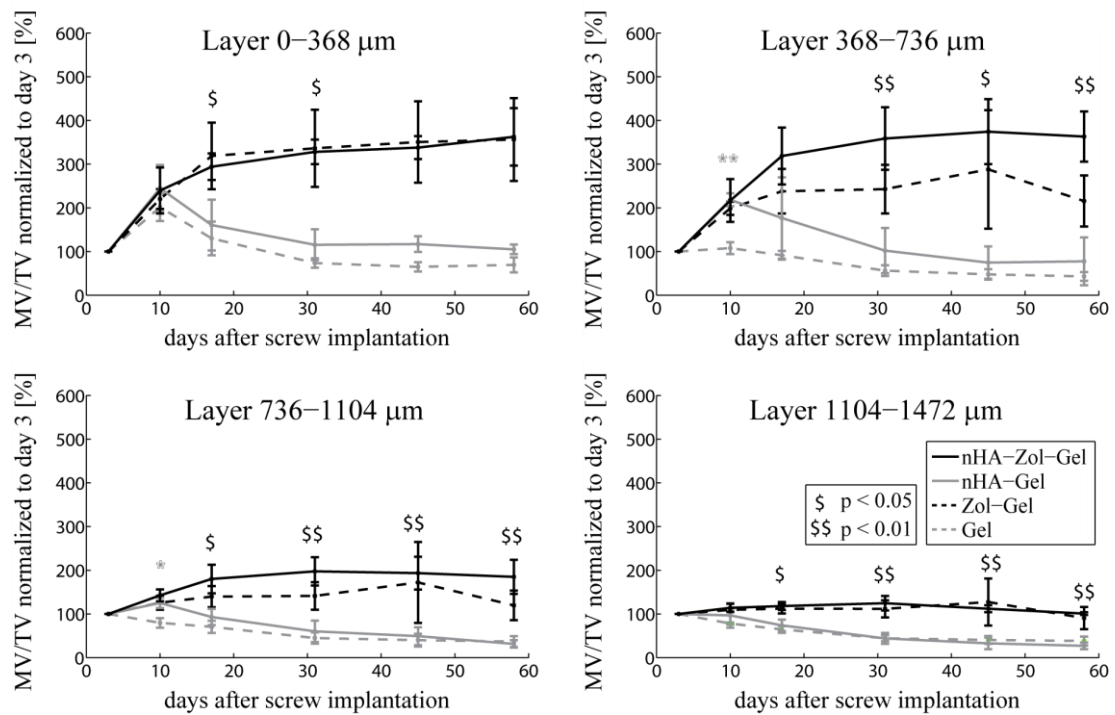


Figure 3.9: Mineralized volume/ tissue volume measured in 4 layers around the screw. The grey asterisks indicate the significant differences between nHA-Gel-group and Gel-group and the dollar signs indicate the significant differences between nHA-Zol-Gel-group and nHA-Gel-group. The data from the Zol-Gel-group and the Gel-group were acquired during an earlier study (chapter 2) and are shown for comparison.

Dynamic Parameters

The analysis of the dynamic parameters gives information about bone formation and resorption processes. In the case of the present study, it is not clear which part of the appearing mineralized structure was new bone and which part was mineralizing biomaterial, therefore we measured a general mineralization rate instead of a bone formation rate. The same applied for the bone resorption rate, which was named demineralization rate for this study and included bone resorption and biomaterial degradation. A 3D rendering of a comparison of two consecutive microCT scans (Figure 3.10) gave a good overview over the mineralizing and demineralizing processes. It could be seen that in both groups there was a significant mineralization around the screw between day 3 and day 10, which was followed by a pronounced demineralization in the nHA-Gel-group. The bone further away from the implantation site, however, was gradually resorbed. The nHA-Zol-Gel-group, on the contrary, showed only very little demineralization in the analyzed region. Those findings were also represented in the measured mineralization and demineralization rate (Figure 3.11 and 3.12).

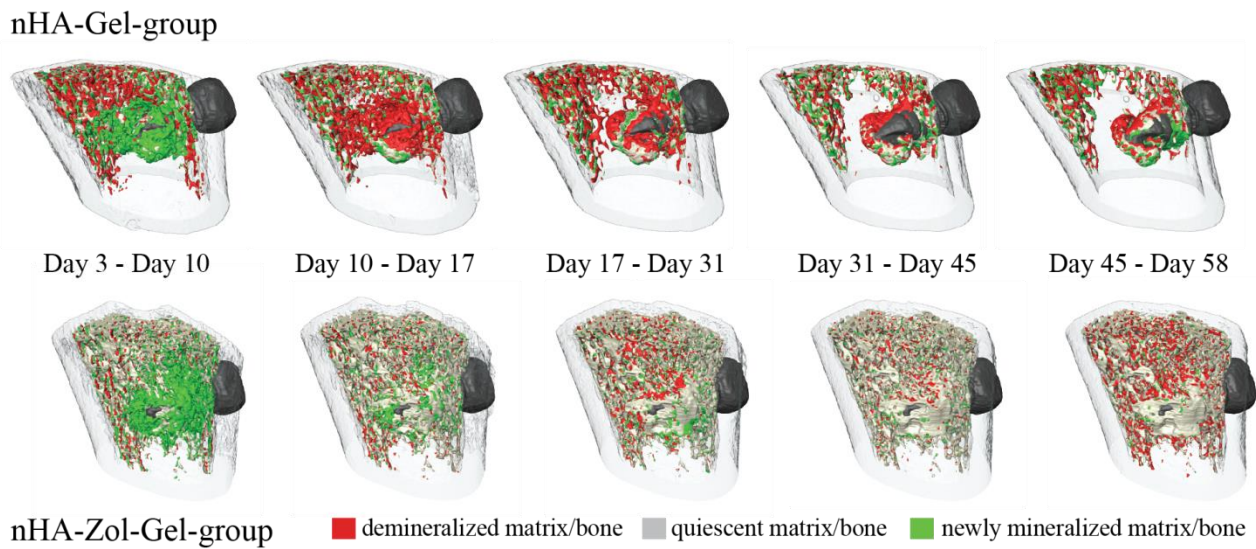


Figure 3.10: Volume rendering of comparisons of always two consecutive microCT scans of two representative samples, one from the nHA-Gel-group (top) and one from the Zol-Gel-group (bottom). The analyzed trabecular region of the bone is displayed in opaque, the screw in dark grey and the cortex in transparent.

No differences in the mineralization rate in direct contact with the screw (layer 0-368 μm) were found between the two groups from this study and the two groups without nHA from our previous study (Figure 3.11). In the second layer (368-736 μm), however, between day 3 and day 10 there was a highly significant difference between the nHA-Gel-group and the Gel-group and a small trend to a higher mineralization rate in the nHA-Zol-Gel-group compared to the group that released the drug directly from the hydrogel (Zol-Gel-group). Those differences equaled out by day 10. The same situation was present also in the outer two layers (736-1472 μm).

When looking at the bone resorption/demineralization rate, we observed the typical difference between the Zoledronate and the non-Zoledronate groups (Figure 3.12). The bone resorption/demineralization peak between days 10 and 31 that is characteristic for the drug-free groups was completely inhibited by the locally delivered Zoledronate. The demineralization rate of the nHA-Zol-Gel-group did not differ at any time and in any region from the one of the Zol-Gel-group. When comparing the nHA-Gel-group with the Gel-group, there was an unexpected trend to a higher demineralization rate in the nHA-group in the outer two layers (736-1472 μm).

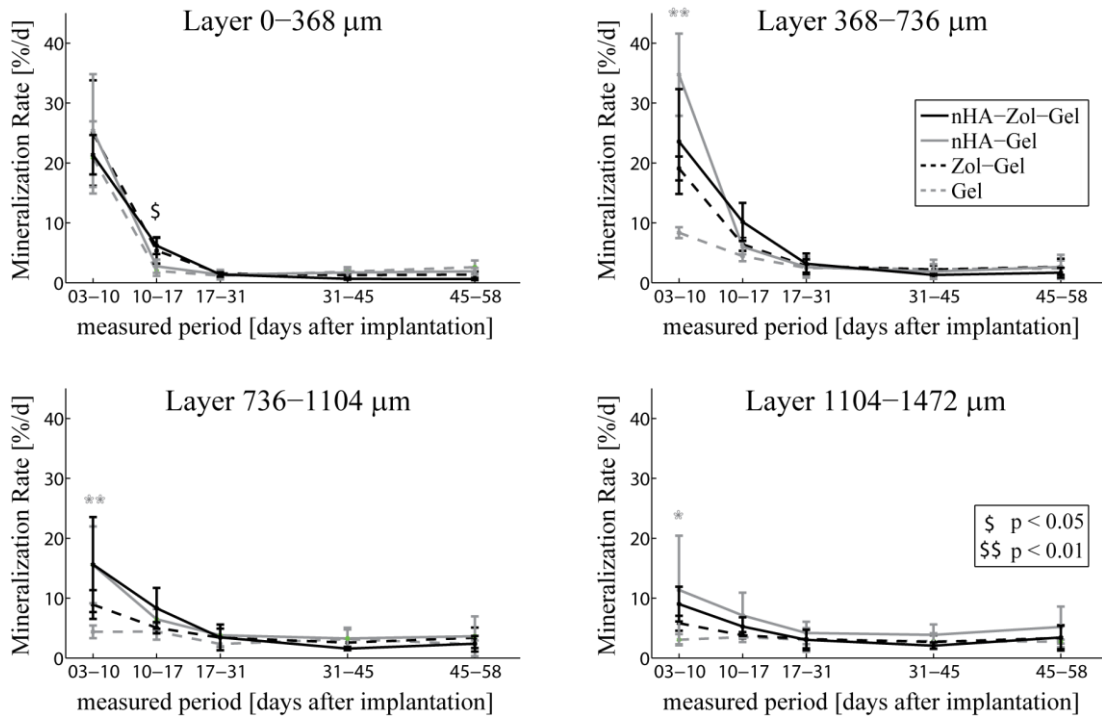


Figure 3.11: Mineralization rate including bone formation and biomaterial mineralization measured in 4 layers around the screw, the grey asterisks indicate the significant differences between nHA-Gel-group and Gel-group, and the dollar signs indicate the significant differences between nHA-Zol-Gel-group and nHA-Gel-group. The data from the Zol-Gel-group and the Gel group were acquired during an earlier study (chapter 2) and are shown only for comparison.

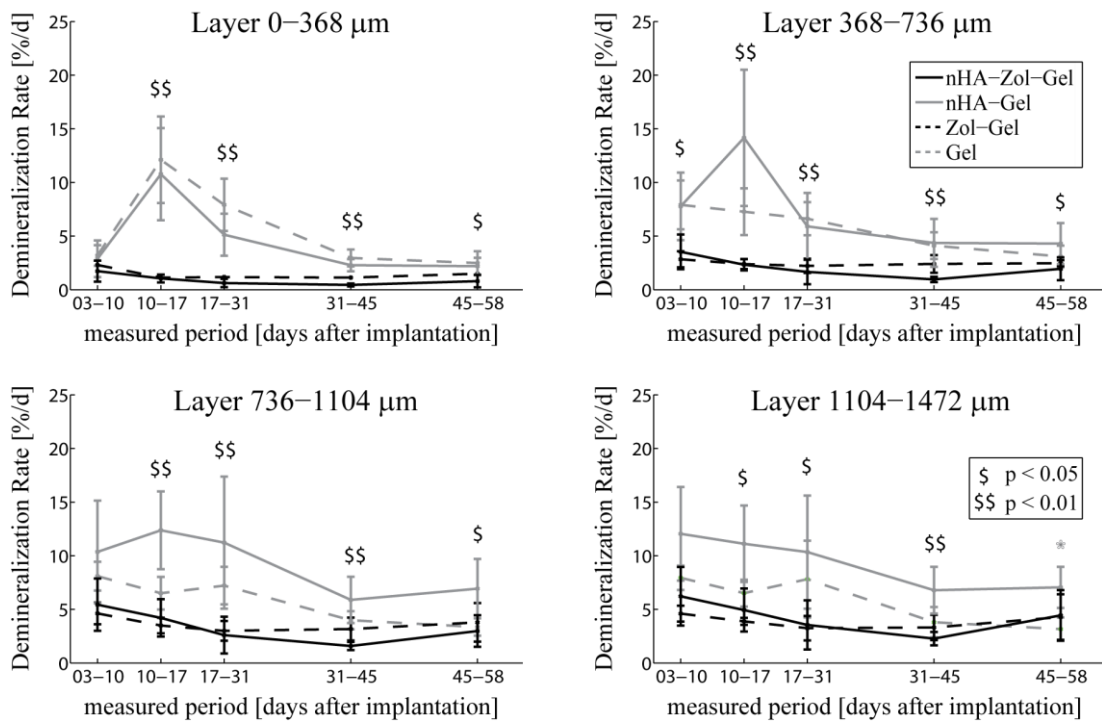


Figure 3.12: Demineralization rate including bone resorption and biomaterial degradation measured in 4 layers around the screw, the grey asterisks indicate the significant differences between nHA-Gel-group and Gel-group and the dollar signs indicate the significant differences between nHA-Zol-Gel-group and nHA-Gel-group. The data from the Zol-Gel-group and the Gel group were acquired during an earlier study (chapter 2) and are shown only for comparison.

3.4.4 Histology

The histological results confirmed the earlier finding that the used hyaluronic acid hydrogel is fully degraded after 58 days of implantation without leaving any visible residues (Figure 3.13 and 3.14). All screws showed a good osteointegration without any inflammation reaction or fibrotic tissue encapsulation. In both nHA-Gel- and nHA-Zol-Gel groups there were highly mineralized regions present within the bone. Those granule shaped spots had a diameter of up to 50 μm in the nHA-Gel-group and extended across wide areas in the nHA-Zol-Gel-group. The X-rays taken of the histology slides indicate that those granules can be denser than bone tissue. It can be excluded that those regions simply represent remaining nHA-particles as those particles have a diameter of less than 200 nm and the observed granules are much bigger.

In the nHA-Gel group, only small amounts of those mineralized spots were found in islands of new bone located mainly close to the screw tip, the region where the hydrogel cumulates during screw insertion. The granules were completely embedded in the bone matrix and the resulting constructs showed a trabecular structure. Large amounts of multinucleated cells such as macrophages and giant foreign body cells were present in the bone marrow around these bone-mineralization islands indicating an on-going resorption of the mineralized hydrogel. No new bone formation could be detected in this group beside a thin layer close to the screw surface and the bone close to the biomaterial. Almost no trabecular bone was left around the screw in the nHA-Gel group 13 weeks after OVX.

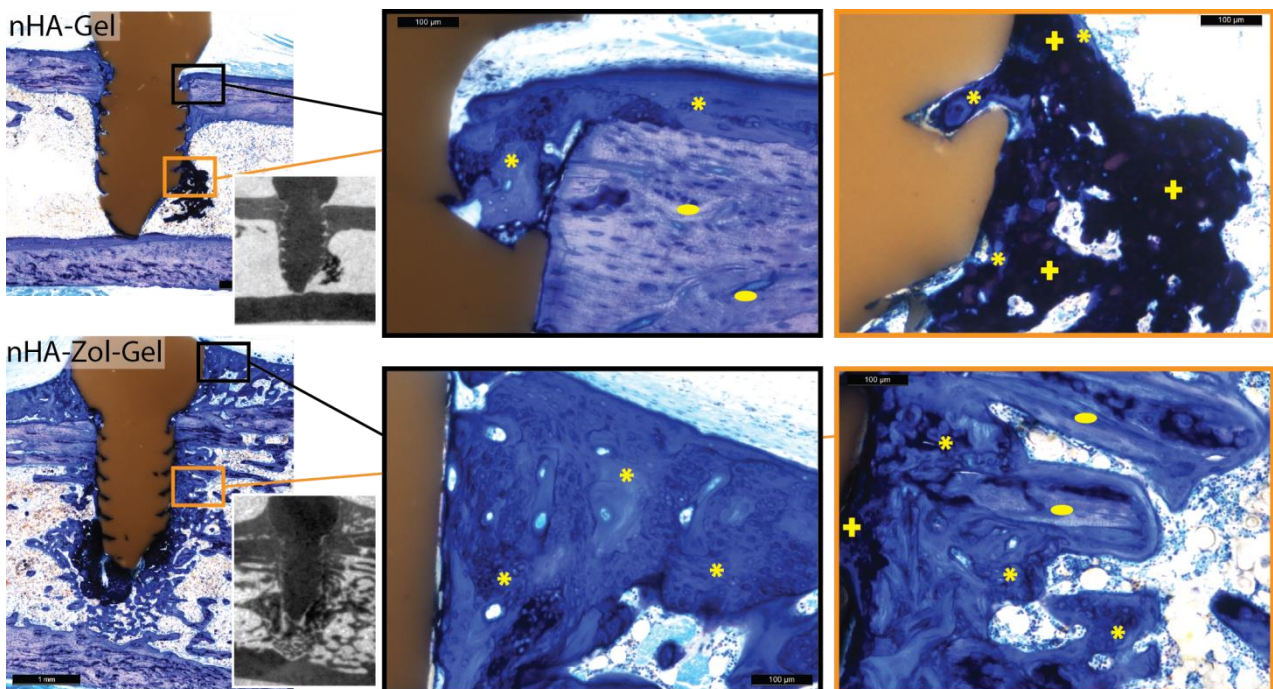


Figure 3.13: Toluidine blue stained ground sections from the nHA-Gel-group (top) and the nHA-Zol-Gel-group (bottom). The yellow asterisks in the darker blue regions indicate immature, non-remodeled bone, the yellow ellipses on brighter blue regions mark remaining old bone. Mineralized hydrogel residues are highlighted with yellow crosses. The small black-and-white panels are X-rays of the histology slides and show the mineralization of each region.

The nHA-Zol-Gel-group showed a completely different situation. Significantly larger mineralized regions were found mainly close to the screw tip but also between the threads. The remaining mineralized biomaterial had a porous structure and was partly penetrated by bone tissue. In contrast to what was seen in the nHA-Gel-group, the bone-mineralization constructs were rather compact and did not show a trabeculae-like structure. Smaller amounts of macrophages but no giant foreign body cells could be detected in the bone marrow close to the biomaterial, which confirms the inhibiting effect of Zoledronate. In general, much more trabecular bone could be found around the screw in the nHA-Zol-Gel-group compared to the nHA-Gel group. New bone formed next to and away from the screw surface and especially also at the interface to the mineralized hydrogel. A significant periosteal callus formation was also seen in the nHA-Zol-Gel-group that was not present to this extent in the nHA-Gel-group.

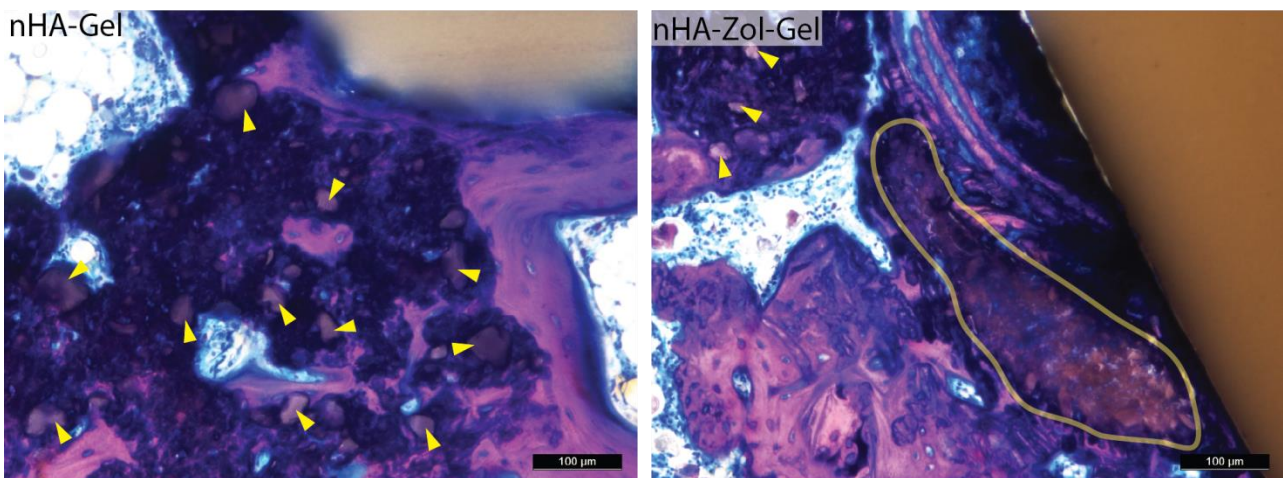


Figure 3.14: Details from the samples shown in Figure 3.13 stained with Giemsa for a better differentiation between bone (pink) and mineralized hydrogel (pink-brownish). In the left image, small granule-shaped mineralized spots from the nHA-Gel-group are marked with yellow arrows. In the right one, an extended mineralized region from the nHA-Zol-Gel group is marked with a yellow line; smaller regions are also highlighted with yellow arrows.

3.5 Discussion

The main goal of the present study was to investigate if a synergistic effect can be achieved by adding hydroxyapatite nanoparticles to Zoledronate-loaded hydrogel. Such an effect can be presumed based on studies that showed enhanced peri-implant bone density after application of HA-particles, an increase of Zoledronate potency in presence of Ca^+ ions and favorable bone ingrowth in bisphosphonate-linked hydrogel containing calcium phosphate particles (Monkkonen, Taskinen et al. 1994; Merrell, Wakchoure et al. 2007; Tami, Leitner et al. 2009; Nejadnik, Yang et al. 2014). The present study was based on a previous study showing that Zoledronate locally delivered from a hyaluronic acid hydrogel increases the early bone formation rate up to 100% while efficiently inhibiting peri-implant bone resorption (chapter 2).

Astonishingly, the main finding of this study was however not directly related to the anti-resorptive bisphosphonate Zoledronate. The *in vivo* study in a rat model of postmenopausal osteoporosis showed an unexpected rapid mineralization of the nHA-loaded hydrogel already between day 3 and 10 after

implantation, with and without the presence of Zoledronate. The drug showed its strong effect from day 17 and efficiently inhibited the resorption of present and newly formed bone as well as the degradation of the biomaterial.

The cell proliferation assay that was performed with murine RAW 264.7 macrophages showed a dose-dependent proliferation decrease for cells that were exposed to Zoledronate concentrations from 0.16 to 40 μM . This inhibitory effect was significantly enhanced by the presence of hydroxyapatite nanoparticles that were added to the solution with a nHA/Zoledronate ratio of 10:1. Due to the high affinity of Zoledronate to hydroxyapatite, it must be assumed that most of the drug was absorbed to the particles and therefore not present in solution (Nancollas, Tang et al. 2006). Light microscopy images showed that the macrophages incorporated the Zoledronate-loaded particles surrounding them. This finding suggests that the cells have taken up the drug together with the nHA-particles. Thompson et al. have shown that aminobisphosphonates are typically internalized by macrophages and osteoclasts via fluid-phase endocytosis (pinocytosis) *in vitro* (Thompson, Rogers et al. 2006). Particles however have been shown to be incorporated by macrophages via pinocytosis only for sizes smaller 500 nm, larger particles are phagocytized (Kruth, Jones et al. 2005; Oh and Park 2014). The particles used for this study have a size of less than 200 nm but form agglomerations, so that both mechanisms have to be considered. A stronger inhibitory effect on macrophages has also been described for bisphosphonate-modified gold nanoparticles (size <100 nm) compared to unbound bisphosphonate (Fanord, Fairbairn et al. 2011). One possible explanation for this phenomenon given in this publication is that a greater concentration of drug molecules is introduced in cells with the particles as carrier. This can also be the case in the present study. An alternative explanation could be an enhancement of the bisphosphonate potency by the presence of calcium, phenomenon that has been demonstrated before (Thompson, Rogers et al. 2006). The Ca^+ ions could originate from a dissolution of the hydroxyapatite in the macrophages (Bloebaum, Lundeen et al. 1998). In order to rule out a negative effect of the nHA powder itself on the macrophages, we also cultured them only with particles. The results show that the cells tolerated well the presence of the particles. This finding is in accordance with literature as other studies have shown the HA-particles with different sizes and shapes do not considerably impact the viability of RAW 264.7 macrophages up to a concentration of 500 $\mu\text{g}/\text{ml}$ (Scheel, Weimans et al. 2009).

Another cell culture experiment with RAW 264.7 macrophages was performed in the frame of this study to investigate the Zoledronate release from pure hydrogel compared to nHA-loaded hydrogel. This indirect assay, which can be considered as a functional assay, was sufficient to confirm the theory that the small Zoledronate molecules are released from the highly porous hydrogel with a burst release. The experiment also confirmed that the presence of the nHA completely changed the release profile. No drug was detectable in solution after 1 hour of incubation, which is supported by the finding of others that mineral-bound bisphosphonates are only released spontaneously in an acidic environment as it can be found for example in the resorption pit of an osteoclast (Rogers, Gordon et al. 2000).

An unexpected original finding of this study was the rapid *in vivo* mineralization of the hydrogel that happened independently from the bisphosphonate in both groups. It is known that calcium phosphate particles can act as nucleation sites in hydrogel matrices that promote a HA precipitation (Gkioni, Leeuwenburgh et al. 2010). This phenomenon has been investigated mainly *in vitro* with simulated body fluids (Chen, Meng et al. 2011). But we could not find any publications showing such a rapid mineralization *in vivo*. Nejadnik et al. just recently published a study investigating the use of pure and bisphosphonate-modified hyaluronic acid with calcium phosphate nanoparticles for bone repair (Nejadnik, Yang et al. 2014). Despite a mineral content of the gel in the same range (6 w/v% versus 10 w/v% in this study), they did not report a considerable mineralization of the hydrogels after 4 weeks of implantation in bony defects created in rat tibiae. However, newly formed bone was analyzed in their study only based on histology. Depending on the staining used, histology might not be the most appropriate technique to detect biomaterial mineralization.

The highly mineralized spots that were found in the present study showed mainly a granule-like structure with a particle size of up to 50 μm which supports the theory that they were formed by hydroxyapatite deposition starting from the nHA-particles as nucleation points. In the nHA-Zol-Gel-group, the granules seemed to have fused even to larger mineralized regions as shown with histology. A complete integration of the newly formed granules into the bone matrix without any signs of inflammation or foreign body reaction confirmed their excellent biocompatibility and osteoconductivity. When comparing the nHA-Gel-group of this study with the Gel-group of a former study that was treated with pure hydrogel (chapter 2), a significant difference in the early mineralization in the three outer analyzed layers (736-1472 μm) was observed. The difference diminished over time and stayed only as a trend in the inner two layers. The explanation for this phenomenon is an initial rapid mineralization of the biomaterial followed by its simultaneously occurring degradation and penetration by bone tissue as shown by structural changes on the time-lapsed microCT scans and the terminal histology results. Large amounts of macrophages and giant foreign body cells could be found in the nHA-Gel-group, which shows an efficient biodegradation of the hydroxyapatite. Similar findings have been published by Arts et al. (Arts, Verdonschot et al. 2006) who have demonstrated that HA nano-powder is integrated in newly formed bone and efficiently recruits macrophages and osteoblasts *in vivo*.

The obvious mineralization of the biomaterial complicated the evaluation of the drug effect on peri-implant bone. The *in vivo* microCT imaging does not allow a differentiation between newly formed woven bone and mineralized hydrogel. When comparing the mineralized tissue volume fraction and the mineralization rate of the nHA-Zol-Gel-group to the Zol-Gel-group of an earlier study (chapter 2) no significant differences can be detected at any time. However, there is a strong trend to more tissue mineralization in the two central layers of the analyzed region (368-736 μm) that appears early and remains during the whole study time. Contributors to this gain of mineralized tissue could be on one side the new woven bone formation and on the other side the biomaterial mineralization. In our earlier study, we stated that the discovered boost in early peri-implant bone formation was caused by an initial “flush” of all bone cells with bisphosphonate

(chapter 2). With the presented release study, we were able to show that this flush does not occur when nHA is included in the hydrogel matrix as the Zoledronate is absorbed to the particles. We did not investigate the release of particles from the gel as it is highly dependent on the shape, swelling state and surrounding tissue of the hydrogel and therefore difficult to mimic *in vitro*. However, it can be assumed that the release of the comparatively huge nHA-particles is significantly slower than the release of the small drug molecules. Orriss et al. showed *in vitro* that bisphosphonates bound to mineral are significantly less effective to osteoblasts compared to unbound bisphosphonate (Orriss, Key et al. 2009). As the non-phagocytic osteoblasts are unlikely to incorporate Zoledronate-loaded particles, less influence on bone formation can be assumed for the nHA-Zol-Gel-group compared to the situation when Zoledronate is delivered from pure hydrogel. This theory is also supported by findings of Arslan et al. who could not find a significant influence of Alendronate soaked HA granules on bone formation compared to saline soaked HA in a OVX mandibular defect model (Arslan, Altundal et al. 2011). Nevertheless, small, but still significant differences could be also shown for the mineralization rate between the nHA-Gel-group and the nHA-Zol-Gel-group. From day 7 to 10 there was a higher mineralization rate seen in the nHA-Gel-group and from day 31-58 in the nHA-Zol-Gel-group. The combination Zoledronate-nHA must then influence bone formation and/or biomaterial mineralization in a different way than pure nHA, the mechanism is however not clear.

When looking at the demineralization rate, the strong inhibitory effect of Zoledronate becomes obvious in the highly significant differences between the nHA-Gel-group and the nHA-Zol-Gel-group. The microCT study and histology revealed that the drug did not only inhibit bone resorption but also biomaterial degradation as can be seen by the absence of macrophages and giant foreign body cells and much larger amounts of mineralized material remaining in the nHA-Zol-Gel-group. Histology also shows that the bone/biomaterial-construct in the nHA-Gel-group had already been remodeled to a trabecular structure whereas it is still rather compact in the nHA-Zol-Gel-group. Surprisingly, there is no difference in demineralization rate between the Zol-Gel-group from the former study and the nHA-Zol-Gel-group from the present study even very distant from the screw (1104-1472 μm) where the bone is very unlikely to be in contact with the hydrogel. Therefore there must be either a release of the drug-loaded particles or a release of the drug alone as it can be caused by the resorptive activity of osteoclasts or macrophages (Coxon, Thompson et al. 2006). The present study unfortunately could not give any answer to the question by which means and how far the drug-loaded particles move in the bone environment *in vivo*.

MicroCT-based histomorphometry was chosen for the present study as we found it to be a very suitable technique for the long-term three-dimensional analysis of peri-implant bone remodeling (chapter 2). The unexpected rapid mineralization found in the present study however interfered with the bone analysis as the microCT scans do not allow a differentiation between bone and mineralizing biomaterial which is an inherent limitation of this study. This differentiation can only be done by means of histology which was scheduled for this study only at the end of the experimental period of 8 weeks. Future studies should therefore include more groups of animals so that histology can be already performed at earlier time points for an observation of synergies between bone formation and biomaterial mineralization. More experiments

are also needed for an understanding of the exact mineralization process and the composition and mechanical competence of the resulting mineral. The *in vivo* mineralization seems to be dependent on size, shape and material of the particles as well as on type, density and degradation profile of the hydrogel as similar studies with comparable materials did not report an *in vivo* mineralization (Nageeb, Nouh et al. 2012; Martínez-Álvarez, González-Meli et al. 2013; Heo, Ko et al. 2014; Nejadnik, Yang et al. 2014). An investigation of the mechanical properties of the resulting material as it could be done by nano-indentation will be key when it comes to evaluate the stability of implants.

The hydrogels containing pure or Zoledronate-loaded nHA-particles are both easy to apply to bone due to their soft consistency, which makes them ideal for an application to irregular shaped cavities like an implant bed or difficult to access bone defects. Both materials have also been shown to mineralize rapidly *in vivo* and to form a kind of osteoconductive mineral scaffold. This biodegradable scaffold is later on penetrated by bone cells and included in newly forming bone. But the indications for both materials still should not be the same. The nHA-loaded hydrogel induced some new bone formation within the biomaterial in the present study but was not able to stabilize the bone loss situation present in the OVX rats (chapter 2). Therefore a large amount of the material was already degraded during the experimental period and could not contribute to an improved implant fixation. The nHA-loaded hydrogel therefore could have more potential in the repair and sealing of bony defects in healthy bone. The hydrogel with nHA and Zoledronate however could be favorable for the repair of bone defects that require at the same time a preservation of the surrounding bone matrix. Attention has to be paid in this case to the drug dose and the density of the resulting mineralized spots. As the Zoledronate has a “protective” effect for the biomaterial and inhibits its degradation, there is a risk that the penetration by the bone tissue can become impossible if the biomaterial becomes too dense and cannot be resorbed.

Despite the synergistic effects between hydroxyapatite nanoparticles and Zoledronate that we were able to show *in vitro*, it was not possible to answer the question if the use of a nHA-Zoledronate-hydrogel is further improving implant fixation compared to a hydrogel loaded only with Zoledronate. There was a non-significant increase of the mineralized tissue volume fraction in an extended range around the implant, but large amounts of biomaterial residues with unknown mechanical properties require mechanical testing before drawing a final conclusion. For the moment we can only conclude that both tested materials seem to be good candidates for bone repair in different specific clinical situations.

3.6 Conclusion

The present study was able to show a synergistic effects between Zoledronate and nHA-particles *in vitro* as the inhibitory effect of the drug on macrophages was enhanced when administering Zoledronate absorbed on hydroxyapatite nanoparticles. Furthermore it could be demonstrated that nano-sized hydroxyapatite also can serve as nucleation points in hyaluronic acid hydrogel *in vivo* in a rat model of postmenopausal osteoporosis. The material is then rapidly mineralizing under formation of micrometer-sized granules.

Those highly mineralized spots have been shown to be highly biocompatible, biodegradable and to serve as scaffolds for new bone formation. The biomaterial mineralization also occurred when Zoledronate was absorbed to the nanoparticles before integrating them into the hydrogel. In this case, however, the forming granules were protected from degradation by the anti-resorptive effect of the bisphosphonate resulting in larger mineralized regions compared to drug free nHA-hydrogel. At the same time, Zoledronate was still released from the biomaterial and inhibited efficiently the resorption of peri-implant bone to a similar extent that pure hydrogel loaded with only the drug. It was however not possible to determine a synergistic effect of the nHA-Zoledronate combination on bone formation *in vivo*, as the microCT-based dynamic histomorphometry that was chosen to monitor the bone remodeling *in vivo*, did not allow a differentiation between bone formation and biomaterial mineralization.

3.7 Acknowledgements

Special thanks to Sandra Jaccoud at the LBO for her assistance during surgeries and cell culture experiments as well as for the preparation of the histology slides. Special thanks also to Eric Thein from CHUV for his assistance during surgeries and to Dr. Salim Darwiche, Dr. Karina Klein and Prof. Brigitte von Rechenberg for the interpretation of the histology slides. This study was partially supported by a KTI grant (Project no. 11098.1).

3.8 References

- Abe, K., Y. Yoshimura, et al. (2012). "Effects of bisphosphonates on osteoclastogenesis in RAW264.7 cells." International Journal of Molecular Medicine **29**(6): 1007-1015.
- Alghamdi, H. S., R. Bosco, et al. (2013). "Osteogenicity of titanium implants coated with calcium phosphate or collagen type-I in osteoporotic rats." Biomaterials **34**(15): 3747-3757.
- Arslan, A., H. Altundal, et al. (2011). "Comparison of the effects of local application of hydroxyapatite graft soaked with alendronate solution and pure hydroxyapatite graft in the mandible of ovariectomized rats." Biotechnology and Biotechnological Equipment **25**(3): 2513-2518.
- Arts, J. J. C., N. Verdonschot, et al. (2006). "The use of a bioresorbable nano-crystalline hydroxyapatite paste in acetabular bone impaction grafting." Biomaterials **27**(7): 1110-1118.
- Bloebaum, R. D., G. A. Lundeen, et al. (1998). "Dissolution of particulate hydroxyapatite in a macrophage organelle model." Journal of Biomedical Materials Research **40**(1): 104-114.
- Boanini, E., P. Torricelli, et al. (2012). "The effect of zoledronate-hydroxyapatite nanocomposites on osteoclasts and osteoblast-like cells in vitro." Biomaterials **33**(2): 722-730.
- Chen, X., Y. Meng, et al. (2011). "A biomimetic material with a high bio-responsibility for bone reconstruction and tissue engineering." Journal of Biomaterials Science, Polymer Edition **22**(1-3): 153-163.
- Coxon, F. P., K. Thompson, et al. (2006). "Recent advances in understanding the mechanism of action of bisphosphonates." Curr Opin Pharmacol **6**(3): 307-312.
- Fanord, F., K. Fairbairn, et al. (2011). "Bisphosphonate-modified gold nanoparticles: A useful vehicle to study the treatment of osteonecrosis of the femoral head." Nanotechnology **22**(3).
- Faucheux, C., E. Verron, et al. (2009). "Controlled release of bisphosphonate from a calcium phosphate biomaterial inhibits osteoclastic resorption in vitro." J Biomed Mater Res A **89**(1): 46-56.
- Gkioni, K., S. C. G. Leeuwenburgh, et al. (2010). "Mineralization of hydrogels for bone regeneration." Tissue Engineering - Part B: Reviews **16**(6): 577-585.
- Heo, D. N., W. K. Ko, et al. (2014). "Enhanced bone regeneration with a gold nanoparticle-hydrogel complex." Journal of Materials Chemistry B **2**(11): 1584-1593.
- Hogan, H. A., S. P. Ruhmann, et al. (2000). "The mechanical properties of cancellous bone in the proximal tibia of ovariectomized rats." Journal of Bone and Mineral Research **15**(2): 284-292.
- Kruth, H. S., N. L. Jones, et al. (2005). "Macropinocytosis is the endocytic pathway that mediates macrophage foam cell formation with native low density lipoprotein." Journal of Biological Chemistry **280**(3): 2352-2360.
- LeGeros, R. Z. (2008). "Calcium phosphate-based osteoinductive materials." Chemical Reviews **108**(11): 4742-4753.
- Lobo-Escolar, A., E. Joven, et al. (2010). "Predictive factors for cutting-out in femoral intramedullary nailing." Injury **41**(12): 1312-1316.
- Martínez-Álvarez, C., B. González-Meli, et al. (2013). "Injection and adhesion palatoplasty: a preliminary study in a canine model." Journal of Surgical Research **183**(2): 654-662.
- Merrell, M. A., S. Wakchoure, et al. (2007). "Differential effects of Ca²⁺ on bisphosphonate-induced growth inhibition in breast cancer and mesothelioma cells." European Journal of Pharmacology **559**(1): 21-31.
- Monkkonen, J., M. Taskinen, et al. (1994). "Growth inhibition of macrophage-like and other cell types by liposome-encapsulated, calcium-bound, and free bisphosphonates in vitro." Journal of Drug Targeting **2**(4): 299-308.
- Nageeb, M., S. R. Nouh, et al. (2012). "Bone engineering by biomimetic injectable hydrogel." Molecular Crystals and Liquid Crystals **555**: 177-188.
- Nancollas, G. H., R. Tang, et al. (2006). "Novel insights into actions of bisphosphonates on bone: differences in interactions with hydroxyapatite." Bone **38**(5): 617-627.
- Nejadnik, M. R., X. Yang, et al. (2014). "Self-healing hybrid nanocomposites consisting of bisphosphonated hyaluronan and calcium phosphate nanoparticles." Biomaterials **35**(25): 6918-6929.
- Oh, N. and J. H. Park (2014). "Endocytosis and exocytosis of nanoparticles in mammalian cells." International Journal of Nanomedicine **9**(SUPPL.1): 51-63.
- Ong, H. T., J. S. C. Loo, et al. (2008). "Exploiting the high-affinity phosphonate-hydroxyapatite nanoparticle interaction for delivery of radiation and drugs." Journal of Nanoparticle Research **10**(1): 141-150.
- Orriss, I. R., M. L. Key, et al. (2009). "Inhibition of osteoblast function in vitro by aminobisphosphonates." J Cell Biochem **106**(1): 109-118.
- Palazzo, B., M. Iafisco, et al. (2007). "Biomimetic hydroxyapatite-drug nanocrystals as potential bone substitutes with antitumor drug delivery properties." Advanced Functional Materials **17**(13): 2180-2188.
- Peter, B., O. Gauthier, et al. (2006). "Local delivery of bisphosphonate from coated orthopedic implants increases implants mechanical stability in osteoporotic rats." J Biomed Mater Res A **76**(1): 133-143.

- Rogers, M. J., S. Gordon, et al. (2000). "Cellular and molecular mechanisms of action of bisphosphonates." Cancer **88**(12 Suppl): 2961-2978.
- Roshan-Ghias, A., F. M. Lambers, et al. (2011). "In vivo loading increases mechanical properties of scaffold by affecting bone formation and bone resorption rates." Bone **49**(6): 1357-1364.
- Scheel, J., S. Weimans, et al. (2009). "Exposure of the murine RAW 264.7 macrophage cell line to hydroxyapatite dispersions of various composition and morphology: Assessment of cytotoxicity, activation and stress response." Toxicology In Vitro **23**(3): 531-538.
- Schulte, F. A., F. M. Lambers, et al. (2011). "In vivo micro-computed tomography allows direct three-dimensional quantification of both bone formation and bone resorption parameters using time-lapsed imaging." Bone **48**(3): 433-442.
- Sörensen, T. C., J. Arnoldi, et al. (2013). "Locally enhanced early bone formation of zoledronic acid incorporated into a bone cement plug in vivo." Journal of Pharmacy and Pharmacology **65**(2): 201-212.
- Stromsoe, K., W. L. Kok, et al. (1993). "Holding power of the 4.5 mm AO/ASIF cortex screw in cortical bone in relation to bone mineral." Injury **24**(10): 656-659.
- Suratwala, S. J., S. K. Cho, et al. (2008). "Enhancement of periprosthetic bone quality with topical hydroxyapatite-bisphosphonate composite." J Bone Joint Surg Am **90**(10): 2189-2196.
- Tami, A. E., M. M. Leitner, et al. (2009). "Hydroxyapatite particles maintain peri-implant bone mantle during osseointegration in osteoporotic bone." Bone **45**(6): 1117-1124.
- Thompson, K., M. J. Rogers, et al. (2006). "Cytosolic entry of bisphosphonate drugs requires acidification of vesicles after fluid-phase endocytosis." Molecular Pharmacology **69**(5): 1624-1632.
- Waarsing, J. H., J. S. Day, et al. (2004). "Detecting and tracking local changes in the tibiae of individual rats: A novel method to analyse longitudinal in vivo micro-CT data." Bone **34**(1): 163-169.
- Wang, L., M. Zhang, et al. (2006). "The first pamidronate containing polymer and copolymer." Chemical Communications(26): 2795-2797.
- Wilmes, B., C. Rademacher, et al. (2006). "Parameters affecting primary stability of orthodontic mini-implants." Journal of Orofacial Orthopedics **67**(3): 162-174.
- Wirth, A. J., J. Goldhahn, et al. (2011). "Implant stability is affected by local bone microstructural quality." Bone **49**(3): 473-478.
- Yoshinari, M., Y. Oda, et al. (2002). "Bone response to calcium phosphate-coated and bisphosphonate-immobilized titanium implants." Biomaterials **23**(14): 2879-2885.
- Zhou, H. and J. Lee (2011). "Nanoscale hydroxyapatite particles for bone tissue engineering." Acta Biomater **7**(7): 2769-2781.

Chapter 4 Evaluation of Implant Fixation with Micro-Finite-Element Analysis

*Paper 3 Time Course of Bone Screw Fixation Following a Local
Delivery of Zoledronate in a Rat Femoral Model
– A Micro-Finite Element Analysis*

(modified version submitted to Journal of Mechanical Behavior of Biomedical Materials)

4.1 Abstract

A good fixation of osteosynthesis implants is crucial for a successful bone healing but often difficult to achieve in osteoporotic patients. One possible solution to this issue is the local delivery of bisphosphonates in direct proximity to the implants, a technique that has been shown to significantly improve implant anchorage. One critical aspect of this method, that has not yet been well investigated, is the time course of the implant fixation following the drug release. Usual destructive mechanical tests would have required large numbers of animals for this kind of investigation, therefore a micro-finite element (microFE) approach was chosen for the analysis of implant fixation in the present study. *In vivo* micro computed tomography (microCT) scans were performed first weekly and later bi-weekly after implantation of polymeric screws in the femoral condyles of 6 ovariectomized rats. In half of the animals, Zoledronate was released from a hydrogel matrix directly in the peri-implant bone stock, the other half of animals received only the screws and served as control. The time course of the implant fixation was investigated with linear elastic microFE models that were created based on the *in vivo* microCT scans. The numerical models were validated against experimental pullout-tests measurements in an additional cadaver study. The microFE analysis revealed a significant difference in force at yield between the Zoledronate treated group and the control group, which was 28% after 17 days of screw implantation, 42% after 31 days, and persisted until the end of the *in vivo* study at day 58 ($p < 0.01$). These results indicate the great potential of Zoledronate-loaded hydrogel for an enhancement of osteosynthesis implant fixation in impaired bone as they show that the implant anchorage improves fast and over a prolonged time.

Keywords: Drug delivery; hydrogel; bisphosphonate; screw fixation, microCT, microFE

4.2 Introduction

The success of orthopedic implants is highly depending on their anchorage in surrounding bone. A good implant fixation requires a good structural integration between bone and implant surface (osteointegration) as well as a strong bone structure around the implant that can resist the loads that are transferred from the implant to the bone (Schiuma, Plecko et al. 2013). Many successful strategies have been developed to improve the implant osteointegration such as surface topography changing treatments, osteoconductive coatings or surface functionalization with biological molecules (Jäger, Zilkens et al. 2007; Zhang, Myers et al. 2014). An improvement of the second aspect, the peri-implant bone quality, is however much more difficult to achieve. Due to the demographic changes in our population, more and more people suffer from age-related diseases impairing the bone structure such as osteoporosis (Hernlund, Svedbom et al. 2013). Affected patients have a significantly increased fracture risk and fracture treatment is challenging in their cases as osteosynthesis implants are difficult to anchor in the deteriorated bone structure (Cummings and Melton 2002; Broderick, Bruce-Brand et al. 2013). High complication rates, which are typical for osteoporotic fracture treatments, show the need for new strategies to enhance implant fixation in low quality bone. One of the most promising approaches that came up during the last years is the local delivery of anti-resorptive drugs such as bisphosphonates in the peri-implant bone. Several studies have shown that this strategy can locally enhance the bone density and therefore increase the mechanical stability of implants in animals and humans (Peter, Gauthier et al. 2006; Gao, Luo et al. 2009; Andersson, Agholme et al. 2010; Abtahi, Tengvall et al. 2012). The increase in implant fixation was measured in most of the published studies with terminal ex vivo mechanical tests such as pullout, pushout test or torque testing. As each destructive mechanical test requires the sacrifice of a group of animals, typically not more than 1 or 2 time points were investigated (Skoglund, Holmertz et al. 2004; Peter, Gauthier et al. 2006; Andersson, Agholme et al. 2010; Qi, Hu et al. 2012). Consequently, only little is known about the time course of the bisphosphonate effect on implant fixation. The temporal effect, however, is a very important aspect regarding the fact that osteosynthesis implants are placed to stabilize bone fractures. A good fracture reposition and stabilization are crucial for a successful fracture healing (Augat, Simon et al. 2005). Therefore, the onset of the positive bisphosphonate effect on screw fixation should ideally occur as soon as possible after implantation and persist until the fracture has completely healed. This aspect has so far not been targeted by any of the published studies.

One very promising approach to monitor implant fixation *in vivo* is a technique introduced by Wirth et al. that combines microCT imaging with a micro-finite element (microFE) analysis for the investigation of the stability of bone-implant constructs (Wirth, Mueller et al. 2010). This group demonstrated an excellent correlation between microFE predicted pullout strength and measured pullout strength in a cadaveric ovine vertebra model. Stadelmann et al. applied this technique for the first time to time-lapsed microCT scans from an *in vivo* rat model and obtained equally good correlations (Stadelmann, Conway et al. 2013). The use of *in vivo* microCT data for the microFE offers the unique possibility to closely monitor implant stability with a significantly reduced number of animals. In addition, important parameters affecting the implant

fixation can be identified easily as the mechanical information gained with the microFE can be directly linked with bone parameters measured on the microCT scans (Wirth, Goldhahn et al. 2011).

The microFE analysis was used in the present study for the first time to investigate the temporal effect of a locally delivered bisphosphonate (Zoledronate in the present study) on the fixation of miniature screws in a rat femoral model of postmenopausal osteoporosis. The goal of this analysis was to determine if the local bisphosphonate delivery can achieve the fast and durable enhancement of implant fixation that is needed for osteosynthesis implants in osteoporotic bone.

4.3 Materials and Methods

The *in vivo* microCT data that provided the basis for the microFE models were obtained from an animal study published earlier by our group (chapter 2). Since the miniature polymer screws used in the *in vivo* study were not suitable for biomechanical pullout tests, we performed a complementary cadaver study with titanium screws on similar bone specimens and screw geometry but different screw material. This cadaver study provided the data to identify a suitable failure criterion for the microFE models.

4.3.1 *In vivo* MicroCT Study

The animal experiments were approved by the local animal care and use committee (license no. 2508.1, EXPANIM, SCAV, Epalinges, Switzerland). Briefly, in this study, eight ovariectomized rats were implanted with radiopaque polyetheretherketone screws in both femoral condyles. In the 4 animals of a first group (Zol-Gel-group), the pre-drilled screw holes (diameter 1.2 mm, depth 3.5 mm) were filled with 5 μ l of a commercially available hyaluronic acid hydrogel (Termira AuxiGel™, Stockholm, Sweden) containing 1 μ g/ml of Zoledronate (Art.-Nr. ALX-430-153-0000, Enzo Life Sciences, Farmingdale, USA). The 4 rats of the second group (Control-group) received only screws. Both femurs of all animals were scanned with a special *in vivo* microCT for small rodents (Skyscan 1076, Bruker microCT, Kontich, Belgium) at day 3, 10, 17, 31, 45, and 58 after screw implantation. The used scanning parameters were published earlier (chapter 2). Hydroxyapatite-polymer phantoms with known bone mineral density served as references for the microCT calibration. Not all samples of this study could be used for the microFE study as some screw heads were broken. The final analyzed samples size in Zol-Gel-group was $n = 6$ for the first 4 measured time points, $n = 3$ for the 5th time point and $n = 4$ for the last time point. The sample size in the Control-group was $n = 6$ for all time points, therefore a total of 67 microCT scans were analyzed. All animals were sacrificed at the time of the last microCT scan.

4.3.2 Experimental Pullout Test

Six adult female Sprague Dawley rat cadavers with a mean weight of 310 ± 30 g were retrieved from another animal study (license no. 2567.a), EXPANIM, SCAV, Epalinges, Switzerland). The rats were lactating for 7 days at the time of sacrifice and therefore presented a significantly reduced bone density compared to normal animals (Miller and Bowman 1998). The 12 femurs of the animals were dissected directly after

sacrifice and kept frozen in saline until use. After thawing, holes with a length of 3.2 mm were drilled unicortically in the femoral condyles with a motorized dentist's drill (DEC 100, Nobelcare, Sweden). Custom-made aluminum screws (thread length 3 mm, diameter 1.4 mm) with a 20 mm long rod attached to them instead of a screw head were inserted manually in the pre-drilled holes (Figure 4.1, left). Aluminum was chosen as screw material because this material has sufficient mechanical competence for the mechanical testing, while being artifact-free in the microCT. The inappropriate biocompatibility of aluminum however makes its *in vivo* use impossible.

The implanted specimens were wrapped in saline soaked gauze to keep them moist during the imaging and microCT scans were performed. The scanning parameters, adapted to the aluminum screws, were the following: spatial resolution 18.4 μm , 0.5 mm aluminum filter, voltage 60 kV, current 167 μA , exposure time 480 ms, rotation step 0.4°, frame averaging 2.

After the scanning, the specimens were positioned in acrylic glass rings (inner diameter 8 mm) with a guiding device that centered the screw in the ring before fixing them with dental cement (Technovit® 3040 powder, Heraeus Kulzer, Hanau, Germany) (Figure 4.1, middle). This fixation technique was chosen in order to mimic the boundary conditions that were later used for the microFE study.

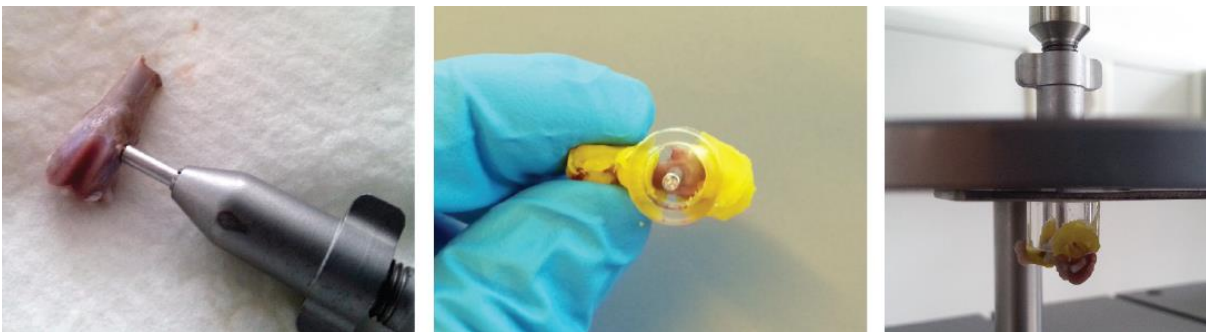


Figure 4.1: Preparation of the rat femurs for the pullout test. Left: implantation of special aluminum screws in the femoral condyles. Middle: fixation of the specimen in acrylic glass rings with dental cement. Left: pullout tests were performed with a tensile testing machine.

The pullout test was performed with a tensile testing machine (ElectroPuls E3000, Instron, High Wycombe, England). The sample in the acrylic glass ring was placed under a plate with a 8 mm-hole that was fixed to the base of the machine. The rod as prolongation of the screw was passed through the hole and fixed in a special gripper that was attached to the head of the tensile testing machine (Figure 4.1, right). The head was moved up with a speed of 1 mm/min. Force and displacement were recorded with a frequency of 50 Hz after a pre-load of 0.5 N was reached. Stiffness, force at yield, and force at pullout were determined for each sample from the resulting force-displacement curves. All calculations for this study have been done with Matlab (Mathworks, Natick, USA).

4.3.3 Image Processing

The image processing process was identical for the *in vivo* study and the cadaver study, only the segmentation thresholds had to be adapted to the different screw materials and scanning parameters. The reconstruction of the projection images was done with NRecon and GPURecon Server (Bruker microCT) following a protocol that was published earlier (chapter 2). Image processing after reconstruction was done with CTan (Bruker microCT) and Amira® (FEI Visualization Sciences Group, Burlington, USA).

The first step of the image processing was a reduction of the dataset size for an easier handling of the datasets. A VOI including the full diameter of the femur from 5 mm distal to 5 mm proximal to the screw was manually defined on all scans using CTan. The background and the patella were then removed with an automated algorithm. The pre-processed datasets were loaded in Amira® for a further processing with a custom written script. A 6 mm high reference dataset was created with the screw in the center and concentric regions measuring 3, 4, 5, 6, 7 and 8 mm in diameter around. All datasets were registered on the reference dataset, ensuring an equal alignment and positioning of all screws for the microFE analysis (Figure 4.2). In a next step, the datasets were transformed to the new position and resampled by a factor of 3 using the standard interpolation mode of Amira®. The new voxel size after resampling was 55.2 μm . The reduction of the dataset size was necessary to make the image stacks compatible with Abaqus (Simulia, Velizy Villacoublay Cedex, France) for the microFE analysis, as this software can run only a limited number of elements. A noise reduction median filter was applied after transformation and resampling to smooth the resulting images. In a next step, the images were segmented by assigning different grey values to screw, background, bone, and bone marrow in each region allowing a separate analysis of bone and microFE results in different distances from the screw (Figure 4.2). The bone volume fraction (BV/TV) including both cortical and cancellous bone was analyzed in the inner region with a diameter of 3 mm on the processed microCT scans.

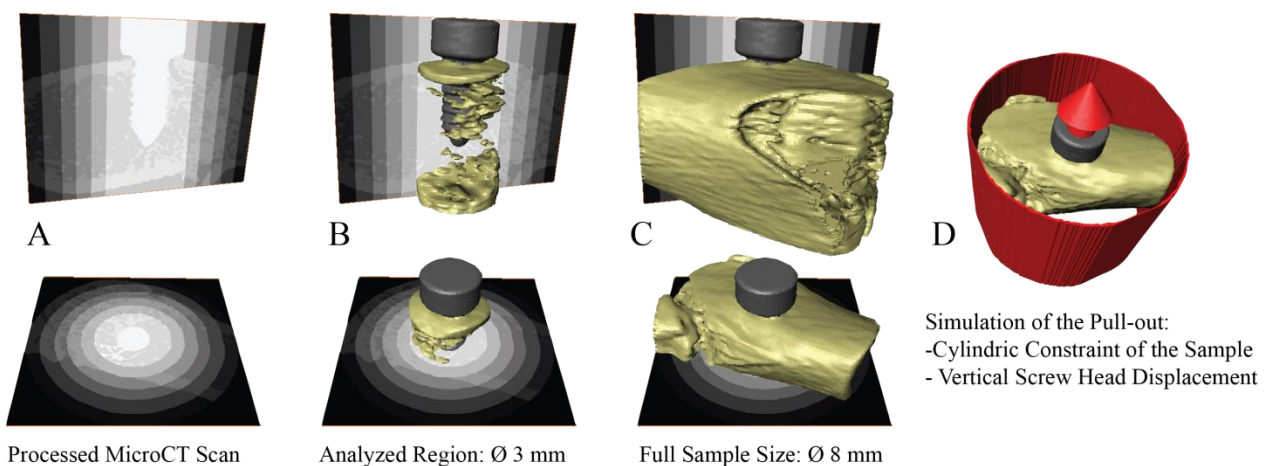


Figure 4.2: Image processing; processed microCT scan with centered screw and different grey values for concentric rings with diameters from 3 to 8 mm (A). bone within the 3 mm ring used for determining the bone volume fraction and the critical strain fraction (B) and full sample size with a diameter of 8 mm (C). MicroFE model of the pullout test (D): the sample was constrained in a ring with 8 mm diameter, the screw head was displaced vertically along the screw axis.

4.3.4 MicroFE Analysis

Creation of MicroFE Models

After image processing, linear elastic microFE models for all microCT scans from the *in vivo* and the cadaver study were created by converting image voxels to linear isotropic hexahedral finite elements (Muller and Ruegsegger 1995). A cube of the same size as a microCT stack was created in the commercially available simulation software Abaqus (Simulia). The cube was meshed with hexahedral elements whereas the edge length of one element in the model was equal to the edge length of one voxel in the pre-processed microCT datasets (55.2 μm). An in-house Matlab (Mathworks, Natick, USA) script was used to assign mechanical properties to the elements according on the grey values in the microCT datasets. Different properties were assigned to bone ($E = 6.8 \text{ GPa}$, $\nu = 0.3$) (Stadelmann, Conway et al. 2013), bone marrow ($E = 0.05 \text{ MPa}$, $\nu = 0.3$) (Perren 1979), the titanium screws of the *in vivo* study ($E = 110 \text{ GPa}$, $\nu = 0.32$) and the aluminum screws of the cadaver study ($E = 70 \text{ GPa}$, $\nu = 0.35$) (Stadelmann, Conway et al. 2013). No difference was made between the properties of cancellous and cortical bone as published before (Kabel, Van Rietbergen et al. 1999). Elements surrounding the bone, which were identified as background during image processing, were removed from the model. The nodes of bone elements located at the intersection with a virtual 8 mm ring around the screw were fully constrained according to the sample fixation during the experimental pullout test (Figure 4.2). A displacement of 0.1 mm along the screw axis was applied to the top surface of the screw head in order to simulate the pullout test. The microFE simulations were performed on a cluster (Castor, EPFL, Switzerland) consisting of 50 nodes with 16 CPUs and 64 GB user memory each. We analyzed the reaction force on the screw head associated to the displacement, the resulting bone stiffness and the corresponding octahedral shear strain (γ_{oct}) in the bone. Post-processing was done with an in-house python script.

Identification of the Failure Criteria

The failure criteria for the microFE models of the present study were identified based on the experimental results of the cadaver study. Therefore, the experimentally measured forces at yield and pullout were compared with the microFE predicted reaction force at different strain states. Bone failure was assumed to occur when a certain bone volume fraction within a predefined VOI exceeded a critical strain level. Instead of using an effective strain criterion as it has been done in other studies (Pistoia, Van Rietbergen et al. 2002; Wirth, Mueller et al. 2010; Stadelmann, Conway et al. 2013), we have chosen an octahedral shear strain criterion as it has been shown to be a good predictor for the spatial distribution of micro-damage within trabecular bone (Nagaraja, Couse et al. 2005).

For the determination of the best failure criteria for the forces at yield and pullout, we analyzed the microFE predicted reaction force at the points where a certain volume fraction of the bone within our pre-defined ROI (highly strained bone volume fraction) passed a certain level of γ_{oct} . To identify the best linear correlation, we analyzed combinations of 3 VOIS (diameter 3 mm, 4 mm, and 5 mm, height constant at 6

mm), 3 levels of γ_{oct} (0.5, 0.7, 1.0%) and 6 highly strained bone volume fractions (from 5 to 30 %). The analyzed strain range was chosen based on values found in the literature (Carter, Caler et al. 1981; Morgan 2009). The combination that provided the highest coefficient of determination (R^2) and the lowest p-value was chosen as critical strain level and critical highly strained bone volume fraction for a prediction of the force at yield and at pullout in the *in vivo* study.

The experimentally measured stiffness from the cadaver study was compared to the microFE predicted stiffness to test for a linear correlation and to determine a scaling factor as microFE is known to significantly overestimate the bone-implant stiffness (Wirth, Mueller et al. 2010).

Analysis of the *In vivo* Data

After identification of the failure criteria and the correlations, the microFE models created from *in vivo* microCT scans were used to predict the force at yield and pullout as well as the bone-implant stiffness for all specimens at the 6 analyzed time points. Furthermore, all possible correlations between BV/TV, stiffness, force at yield and force at pullout were examined for both the cadaver and the *in vivo* study. Finally, BV/TV from the cadaveric study was compared with the initial BV/TV of the *in vivo* Control-group to test the comparability between the results.

4.3.5 Statistical Analysis

The statistics analysis was done with Matlab. Significant differences between the two groups were assumed for a p-value smaller than 0.05 and tested with a Wilcoxon rank sum test as not all results were normally distributed.

4.4 Results

4.4.1 Experimental Pullout Test

Nine specimens were analyzed in total, 3 had to be excluded due to an atypical force-displacement curve without detectable yield that suggested that the screws were loose already at the beginning of the test. The average force at yield was 15.4 ± 2.4 N (from 11.1 N to 20.1 N), the average force at pullout was 21.6 ± 4.0 N (from 13.0 N to 29.5 N), and the average bone-implant stiffness was 107.6 ± 25.7 N/mm (from 59.2 N/mm to 150.1 N/mm). A close inspection of the screws after pullout did not show any damage to the screw threads.

4.4.2 Identification of the Failure Criteria for the MicroFE Models

Nine microFE models were created, one for each experimentally analyzed cadaveric femur. All of them run successfully. The meshing took in average 4 min, the resulting number of elements ranged between 680'000 and 980'000. The degrees of freedom in the models ranged from 2.1 to 3.1 million, the simulation time needed was around 6 hours for each sample. The coefficients of determination (R^2) and p-values of all

analyzed combinations of VOI, highly strained bone volume fraction and γ_{oct} can be found in Table 4.1 for the force at yield and in Table 4.2 for the force at pullout.

Force at yield		Highly strained bone volume fraction											
	γ_{oct} level	5%		10%		15%		20%		25%		30%	
		R ²	p	R ²	p	R ²	p	R ²	p	R ²	p	R ²	p
VOI Ø 3 mm	0.5%	0.576	0.0178	0.574	0.0181	0.594		0.643	0.0151	<i>0.726</i>	<i>0.0036</i>	<i>0.751</i>	<i>0.0025</i>
	0.7%	0.567	0.0192	0.576	0.0178	0.597		0.645	0.0147	<i>0.733</i>	<i>0.0032</i>	-	-
	1%	0.571	0.0184	0.580	0.0172	-	-	-	-	-	-	-	-
VOI Ø 4 mm	0.5%	0.541	0.0238	0.540	0.0241	0.561		0.590	0.0156	0.583	0.0166	-	-
	0.7%	0.539	0.0244	0.541	0.0238	0.561		-	-	-	-	-	-
	1%	0.541	0.0239	0.544	0.0233	-	-	-	-	-	-	-	-
VOI Ø 5 mm	0.5%	0.430	0.0222	0.563	0.0199	0.573		0.548	0.0226	-	-	-	-
	0.7%	0.553	0.0217	0.563	0.0199	0.575		-	-	-	-	-	-
	1%	0.556	0.0211	-	-	-	-	-	-	-	-	-	-

Table 4.1: Coefficients of determination (R^2) and p-values for the linear correlation between the measured and predicted force at yield for different octahedral shear strain levels and different highly strained bone volume fractions measured in 3 VOIs. Empty cells mark combinations where the strain levels were not reached in the specified bone volume fraction (italic values: $p < 0.01$).

Force at pullout		Highly strained bone volume fraction											
	γ_{oct} level	5%		10%		15%		20%		25%		30%	
		R ²	p	R ²	p	R ²	p	R ²	p	R ²	p	R ²	p
VOI Ø 3 mm	0.5%	0.423	0.0580	0.423	0.0580	0.448	0.0487	0.502	0.0326	0.592	0.0154	<i>0.651</i>	<i>0.0086</i>
	0.7%	0.413	0.0622	0.425	0.0572	0.450	0.0480	0.505	0.0320	0.605	0.0136	-	-
	1%	0.417	0.0601	0.427	0.0561	-	-	-	-	-	-	-	-
VOI Ø 4 mm	0.5%	0.409	0.0636	0.416	0.0609	0.448	0.0485	0.500	0.0332	0.526	0.0270	-	-
	0.7%	0.405	0.0654	0.417	0.0603	0.449	0.0482	-	-	-	-	-	-
	1%	0.406	0.0647	0.419	0.0594	-	-	-	-	-	-	-	-
VOI Ø 5 mm	0.5%	0.430	0.0553	0.459	0.0450	0.501	0.0337	0.507	0.0315	-	-	-	-
	0.7%	0.433	0.0540	0.458	0.0451	0.501	0.0328	-	-	-	-	-	-
	1%	0.436	0.0528	-	-	-	-	-	-	-	-	-	-

Table 4.2: Coefficients of determination (R^2) and p-values for the linear correlation between the measured and predicted force at pullout for different octahedral shear strain levels and different highly strained bone volume fractions measured in 3 volumes of interest. Empty cells mark combinations where the strain levels were not reached in the specified bone volume fractions (italic values: $p < 0.01$).

For both force at pullout and force at yield, the best correlations between numerical predictions and experimental measurements were obtained for a highly strained bone volume fraction of 30% at an octahedral shear strain level of 0.5% measured within a cylindrical VOI with a diameter of 3 mm. This finding is in agreement with a linear correlation between experimental force at yield and experimental force at pullout ($R^2 = 0.887$, $p = 0.0002$). The correlation between measured and predicted force at yield was better ($R^2 = 0.751$ / $p = 0.0025$) than between measured and predicted force at pullout ($R^2 = 0.651$ / $p = 0.0086$). Both predicted forces were overestimated by the numerical model by a factor of 6.4 and 10.5.

Therefore, the predicted forces for the *in vivo* study were corrected based on the identified correlations (Figure 4.3).

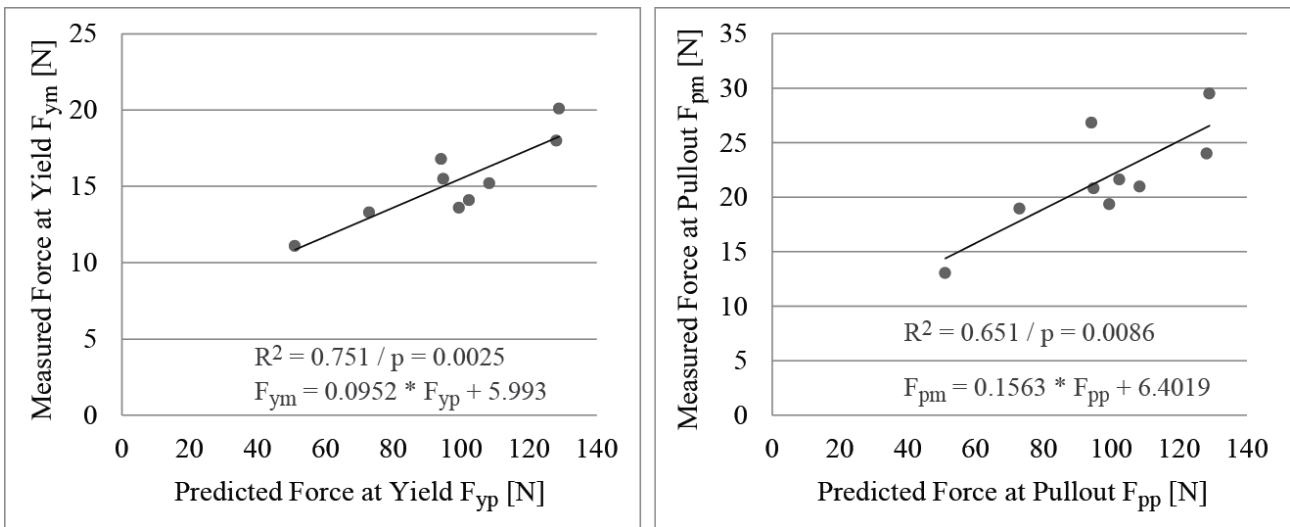


Figure 4.3: Correlation between measured and predicted force at yield (left) and measured and predicted force at pullout (right); the experimental and numerical results were obtained from the rat cadaver study.

A significant but weaker linear correlation was obtained for the measured and predicted bone-implant stiffness ($R^2 = 0.524$, $p = 0.0275$) (Figure 4.4). The predicted stiffness was highly overestimated by a factor of 32.7 and again corrected based on the correlation for the *in vivo* study.

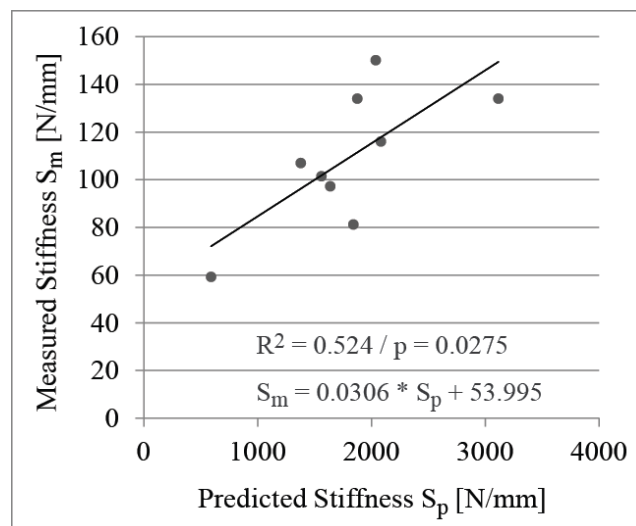


Figure 4.4: Correlation between measured and predicted bone-implant stiffness; the experimental and numerical results were obtained from the rat cadaver study.

4.4.3 Analysis of the *In vivo* Study

All 67 microFE models were created and analyzed successfully. Values for the force at yield and force at pullout as well as for the bone-implant stiffness were predicted for all samples at all analyzed time points (Figure 4.5).

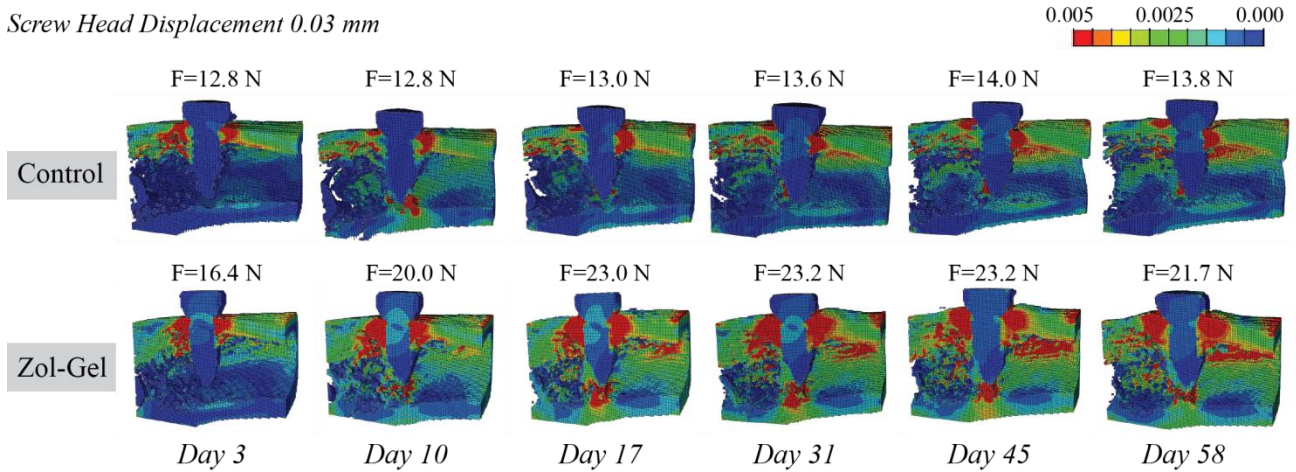


Figure 4.5: One sample from each group showing the octahedral shear strain maps and corrected reaction forces at each time point determined for a screw head displacement of 0.03 mm

The initial predicted force at yield was 16.4 ± 1.1 N in the Control-group and 16.1 ± 1.0 N in the Zol-Gel-group (Figure 4.6 left). In the Control-group, it increased by 9% to 17.8 ± 1.3 N between day 3 and day 10 and then did not show any marked changes until day 58. For the Zol-Gel-group, however, a total increase in the predicted force at yield of 50% to 24.1 ± 1.4 N was found between day 3 and day 31 followed by a slight decrease by 4% until day 58. The difference between the two groups was highly statistically significant starting from day 17. A similar time course was also found for the force at pullout (Figure 4.6 right) and the predicted stiffness (Figure 4.7) due to the correlations between all parameters. The force at pullout increased in the Control-group from 23.4 ± 1.7 N at day 3 by 10% to a maximum of 25.8 ± 2.2 N at day 10 and did not change significantly any more until the end of the study. The Zol-Gel-group started with a force at pullout of 23.0 ± 1.6 N that increased in total by 57% up to 36.0 ± 0.8 at day 31 followed by slight decrease of 3% until day 58. The initial value of the predicted stiffness was 145.5 ± 12.7 N/mm in the Control-group and 147.3 ± 17.8 N/mm in the Zol-Gel-group and rose by 16% to 169.9 ± 23.0 N/mm at day 58 in the Control-group and by 55% to 229.1 N/mm at day 45 in the Zol-Gel-group. Again, a statistically significant difference was found between the groups starting from day 17.

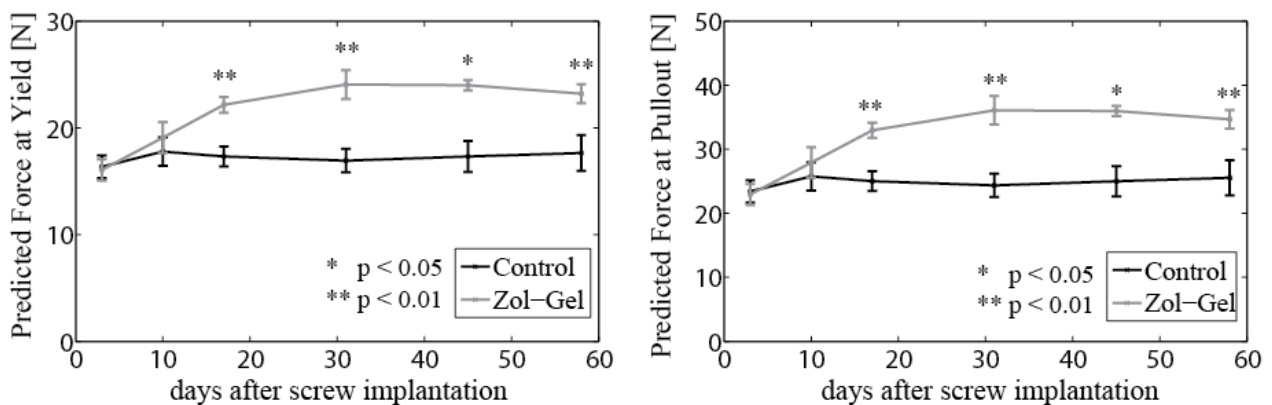


Figure 4.6: Time course of the predicted force at yield (left) and force at pullout (right) for the two groups of the *in vivo* study. The values were corrected based on the correlations identified in the cadaver study.

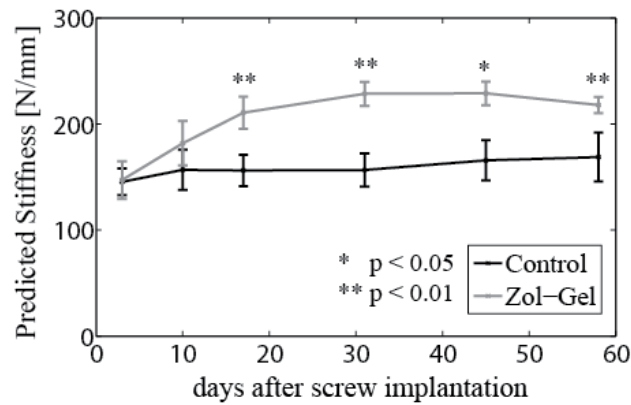


Figure 4.7: Time course of the predicted stiffness for the two groups of the *in vivo* study. The values were corrected based on the correlations identified in the cadaver study.

The test for linear correlation of all measured parameters of the cadaver study revealed a strong linear correlation between force at yield and force at pullout ($R^2=0.886$), weak correlations between BV/TV and force at yield ($R^2=0.468$), BV/TV and stiffness ($R^2=0.480$), and force at yield and stiffness ($R^2=0.583$). No correlation was found for the other combinations (Table 4.3). For the measured BV/TV and all predicted parameters of the *in vivo* study, we found high linear correlations between BV/TV and force at yield/pullout ($R^2=0.822$) and stiffness and force at yield/pullout ($R^2=0.862$) and a lower correlation for BV/TV and stiffness ($R^2=0.671$) (Table 4.3). As force at yield and force at pullout are determined based on the same reaction force from the model, their correlation is one and they have equal R^2 when compared with other parameters. The very low p-values found for the correlations of the *in vivo* study are caused by the high number of samples ($n=67$).

- Linear correlation with -		Cadaver study (n=9)		<i>In vivo</i> study (n=67)	
		R^2	p	R^2	p
BV/TV	Force at yield	<u>0.468</u>	<u>0.042</u>	<i>0.822</i>	<i>0.0000</i>
BV/TV	Force at pullout	0.349	0.0942	<i>0.822</i>	<i>0.0000</i>
BV/TV	Stiffness	<u>0.480</u>	<u>0.0386</u>	<i>0.671</i>	<i>0.0000</i>
Stiffness	Force at yield	<u>0.583</u>	<u>0.0166</u>	<i>0.862</i>	<i>0.0000</i>
Stiffness	Force at pullout	0.378	0.0781	<i>0.862</i>	<i>0.0000</i>
Force at yield	Force at pullout	<i>0.886</i>	<i>0.0002</i>	<i>1</i>	<i>0.0000</i>

Table 4.3: Coefficients of determination (R^2) and p-values for the linear correlations between all measured parameters of the cadaver study and the measured BV/TV and all predicted parameters of the *in vivo* study (underlined values: $p<0.05$, italic values: $p<0.01$).

4.5 Discussion

The goal of the present study was to investigate the temporal influence of locally delivered Zoledronate on the implant fixation in a rat model of postmenopausal osteoporosis. This was done based on time-lapsed *in vivo* microCT scans that were taken weekly to bi-weekly from the screw implantation sites. The scans were used to create linear elastic microFE models that could predict force at yield and pullout as well as stiffness

of the bone-implant construct. With this microFE approach, we were able to confirm for the first time numerically the positive effect of locally delivered Zoledronate on implant fixation. More importantly, the combination of *in vivo* microCT with microFE analysis revealed insights in the time course of the Zoledronate effect showing that a significant enhancement of screw fixation can be expected in rats as early as 17 days after implantation and can persist for minimum 6 weeks after onset. This result is of great importance considering the aim of the local bisphosphonate delivery, which is the rapid stabilization of osteosynthesis implants in osteoporotic patients. The possibility for an early loading of the implant is crucial for a mobilization of the patients. Therefore, the drug effect should occur as soon as possible after implantation and persist until the fracture has healed completely.

A close investigation of the results from this study highlighted that the load in this femoral model of postmenopausal osteoporosis is mainly transmitted from the screw in the cortical bone as only little amounts of cancellous bone structure are left over. The increase in force at yield and pullout as well as the stiffness in the Zol-Gel-groups is also caused to a high extent by the periosteal callus formation and resulting thickening of the cortex, which was observed in this group around the screw head (chapter 2). The newly formed trabecular bone seems to play a less significant role for the load transfer. No significant callus formation was observed in the control group, which explains the small increase in predicted force at yield, by only 9% that occurred already during the first 10 days. Stadelmann et al. investigated the time course of the implant fixation in rat tibia without any pharmacological treatment (Stadelmann, Conway et al. 2013). They reported a time course similar to the one found in the present study for the force at yield with a peak at day 9, the reported maximum gain in force at yield however was much higher with 71% (Stadelmann, Conway et al. 2013). This significant difference might have been caused by the difference in screw size and geometry as well as by the intact trabecular bone structure of the healthy rats used in their study. The values for force at yield and pullout as well as for the stiffness reported in the present study are in general low compared to published data from other rat studies (Andersson, Agholme et al. 2010; Stadelmann, Conway et al. 2013). This can be explained by the experimental pullout test conditions of the present study including small screw size, the non-osteointegrated state of the screws and the low bone density of the rat cadavers used. When comparing the results obtained in this study with previously published experimental data, excellent accordance can be found. Skoglund et al. performed pullout tests with miniature screws implanted in rat tibiae. They reported a 15% larger force at pullout and 28% higher stiffness in animals that received miniature screws with a local dose of Ibandronate compared to control 14 days after implantation (Skoglund, Holmertz et al. 2004). We found an increase in predicted force at pullout of 8% after 10 days and 32% after 17 days as well as an increase in stiffness of 16% after 10 days and 35% after 17 days for the Zoledronate treated animals. Other studies obtained also similar values two weeks after screw implantation and bisphosphonate release (Tengvall, Skoglund et al. 2004; Wermelin, Aspenberg et al. 2008). One more study from the Aspenberg group reported a 41% increase in pullout force for bisphosphonate coated screws after 4 weeks (Agholme, Andersson et al. 2011) which corresponds again very well with the 42% increase that we found after the same time period. We found only one long term study published by Wermelin et al. that investigated the temporal effect of Pamidronate and Ibandronate

immobilized on stainless steel screws via a fibrinogen layer on screw fixation (Wermelin, Tengvall et al. 2007). For screws that were implanted close to the diaphyseal area in rat tibiae, a position comparable in terms of trabecular bone density to our OVX femoral model, they reported an increasing difference in pullout load between control and bisphosphonate animals until week 4 (69%) which diminished at week 8 (43%). In the present study the peak difference between Control-group and Zol-Gel group was also identified at week 4 (42%) and slightly diminished at week 6 (39%) and week 8 (31.5%). Lower values in the present study might again be caused by smaller screws and the reduce trabecular bone density.

The screws used in the present *in vivo* study were made from a special barium sulfate-loaded PEEK that is visible on microCT scans but, unlike titanium or stainless steel implants, does not cause artifacts. This way we eliminated one of the limitations of other microFE studies which were based on *in vivo* microCT presenting metal artifact biased peri-implant bone structure (Wirth, Mueller et al. 2010; Stadelmann, Conway et al. 2013). At the same time, the comparatively soft polymer screws did not allow us performing pullout tests for a validation of the model. Therefore, we did a complementary study with rat cadavers for an identification of the possible correlations, which was designed to be as similar as possible to the actual *in vivo* study. The aluminum screws used for the cadaver study had an identical geometry than the PEEK screws of the *in vivo* study. Aluminum was chosen as screw material, as it is artifact-free in the microCT and has at the same time sufficient mechanical properties for a pullout test. The bone loss situation was comparable in the lactating rats of the cadaver study and the OVX rats of the *in vivo* study as confirmed by comparison of the BV/TV. In the cadaver study we found a good linear correlation between predicted and measured force at yield ($R^2 = 0.75 / p=0.003$) and a weaker correlation for the force at pullout ($R^2 = 0.65 / p=0.009$) within a VOI of 3 mm diameter, with an octahedral shear strain level of 0.5% and a highly strained bone volume fraction of 30%. A significant but weaker linear correlation was also found for the measured and predicted stiffness ($R^2 = 0.52 / p=0.03$). Wirth *et al.* and Stadelmann *et al.* also reported a good correlation for the failure load but did not find any correlation between predicted and measured stiffness in cadaver or *ex vivo* studies (Wirth, Mueller et al. 2010; Stadelmann, Conway et al. 2013). One possible explanation for this difference is probably due to our osteoporotic model with a load transfer from the comparatively small screws mainly into the cortices.

The numerical models used for the present study were purely linear elastic, therefore only the linear elastic first part of the pullout test could be reliably predicted. The weak linear correlation that was found in this study between the measured and predicted force at pullout is caused by a linear correlation between the measured force at yield and the measured force at pullout. This linear correlation is not typical for pullout tests with bone screws (Stadelmann, Conway et al. 2013) and must be considered as being model-specific. Another limitation concerns the interface between screw and bone, which was considered as being rigid in the numerical models. This assumption might be justifiable for fully osteointegrated screws but is questionable for screws directly after insertion or implanted into cadaveric bone. However, in screws unlike in pins, the threaded part of the screw achieves a form closure and prevents friction to have a decisive contribution to the pullout forces (Wirth, Mueller et al. 2010; Stadelmann, Conway et al. 2013).

A down sampling of the element size from 18.4 μm (microCT resolution) to 55.2 μm was necessary to reduce computational costs, but it might have also distorted thin trabecular structures (Cooper, Turinsky et al. 2007). However, as mentioned above, the main loads in this osteoporotic model are taken by the cortices. Those are comparatively wider and therefore less sensitive to the bias that is caused by a reduction of the resolution. One further limitation that affects microCT based studies in general is the fact that computed tomography can detect the degree of mineralization of the bone but is unable to differentiate between mature lamellar bone and unstructured woven bone (Mulder, Koolstra et al. 2008). Woven bone can have a higher degree of mineralization than lamellar bone, but its irregular oriented collagen fibers and irregular mineralization patterns make it mechanically inferior (Currey 1998). The microFE approach considers all bone parts that exceed a certain mineralization degree (grey value threshold for bone segmentation) as equally mechanical competent. This might be a disadvantage in the current study as the bone trauma caused by the insertion of an implant is known to cause a rapid formation of woven bone in direct proximity of the implant (Marco, Milena et al. 2005). We recently showed that this early peri-implant bone formation is even enhanced by a fast local delivery of Zoledronate (chapter 2). Studies have also shown that the bisphosphonate can delay the remodeling of the newly formed woven bone to lamellar bone (McDonald, Dulai et al. 2008), however the intrinsic mechanical properties of healing bone should not be affected by the bisphosphonate (Amanat, He et al. 2008). All those processes and factors are not taken into account in the microFE analysis. For future studies, one possible improvement for this limitation could be the combination of dynamic histomorphometry and microFE (Schulte, Lambers et al. 2011) (chapter 2) to identify newly formed bone. Depending on the maturity of the bone, the bone properties could then be adapted in the microFE model.

Despite several inherent limitations, the good correlations between the results of the present study and published experimental and numerical data confirm the great potential of microFE analysis to predict the time course of implant fixation *in vivo* and how it is altered by the presence of the locally delivered Zoledronate.

4.6 Conclusion

With the present study, we were able to show the time course of the Zoledronate effect on implant fixation *in vivo* based on microFE analysis. The locally delivered bisphosphonate was predicted by the microFE model to significantly improve force at yield and pullout as well as stiffness already 2 weeks after screw implantation in a femoral rat model of postmenopausal osteoporosis. The difference between the groups persisted until the end of the study after 8 weeks. Those results indicate that the local delivery of bisphosphonates from a hydrogel matrix can improve the fixation of implants in impaired bone rapidly and over a long time. These are very important aspects considering the fact that the bisphosphonate delivery system is intended to stabilize osteosynthesis implant systems in osteoporotic bone.

4.7 Acknowledgements

Special thanks to Sandra Jaccoud at the LBO for her assistance during rat surgeries and dissection.

4.8 References

- Abtahi, J., P. Tengvall, et al. (2012). "A bisphosphonate-coating improves the fixation of metal implants in human bone. A randomized trial of dental implants." *Bone* **50**(5): 1148-1151.
- Agholme, F., T. Andersson, et al. (2011). "Local bisphosphonate release versus hydroxyapatite coating for stainless steel screw fixation in rat tibiae." *Journal of Materials Science: Materials in Medicine*: 1-10.
- Amanat, N., L. H. He, et al. (2008). "The effect of zoledronic acid on the intrinsic material properties of healing bone: an indentation study." *Med Eng Phys* **30**(7): 843-847.
- Andersson, T., F. Agholme, et al. (2010). "Surface immobilized zoledronate improves screw fixation in rat bone: a new method for the coating of metal implants." *J Mater Sci Mater Med* **21**(11): 3029-3037.
- Augat, P., U. Simon, et al. (2005). "Mechanics and mechano-biology of fracture healing in normal and osteoporotic bone." *Osteoporos Int* **16 Suppl 2**: S36-43.
- Broderick, J. M., R. Bruce-Brand, et al. (2013). "Osteoporotic Hip fractures: The burden of fixation failure." *The Scientific World Journal* **2013**(515197).
- Carter, D. R., W. E. Caler, et al. (1981). "Fatigue behavior of adult cortical bone: The influence of mean strain and strain range." *Acta Orthopaedica Scandinavica* **52**(5): 481-490.
- Cooper, D., A. Turinsky, et al. (2007). "Effect of voxel size on 3D micro-CT analysis of cortical bone porosity." *Calcified Tissue International* **80**(3): 211-219.
- Cummings, S. R. and L. J. Melton (2002). "Osteoporosis I: Epidemiology and outcomes of osteoporotic fractures." *Lancet* **359**(9319): 1761-1767.
- Currey, J. D. (1998). "Mechanical properties of vertebrate hard tissues." *Proceedings of the Institution of Mechanical Engineers, Part H: Journal of Engineering in Medicine* **212**(6): 399-411.
- Gao, Y., E. Luo, et al. (2009). "Effect of combined local treatment with zoledronic acid and basic fibroblast growth factor on implant fixation in ovariectomized rats." *Bone* **44**(2): 225-232.
- Hernlund, E., A. Svedbom, et al. (2013). "Osteoporosis in the European Union: Medical management, epidemiology and economic burden: A report prepared in collaboration with the International Osteoporosis Foundation (IOF) and the European Federation of Pharmaceutical Industry Associations (EFPIA)." *Archives of Osteoporosis* **8**(1-2).
- Jäger, M., C. Zilkens, et al. (2007). "Significance of nano- and microtopography for cell-surface interactions in orthopaedic implants." *Journal of Biomedicine and Biotechnology* **2007**.
- Kabel, J., B. Van Rietbergen, et al. (1999). "The role of an effective isotropic tissue modulus in the elastic properties of cancellous bone." *Journal of Biomechanics* **32**(7): 673-680.
- Marco, F., F. Milena, et al. (2005). "Peri-implant osteogenesis in health and osteoporosis." *Micron* **36**(7-8): 630-644.
- McDonald, M. M., S. Dulai, et al. (2008). "Bulus or weekly zoledronic acid administration does not delay endochondral fracture repair but weekly dosing enhances delays in hard callus remodeling." *Bone* **43**(4): 653-662.
- Miller, S. C. and B. M. Bowman (1998). "Comparison of bone loss during normal lactation with estrogen deficiency osteopenia and immobilization osteopenia in the rat." *Anatomical Record* **251**(2): 265-274.
- Morgan, E. K., TM; Yeh, OC (2009). *Bone Mechanics. Biomedical engineering and design handbook*. M. Kutz. New York, McGraw-Hill. **1**.
- Mulder, L., J. H. Koolstra, et al. (2008). "Relationship between tissue stiffness and degree of mineralization of developing trabecular bone." *Journal of Biomedical Materials Research - Part A* **84**(2): 508-515.
- Muller, R. and P. Ruegsegger (1995). "Three-dimensional finite element modelling of non-invasively assessed trabecular bone structures." *Medical Engineering and Physics* **17**(2): 126-133.
- Nagaraja, S., T. L. Couse, et al. (2005). "Trabecular bone microdamage and microstructural stresses under uniaxial compression." *Journal of Biomechanics* **38**(4): 707-716.
- Perren, S. M. (1979). "Physical and biological aspects of fracture healing with special reference to internal fixation." *Clinical Orthopaedics and Related Research* **NO. 138**: 175-196.
- Peter, B., O. Gauthier, et al. (2006). "Local delivery of bisphosphonate from coated orthopedic implants increases implants mechanical stability in osteoporotic rats." *J Biomed Mater Res A* **76**(1): 133-143.
- Pistoia, W., B. Van Rietbergen, et al. (2002). "Estimation of distal radius failure load with micro-finite element analysis models based on three-dimensional peripheral quantitative computed tomography images." *Bone* **30**(6): 842-848.
- Qi, M., J. Hu, et al. (2012). "Effect of zoledronate acid treatment on osseointegration and fixation of implants in autologous iliac bone grafts in ovariectomized rabbits." *Bone* **50**(1): 119-127.
- Schiuma, D., M. Plecko, et al. (2013). "Influence of peri-implant bone quality on implant stability." *Medical Engineering and Physics* **35**(1): 82-87.

- Schulte, F. A., F. M. Lambers, et al. (2011). "In vivo micro-computed tomography allows direct three-dimensional quantification of both bone formation and bone resorption parameters using time-lapsed imaging." Bone **48**(3): 433-442.
- Skoglund, B., J. Holmertz, et al. (2004). "Systemic and local ibandronate enhance screw fixation." J Orthop Res **22**(5): 1108-1113.
- Stadelmann, V. A., C. M. Conway, et al. (2013). "In vivo monitoring of bone-implant bond strength by microCT and finite element modelling." Computer Methods in Biomechanics and Biomedical Engineering **16**(9): 993-1001.
- Tengvall, P., B. Skoglund, et al. (2004). "Surface immobilized bisphosphonate improves stainless-steel screw fixation in rats." Biomaterials **25**(11): 2133-2138.
- Wermelin, K., P. Aspenberg, et al. (2008). "Bisphosphonate coating on titanium screws increases mechanical fixation in rat tibia after two weeks." J Biomed Mater Res A **86**(1): 220-227.
- Wermelin, K., P. Tengvall, et al. (2007). "Surface-bound bisphosphonates enhance screw fixation in rats--increasing effect up to 8 weeks after insertion." Acta Orthop **78**(3): 385-392.
- Wirth, A. J., J. Goldhahn, et al. (2011). "Implant stability is affected by local bone microstructural quality." Bone **49**(3): 473-478.
- Wirth, A. J., T. L. Mueller, et al. (2010). "Mechanical competence of bone-implant systems can accurately be determined by image-based micro-finite element analyses." Archive of Applied Mechanics **80**(5): 513-525.
- Zhang, B. G. X., D. E. Myers, et al. (2014). "Bioactive coatings for orthopaedic implants-recent trends in development of implant coatings." International Journal of Molecular Sciences **15**(7): 11878-11921.

Chapter 5 Discussion and Perspectives

5.1 Clinical Situation and Specifications for the Drug Delivery System

Osteoporosis is one of the major health problems in our aging population. This metabolic bone disease, characterized by a reduced bone mass and a deteriorated bone microstructure, affected 27.5 million individuals in the European Union in 2010, this number is expected to rise by 23% to 2025 (Hernlund, Svedbom et al. 2013). The main clinical consequences of osteoporosis are fragility fractures that are associated with severe pain and suffering, disability and even death for the patients and a substantial economic burden for the society. The costs caused by osteoporosis were estimated to € 37 billion in 2010 in the European Union, whereas 66% were spent for incident fractures and 29% for long term fracture care (Hernlund, Svedbom et al. 2013). The main challenge for the treatment of osteoporotic fractures is a reliable anchorage of osteosynthesis implants in the impaired bone (Cornell 2003; Broderick, Bruce-Brand et al. 2013). A stable internal or external fixation, however, is crucial for a rapid bone healing, return of function and the prevention of complications (Lampropoulou-Adamidou, Karampinas et al. 2014). Therefore many new strategies to improve implant fixation have been developed and tested during the last decade, including mechanical and pharmaceutical approaches (Pioletti, Gauthier et al. 2008; Aspenberg 2009; Augat and Bühren 2010; Kammerlander, Erhart et al. 2013). The demands on new techniques and devices are high. In order to reduce the morbidity of the mainly elderly osteoporotic patients, their mobilization after fracture treatment has to occur as soon as possible (Beaupre, Binder et al. 2013; Liem, Kammerlander et al. 2013). Consequently, the fixation of osteosynthesis implants in the distorted osteoporotic bone has to be optimally strong and reliable from the time of implantation until the end of the bone healing process. At the same time, the device should ideally have no negative long-term effects on the bone and should not interfere with revision surgeries or implant removal. Until now, no technique was found that could meet all those requirements. New implant designs and mechanical fixation concepts like locking plates have shown to improve the load transmission and distribution in deteriorated bone (Kammerlander, Erhart et al. 2013; Lampropoulou-Adamidou, Karampinas et al. 2014). However, the insufficient bone strength remains an unsolved underlying problem of the difficult implant fixation; therefore, the success of this approach is limited. Another strategy is the augmentation of implants, in this case mostly bone screws, with PMMA or calcium phosphate bone cements (Amendola, Gasbarrini et al. 2011; Larsson, Stadelmann et al. 2012; Namdari, Rabinovich et al. 2013). This approach has been shown to enhance significantly the primary stability of implants (Fensky, Nüchtern et al. 2013; Gradl, Knobe et al. 2013). But as those cements are either non-degradable (PMMA) or only slowly degradable (calcium phosphate), they can be dangerous when leaking into fracture sites or surrounding organs and soft tissues (Sermon, Hofmann-Fliri et al. 2014) and they might impair the surrounding bone on the long term (Huang,

Yan et al. 2005; Lindner, Kanakaris et al. 2009). The most promising pharmaceutical approach investigated during the last years is the local delivery of anabolic or anti-catabolic drugs to the peri-implant bone. Most of the published studies addressed the release of the anti-resorptive bisphosphonates (BPs) and could show positive effects on peri-implant bone density and implant fixation in animal models and humans (Peter, Gauthier et al. 2006; Abtahi, Tengvall et al. 2012; Bobyn, Thompson et al. 2014). Anabolic substances like strontium ranelate or growth factors have been tested as well but shown to be less efficient in improving implant fixation (Andersen, Offermanns et al. 2013; Fu, Zhang et al. 2014; Ross, Hamilton et al. 2014). Drug delivery systems can significantly enhance the osteointegration and peri-implant bone density in the longer term but all of them failed so far to improve the primary stability of the implants. Attempts have been made recently to optimize the results by combining different approaches for example by loading bone cements with BPs (Sörensen, Arnoldi et al. 2013), but the perfect solution still could not be found.

5.2 Hydrogel as Drug Delivery System for Bisphosphonates

The main goal of the present doctoral thesis was the development of a BP delivering hydrogel targeting the improvement of implant fixation in osteoporotic bone. The studies performed in the frame of this thesis revealed that hyaluronic acid hydrogels are suitable drug delivery systems for BPs that show inherent advantages over other known release systems. The first positive aspect of using a hydrogel as drug delivery system is the simplicity of the application. The mechanical properties of the hyaluronic acid hydrogel can be tailored to specific implantation sites by selecting appropriate polymer concentrations or molecule sizes as well as by crosslinking processes (Holloway, Ma et al. 2014). The gel can be applied to the prepared implant bed by simple injection, as a pre-shaped bulk material or even in lyophilized dry form. At the same time, the viscosity of the hydrogel keeps the drug from being washed away, as would occur when applying a simple drug solution. We could show in this thesis that the gel is pushed in the bone cavities during implant insertion. This way, even bone further away from the implant comes in direct contact with the drug.

This seems to be an important aspect as BPs have a high affinity to bone mineral and therefore stay highly localized when released into bone (Nancollas, Tang et al. 2006; McKenzie, Dennis Bobyn et al. 2011). The animal studies of this thesis revealed the strongest drug effect on bone formation and resorption within the bone region where a direct contact between Zoledronate-loaded hydrogel and trabecular bone was assumed (0-750 μm from the screw surface) (chapter 2). A weaker effect, however, was also seen in the region between 750-1500 μm from the surface suggesting that there was nevertheless some diffusion of the drug. Earlier studies of our group performed with Zoledronate absorbed to hydroxyapatite coated titanium implants showed with similar drug doses only very localized effects within a range of 70-250 μm from the implant surface in rats and 400 μm from the implant surface in sheep (Peter, Pioletti et al. 2005; Peter, Gauthier et al. 2006; Stadelmann, Gauthier et al. 2008). Those results confirm also the findings of other publications stating that BPs are not easily released from mineral surfaces as a release requires certain conditions such as an acidic environment (Ebetino, Francis et al. 1998). In addition, once the BP molecule is dissociated from the bone, long diffusion paths are inhibited by a fast re-absorption (Russell,

Watts et al. 2008). Taken together, the results of this thesis clearly suggest that the penetration of the bone with a BP-loaded matrix has the advantage of a significantly enlarged range of action compared to a delivery from the implant surface as it is achieved with a drug releasing coating.

Another positive aspect of the BP release via a hydrogel seems to be the fast release of the small drug molecules from the highly porous polymeric matrix. We were able to confirm this burst release with an indirect cell assay demonstrating that around 75% of the drug are released from a hyaluronic acid hydrogel within one hour of incubation in water (chapter 3). We stated that this initial “Zoledronate flush” of the peri-implant bone might be responsible for the positive effect on early bone formation that we demonstrated *in vivo* (chapter 2). Numerous *in vitro* studies have shown that BPs can have positive or negative effects on osteoblasts, depending on the drug dose and study design (Pan, To et al. 2004; Greiner, Kadow-Romacker et al. 2006; Idris, Rojas et al. 2008; Orriss, Key et al. 2009). The *in vitro* cell assay results, however, are very difficult to use for a prediction of the *in vivo* situation as the fast absorption of BPs to bone prevents osteoblasts from being exposed to high drug concentrations in solution, as it is the case in cell culture assays. Unlike osteoclasts, osteoblasts do not have the ability to liberate BPs from the bone surface (Rogers, Gordon et al. 2000; Coxon, Thompson et al. 2008). A burst release of the BP in direct proximity to the osteogenic cells, however, might be sufficient to stimulate other cell types than osteoclasts and macrophages.

The superiority of a burst release of BPs release to a slow controlled release is also suggested by the results of a rat fracture healing study performed by McDonald et al. (McDonald, Dulai et al. 2008). The group demonstrated that a systemic bolus administration of Zoledronate increased callus size and strength while allowing hard callus remodeling only with a short delay compared to control. A distribution of the same Zoledronate dose over a period of 5 weeks, however, significantly affected the remodeling long after cessation of the treatment. This is also important information considering the fact that the Zoledronate-loaded hydrogel is intended to be used to stabilize osteosynthesis implants in proximity to a fracture site, therefore a drug effect on the fracture healing cannot be excluded. The positive effect of BPs on early callus size and strength described by McDonald et al. and other studies (Fleisch 2001; Amanat, Brown et al. 2005; McDonald, Dulai et al. 2008; Matos, Tannuri et al. 2010) is desirable. An inhibition of the hard callus remodeling as it has been associated with a prolonged BP administration, nevertheless has to be avoided.

To sum up, there is much to suggest that hydrogels and in particular the biodegradable hyaluronic acid are favorable biomaterials for a local release of bisphosphonates in peri-implant bone presenting many advantages over other systems such as slow releasing coatings.

5.3 Applicability of the New Drug Delivery System

The ideal application areas for pure hydrogel containing only the BP are bone regions with insufficient bone density and bone strength, where the formation of new bone needs to be encouraged while avoiding a resorption of the existing bone stock. This is typically the case in the surrounding of osteosynthesis

implants such as bone screws especially if those have to be anchored in the trabecular bone of the epiphyseal and metaphyseal regions of long bones. Implant placement in these sites is known to be particularly difficult in osteoporotic patients (Stromsoe 2004). The microFE study that was performed for this thesis nevertheless revealed that the gain in stiffness and force at pullout in Zoledronate treated OVX rats was caused to a high extent by a periosteal callus formation around the screw with resulting thickening of the cortex (chapter 4). This result suggests that an application of the BP-loaded hydrogel could also be favorable in the diaphyseal regions of long bones.

Another possible application for the BP-hydrogel could be the bone stock around joint replacing endoprostheses. Hilding et al. demonstrated that locally applied Ibandronate significantly reduced the migration of cemented total knee prostheses in humans (Hilding and Aspenberg 2007). A meta-analysis of 14 randomized trials revealed that systemically administered BPs could also significantly inhibit peri-implant bone loss up to 72 months after joint replacement surgery without reporting any serious side effects related to the drug (Lin, Yan et al. 2012). Those promising findings encourage a further investigation of the use of BP-hydrogels for an enhanced osteointegration of long-term implants such as endoprostheses while preventing peri-implant bone loss.

In the frame of this thesis, we also tested the hyaluronic acid hydrogel in combination with Zoledronate-loaded hydroxyapatite nano-particles (nHA) in our rat model. Prior cell culture assays had shown an enhancement of the inhibitory effect on murine macrophages by the presence of the hydroxyapatite particles (chapter 3). *In vivo* we had the much-unexpected effect of a rapid mineralization of the hydrogel due to the presence of the nHA. The mineralized and therefore microCT-detectable hydrogel inhibited an investigation of the precise bone formation and resorption processes as bone and mineralized material could not be distinguished on the microCT scans. Histology performed at the end of the study showed in both experimental groups, receiving either nHA-hydrogel and or nHA-hydrogel with Zoledronate, the formation of mineralized granules that served as scaffold for new bone formation. In the animals that had the nHA loaded with Zoledronate, we detected a complementary anti-resorptive effect on both the mineralized hydrogel and the surrounding bone. The finding that the hydrogel might serve as *in situ* forming scaffold requires a closer investigation but it might extend the area of application for the particle-loaded hydrogel to non-load-bearing, difficult-to-access bone defects. The hydrogel loaded only with the HA-particles could be used in patients with normal bone quality to fill bone defects that appear for example after implant or bone tumor removal to encourage new bone formation without leaving bulky residues as can be seen after the use of bone cements. A loading of the HA-particles with a BP might be very useful for cases where bone loss is a concern, for example in osteoporotic patients or for the gap filling around implants where peri-implant bone loss is expected.

5.4 Perspectives

5.4.1 Testing the Model and Dose Dependency of the Results

The *in vivo* studies performed as part of this thesis used only one drug dose of 5 µg per implant. This dose was based on similar studies that reported a positive effect on peri-implant bone for locally applied Zoledronate doses from less than 1 µg to 20 µg (Peter, Gauthier et al. 2006; Greiner, Wildemann et al. 2008; Andersson, Agholme et al. 2010). We were the first to show with a microCT based dynamic bone monitoring that Zoledronate released from hyaluronic acid hydrogel has a positive effect on early bone formation rate (chapter 2). *In vitro* studies nevertheless have shown that BP effects on osteogenic cells are highly dose dependent (Greiner, Kadow-Romacker et al. 2006; Orriss, Key et al. 2009). Therefore further dose-response studies with Zoledronate-loaded hydrogels are necessary to evaluate the dose dependency of the anti-resorptive effect on osteoclasts and, even more important, the positive effect on early bone formation.

Finally, the insertion of non-load-bearing miniature screws in ovariectomized rats is a strong simplification of the real situation, which is the use of osteosynthesis systems in osteoporotic patients. Despite the very promising results in the rat study, more sophisticated studies with load-bearing implants in larger animal models will have to be performed for a reliable prediction of the actual time course and range of action of the drug effect that can be expected in humans.

5.4.2 Investigation of the Enhanced Early Bone Formation

MicroCT-based dynamic histomorphometry enabled us to detect an enhancement of the early bone formation in our animal studies (chapter 2). This technique nevertheless cannot show how this process is driven on a cellular level. Therefore further *in vivo* studies with histology scheduled already shortly after implantation are needed to understand how Zoledronate released from hyaluronic acid hydrogels can influence early bone formation. Those histology-focused experiments are ideally combined with the above-mentioned dose-response studies in order to get a comprehensive view of the Zoledronate effect on osteogenic cells *in vivo*.

5.4.3 Investigation of the *in vivo* Hydrogel Mineralization

One very interesting aspect that was detected in the frame of this thesis but unfortunately could not be investigated more in detail is the rapid *in vivo* mineralization of the hyaluronic acid hydrogel in the presence of HA nanoparticles (chapter 3). It is well described in the literature that hydrogel can mineralize when calcium phosphate is added as nucleation points (Gkioni, Leeuwenburgh et al. 2010), but we could not find any studies reporting a mineralization of the gel with similar density than bone after 10 days of implantation. Even a group that used BP-bound calcium phosphate-containing hyaluronic acid hydrogels for bone repair did not report any significant mineralization after 4 weeks of implantation (Nejadnik, Yang et al. 2014). Again, *in vivo* studies with histology scheduled at early time points have to be performed to

understand the mineralization processes and how they interfere with bone formation and resorption and the hydrogel degradation. For this purpose, a bone defect model should be chosen instead of the peri-implant bone model, as the “*in situ* scaffold forming” hydrogel is a promising candidate for bone defect repair. Another very important aspect to investigate is the composition of the mineralized hydrogel as it could be done with energy-dispersive X-ray (EDX) spectroscopy and its mechanical properties by nano-indentation. This way information about a possible augmentation or weakening of the bone by the presence of the mineralized granules can be gained. Furthermore, the *in vitro* mineralization capability of hydrogels should be tested for example by immersion of the gels in simulated body fluids. *In vitro* experiments would give a fast and easy possibility to identify critical parameters for the mineralization such as particle material, size, shape or concentration as well as the type, density and degradation profile of the hydrogel. Further analyses are also required to investigate the interaction between the hydrogel mineralization and the BP as well as the delivery of the drug and/or the drug loaded particles from the gel.

5.4.4 Improvement of Implant Primary Stability

One secondary objective of this thesis that finally could not be achieved was to prove that reinforcing the hydrogel with a sufficient amount of particles could improve the primary stability of the screws immediately after surgery. There are publications indicating that filling the space between the trabeculae can significantly improve pullout strength in human cancellous bone (Steeves, Stone et al. 2005). We followed this theory and performed pullout tests with either rat cadavers or artificial bone after application of hydrogels loaded with big amounts of hydroxyapatite or composite microspheres (annex). With both models, we could not confirm an enhancement of the force at pullout due to the application of the hydrogels. We concluded that both models were not appropriate to show this effect, as the cortex was very thick compared to the screw length in the rat cadaver model and the artificial polyurethane foam had no “cortex” at all and was simply too different from real bone. Further investigations should be done with either cadaveric human bone and if not available, bovine or ovine cadaveric bone. Complementary tests such as insertion and removal torque tests or resonance frequency analysis could also give a more global idea of the implant stability than a simple pullout test (Atsumi, Park et al. 2007). If it can be shown that a particle-BP-loaded hydrogel can improve both primary and secondary implant stability in osteoporotic bone, then a major step would have been taken towards the perfect implant fixation strategy that we described in chapter 5.1.

5.4.5 The Path towards a Clinical Study

Due to the industrial background of this thesis, all the research has to focus on a clinical study as milestone towards a final product. The performance of a clinical study requires the compliance with many rules and standards. First, all materials that are intended to be used in humans have to be certified for this purpose. The materials used for the experiments of this thesis were not all licensed for human use, therefore the next important step, before continuing with the above-described complementary studies, will be to find identical raw materials that are approved for implantation in humans. The next step will then be the

fabrication of the hydrogel that has to meet GMP standards. Therefore, a certified production site has to be found. Other important aspects are the sterilization, storage and application of the hydrogels. Suitable techniques, protocols and devices need to be developed and evaluated. All those procedures already have to be considered while continuing the research on this promising project to ensure a smooth transition to industry at the end.

5.5 References

- Abtahi, J., P. Tengvall, et al. (2012). "A bisphosphonate-coating improves the fixation of metal implants in human bone. A randomized trial of dental implants." *Bone* **50**(5): 1148-1151.
- Amanat, N., R. Brown, et al. (2005). "A single systemic dose of pamidronate improves bone mineral content and accelerates restoration of strength in a rat model of fracture repair." *J Orthop Res* **23**(5): 1029-1034.
- Amendola, L., A. Gasbarrini, et al. (2011). "Fenestrated pedicle screws for cement-augmented purchase in patients with bone softening: A review of 21 cases." *Journal of Orthopaedics and Traumatology* **12**(4): 193-199.
- Andersen, O. Z., V. Offermanns, et al. (2013). "Accelerated bone ingrowth by local delivery of strontium from surface functionalized titanium implants." *Biomaterials* **34**(24): 5883-5890.
- Andersson, T., F. Agholme, et al. (2010). "Surface immobilized zoledronate improves screw fixation in rat bone: a new method for the coating of metal implants." *J Mater Sci Mater Med* **21**(11): 3029-3037.
- Aspenberg, P. (2009). "Bisphosphonates and implants: an overview." *Acta Orthop* **80**(1): 119-123.
- Atsumi, M., S. H. Park, et al. (2007). "Methods used to assess implant stability: Current status." *International Journal of Oral and Maxillofacial Implants* **22**(5): 743-754.
- Augat, P. and V. Bühren (2010). "[Modern implant design for the osteosynthesis of osteoporotic bone fractures]." *Orthopade* **39**(4): 397-406.
- Beaupre, L. A., E. F. Binder, et al. (2013). "Maximising functional recovery following hip fracture in frail seniors." *Best Practice and Research: Clinical Rheumatology* **27**(6): 771-788.
- Bobyn, J. D., R. Thompson, et al. (2014). "Local alendronic acid elution increases net periimplant bone formation: A micro-CT analysis." *Clin Orthop Relat Res* **472**(2): 687-694.
- Broderick, J. M., R. Bruce-Brand, et al. (2013). "Osteoporotic Hip fractures: The burden of fixation failure." *The Scientific World Journal* **2013**(515197).
- Cornell, C. N. (2003). "Internal fracture fixation in patients with osteoporosis." *J Am Acad Orthop Surg* **11**(2): 109-119.
- Coxon, F. P., K. Thompson, et al. (2008). "Visualizing mineral binding and uptake of bisphosphonate by osteoclasts and non-resorbing cells." *Bone* **42**(5): 848-860.
- Ebetino, F. H., M. D. Francis, et al. (1998). "Mechanisms of action of etidronate and other bisphosphonates." *Reviews in Contemporary Pharmacotherapy* **9**(4): 233-243.
- Fensky, F., J. V. Nüchtern, et al. (2013). "Cement augmentation of the proximal femoral nail antirotation for the treatment of osteoporotic pertrochanteric fractures - A biomechanical cadaver study." *Injury* **44**(6): 802-807.
- Fleisch, H. (2001). "Can bisphosphonates be given to patients with fractures?" *J Bone Miner Res* **16**(3): 437-440.
- Fu, Y., Q. Zhang, et al. (2014). "Controlled-release of bone morphogenetic protein-2 from a microsphere coating applied to acid-etched Ti6AL4V implants increases biological bone growth in vivo." *Journal of Orthopaedic Research* **32**(6): 744-751.
- Gkioni, K., S. C. G. Leeuwenburgh, et al. (2010). "Mineralization of hydrogels for bone regeneration." *Tissue Engineering - Part B: Reviews* **16**(6): 577-585.
- Gradl, G., M. Knobe, et al. (2013). "Biomechanical evaluation of locking plate fixation of proximal humeral fractures augmented with calcium phosphate cement." *Journal of Orthopaedic Trauma* **27**(7): 399-404.
- Greiner, S., A. Kadow-Romacker, et al. (2006). "The effect of zoledronic acid incorporated in a poly(D,L-lactide) implant coating on osteoblasts in vitro." *J Biomed Mater Res A* **80**(4): 769-775.
- Greiner, S. H., B. Wildemann, et al. (2008). "Local application of zoledronic acid incorporated in a poly(D,L-lactide)-coated implant accelerates fracture healing in rats." *Acta Orthop* **79**(5): 717-725.
- Hernlund, E., A. Svedbom, et al. (2013). "Osteoporosis in the European Union: Medical management, epidemiology and economic burden: A report prepared in collaboration with the International Osteoporosis Foundation (IOF) and the European Federation of Pharmaceutical Industry Associations (EFPIA)." *Archives of Osteoporosis* **8**(1-2).
- Hilding, M. and P. Aspenberg (2007). "Local peroperative treatment with a bisphosphonate improves the fixation of total knee prostheses: a randomized, double-blind radiostereometric study of 50 patients." *Acta Orthop* **78**(6): 795-799.
- Holloway, J. L., H. Ma, et al. (2014). "Modulating hydrogel crosslink density and degradation to control bone morphogenetic protein delivery and in vivo bone formation." *Journal of Controlled Release*.
- Huang, K. Y., J. J. Yan, et al. (2005). "Histopathologic findings of retrieved specimens of vertebroplasty with polymethylmethacrylate cement: case control study." *Spine* **30**(19): E585-588.
- Idris, A. I., J. Rojas, et al. (2008). "Aminobisphosphonates cause osteoblast apoptosis and inhibit bone nodule formation in vitro." *Calcif Tissue Int* **82**(3): 191-201.

- Kammerlander, C., S. Erhart, et al. (2013). "Principles of osteoporotic fracture treatment." Best Practice and Research: Clinical Rheumatology **27**(6): 757-769.
- Lampropoulou-Adamidou, K., P. K. Karampinas, et al. (2014). "Currents of plate osteosynthesis in osteoporotic bone." European Journal of Orthopaedic Surgery and Traumatology **24**(4): 427-433.
- Larsson, S., V. A. Stadelmann, et al. (2012). "Injectable calcium phosphate cement for augmentation around cancellous bone screws. In vivo biomechanical studies." Journal of Biomechanics **45**(7): 1156-1160.
- Liem, I. S., C. Kammerlander, et al. (2013). "Identifying a standard set of outcome parameters for the evaluation of orthogeriatric co-management for hip fractures." Injury **44**(11): 1403-1412.
- Lin, T., S. G. Yan, et al. (2012). "Bisphosphonates for periprosthetic bone loss after joint arthroplasty: A meta-analysis of 14 randomized controlled trials." Osteoporosis International **23**(6): 1823-1834.
- Lindner, T., N. K. Kanakaris, et al. (2009). "Fractures of the hip and osteoporosis: The role of bone substitutes." Journal of Bone and Joint Surgery - Series B **91**(3): 294-303.
- Matos, M. A., U. Tannuri, et al. (2010). "The effect of zoledronate during bone healing." J Orthop Traumatol **11**(1): 7-12.
- McDonald, M. M., S. Dulai, et al. (2008). "Bolus or weekly zoledronic acid administration does not delay endochondral fracture repair but weekly dosing enhances delays in hard callus remodeling." Bone **43**(4): 653-662.
- McKenzie, K., J. Dennis Bobyn, et al. (2011). "Bisphosphonate Remains Highly Localized After Elution From Porous Implants." Clin Orthop Relat Res **469**(2): 514-522.
- Namdari, S., R. Rabinovich, et al. (2013). "Absorbable and non-absorbable cement augmentation in fixation of intertrochanteric femur fractures: Systematic review of the literature." Archives of Orthopaedic and Trauma Surgery **133**(4): 487-494.
- Nancollas, G. H., R. Tang, et al. (2006). "Novel insights into actions of bisphosphonates on bone: differences in interactions with hydroxyapatite." Bone **38**(5): 617-627.
- Nejadnik, M. R., X. Yang, et al. (2014). "Self-healing hybrid nanocomposites consisting of bisphosphonated hyaluronan and calcium phosphate nanoparticles." Biomaterials **35**(25): 6918-6929.
- Orriss, I. R., M. L. Key, et al. (2009). "Inhibition of osteoblast function in vitro by aminobisphosphonates." J Cell Biochem **106**(1): 109-118.
- Pan, B., L. B. To, et al. (2004). "The nitrogen-containing bisphosphonate, zoledronic acid, increases mineralisation of human bone-derived cells in vitro." Bone **34**(1): 112-123.
- Peter, B., O. Gauthier, et al. (2006). "Local delivery of bisphosphonate from coated orthopedic implants increases implants mechanical stability in osteoporotic rats." J Biomed Mater Res A **76**(1): 133-143.
- Peter, B., D. P. Pioletti, et al. (2005). "Calcium phosphate drug delivery system: influence of local zoledronate release on bone implant osteointegration." Bone **36**(1): 52-60.
- Pioletti, D. P., O. Gauthier, et al. (2008). "Orthopedic implant used as drug delivery system: clinical situation and state of the research." Curr Drug Deliv **5**(1): 59-63.
- Rogers, M. J., S. Gordon, et al. (2000). "Cellular and molecular mechanisms of action of bisphosphonates." Cancer **88**(12 Suppl): 2961-2978.
- Ross, R. D., J. L. Hamilton, et al. (2014). "Pharmacologic augmentation of implant fixation in osteopenic bone." Current Osteoporosis Reports **12**(1): 55-64.
- Russell, R. G., N. B. Watts, et al. (2008). "Mechanisms of action of bisphosphonates: similarities and differences and their potential influence on clinical efficacy." Osteoporos Int **19**(6): 733-759.
- Sermon, A., L. Hofmann-Fliri, et al. (2014). "Cement augmentation of hip implants in osteoporotic bone: How much cement is needed and where should it go?" Journal of Orthopaedic Research **32**(3): 362-368.
- Sörensen, T. C., J. Arnoldi, et al. (2013). "Locally enhanced early bone formation of zoledronic acid incorporated into a bone cement plug in vivo." Journal of Pharmacy and Pharmacology **65**(2): 201-212.
- Stadelmann, V. A., O. Gauthier, et al. (2008). "Implants delivering bisphosphonate locally increase periprosthetic bone density in an osteoporotic sheep model. A pilot study." Eur Cell Mater **16**: 10-16.
- Steeves, M., C. Stone, et al. (2005). "How pilot-hole size affects bone-screw pullout strength in human cadaveric cancellous bone." Can J Surg **48**(3): 207-212.
- Stromsoe, K. (2004). "Fracture fixation problems in osteoporosis." Injury **35**(2): 107-113.

Annex

A.1 Chronology of the Project: From Coating to Hydrogel

A.1.1 Evaluation of a Drug Delivering Coating

The initial idea of the CTI project behind this doctoral thesis was the development of a biodegradable, drug delivering polymer coating based on a published technique (Greiner, Wildemann et al. 2008; Back, Pauly et al. 2012). Different biodegradable polylactides (PLLAs) or polylactide-co-glycolides (PLGAs) (Resomer® R 203 S / RG 756 / LR 706 S, Evonik Industries AG, Essen, Germany) were tested for this purpose. The polymers were dissolved in different solvents and applied to titanium or stainless steel bone screws (Stryker Trauma, Selzach, Switzerland) via a dip-coating process. After several pilot studies, we were facing two major issues with this technique. First, no suitable solvent could be found that can dilute both the biodegradable polymers and the Zoledronate, the bisphosphonate used for this project. As a result, a uniform distribution of the drug in the coating was not possible. The second problem was the insufficient abrasion resistance of the coating as it could be shown with screw-in tests in artificial bones (Sawbones 1522-02, Vashon Islands, WA, US) (Figure A.1).

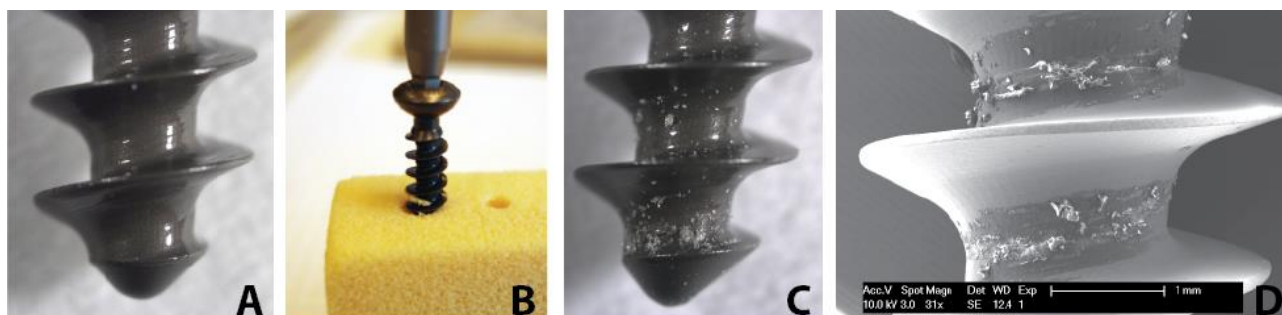


Figure A.1: Titanium cancellous bone screw coated with a polylactide (Resomer® R 203 H) directly after dip-coating (A), while being inserted in artificial bone (B), and after removal from the artificial bone (C). Scanning electron microscope image of the residues of a Resomer® R 203 coating containing hydroxyapatite nanoparticles after insertion in artificial bone (D).

Extended dilution tests with numerous solvents (ethyl acetate, acetone, chloroform, DMSO and mixtures thereof) were performed to find a suitable solvent for polymer and drug. They revealed that Zoledronate is only soluble in water up to a concentration of around 3 mg/ml and in basic aqueous solutions with higher concentrations. None of the tested solvents was able to dissolve the drug. Consequently, we changed the strategy and used different water-soluble polyvinyl alcohols (PVA, art.-nr. 363138 / 363138, Sigma-Aldrich, MO, St. Louis, US) to integrate the drug. First abrasion tests showed that this polymer is even less resistant

than the PLLAs/PLGAs. Therefore we applied a layer of PVA incorporating the drug under a layer of PLLA, a combination that showed still a poor abrasion resistance. Different strategies were tested to enhance the adhesion of the coating to the screws. The screws were pre-treated with either hydrofluoric acid etching or a silanization to improve the polymer attachment to the metal surface. A second approach attempted to reinforce the polymer with hydroxyapatite nanoparticles (art.-nr. 677418, Sigma-Aldrich, St. Louis, MO, USA) that acted at the same time as a drug carrier and helped to circumvent the solvent issue. None of the tested techniques could significantly improve the abrasion resistance of the coating; therefore, we switched to a new approach for the drug delivery system.

A.1.2 Evaluation of a Solid Drug Delivering Bone Plug

As we were not able to attach the drug delivery system on the bone screws, we investigated the possibility of separating screw and drug delivery system and to develop a drug releasing screw anchor that is inserted in the predrilled hole before screw insertion. Tube-shaped prototypes were first produced from hydroxyapatite-polymer microspheres formed with a solvent evaporation technique (Kofron, Cooper et al. 2007). The Zoledronate was loaded on the hydroxyapatite by a simple absorption. The microspheres were heat sintered to tubular structures (Figure A.2 A). First tests with artificial bone looked promising (Figure A.2 B) and first pullout tests demonstrated a gain in screw fixation of up to 15% when using this “bone plugs”. Further tests with a different Sawbone type with higher porosity and a structure more similar to human bone, however, revealed serious difficulties to insert the screw in the compact plug. Consequently, the strategy was changed once more and the microspheres were inserted in a hydrogel matrix (first cross-linked PVA, later hyaluronic acid) instead of sintering them. This approach helped to circumvent problems with the insertion of the material in the hole, as the new material could be injected and facilitated significantly the penetration with the screw. Nevertheless, as mentioned in the discussion, we could not show an improved implant fixation with this approach neither with the Sawbone model nor with a rat cadaveric model.

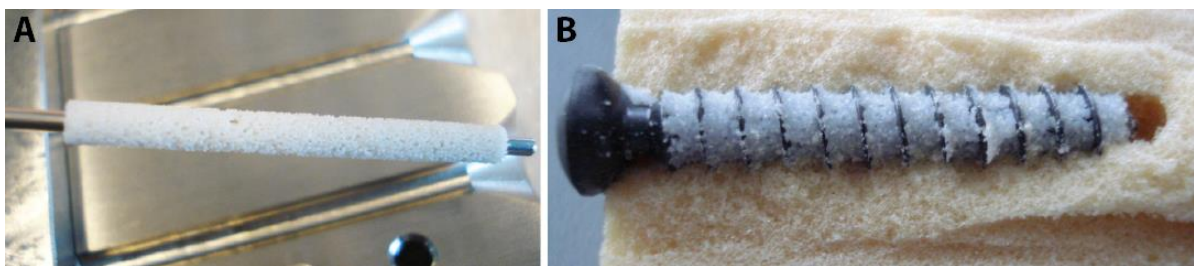


Figure A.2: Bone plugs formed by heat sintering of hydroxyapatite-poly(lactide)-microspheres (A), implanted with a cancellous bone screw in artificial bone (B).

A.2 Hollow Hydroxyapatite-Polylactide Microspheres

The above-mentioned composite microspheres were produced by diluting 15% of biodegradable PLLA (Resomer® R 203 S, Evonik Industries AG, Essen, Germany) in chloroform (Sigma-Aldrich, St. Louis, MO, USA). Hydroxyapatite-nanoparticles with a diameter of less than 200 nm (art-nr. 677418, Sigma-Aldrich, St. Louis, MO, USA) were added to the solution with a ratio polymer/HA of 3:1. The resulting dispersion was poured into a 1% aqueous PVA solution (Mowiol® 8-88, Sigma-Aldrich, MO, St. Louis, US) under continuous stirring at 650 rpm with an overhead stirrer (Heidolph RZR 2020, Schwabach, Germany). After mechanical stirring for 15 h, the microspheres were removed from the PVA solution with filter paper, rinsed with bi-distilled water and dried. The microspheres were fractionated with sieves into 3 groups of 45-100 µm, 100-300 µm and 300-500 µm.

A close inspection of the microspheres with microCT and SEM revealed that they are hollow (Figure A.3). This is a great advantage for their use in bone augmentation, as their large surface to volume ratio will speed up the degradation of the spheres while giving room for new bone formation. We could also show that the hydroxyapatite particles are present mainly on the inner and outer surface of the spheres (Figure 6:3) which enhances their biocompatibility and potential for osteoconduction. An *in vivo* pilot study with one rat showed already an excellent osteointegration of the microspheres.

Further research will be necessary but the hollow microspheres seem to be a promising candidate for reinforcing the drug-loaded hydrogels presented in this PhD thesis.

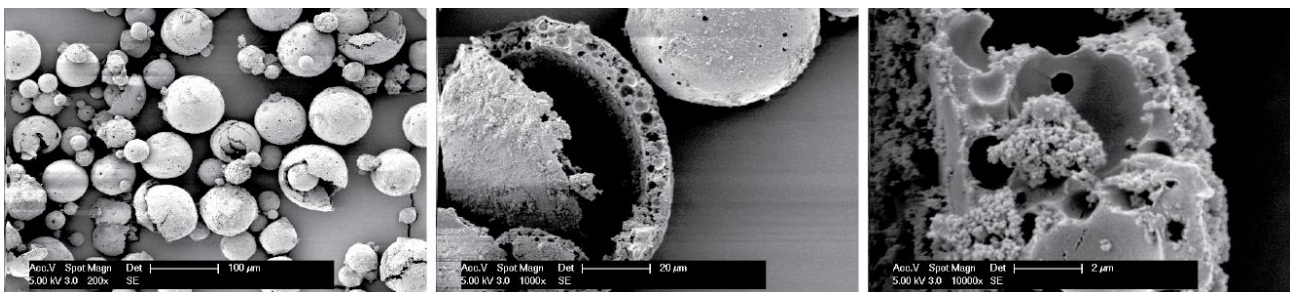


Figure A.3: Scanning electron microscope images of the hollow poly(lactide-co-glycolide)-hydroxyapatite composite microspheres with diameters ranging from 45-100 µm. They were fabricated via a solvent-evaporation technique.

A.3 References

- Back, D. A., S. Pauly, et al. (2012). "Effect of local zoledronate on implant osseointegration in a rat model." BMC Musculoskeletal Disorders **13**.
- Greiner, S. H., B. Wildemann, et al. (2008). "Local application of zoledronic acid incorporated in a poly(D,L-lactide)-coated implant accelerates fracture healing in rats." Acta Orthop **79**(5): 717-725.
- Kofron, M. D., J. A. Cooper, Jr., et al. (2007). "Novel tubular composite matrix for bone repair." J Biomed Mater Res A **82**(2): 415-425.

Ulrike Kettenberger

EDUCATION

Sept. 2010 – Sept 2014	PhD Candidate in Bioengineering and Biotechnology Swiss Federal Institute of Technology EPFL (Lausanne, Switzerland)
Oct. 2004 – May 2009	Diploma / Master of Science in Mechanical Engineering Technical University of Munich TUM (Munich, Germany)

PROFESSIONAL EXPERIENCE

Feb. 2010 – Jul. 2010	Degradable Solutions AG (Schlieren, Switzerland) Project work: Development of an insertion device for suture anchors
Jul. 2009 – Oct. 2009	Centre for Advanced Composite Materials (University of Auckland, NZ) Research assistant: Optimization of microfibril reinforced composites
Nov. 2008 – Apr. 2009	B.Braun Aesculap AG (Tuttlingen, Germany) Diploma thesis: Development of a surface replacement for facet joints
Mar. 2008 – Jul. 2008	Phonak Hearing Systems AG (Stäfa, Switzerland) Internship: Development of a windbreak for hearing systems
Nov. 2007 – Feb. 2008	Department and Chair for Medical Engineering (TUM Munich) Student assistant: Development of an intravesicular drug delivery implant
Dec. 2006 – Oct. 2007	Department of Micro and Medical Device Technology (TUM Munich) Student assistant: Project work in collaboration with BMW AG Munich

PUBLICATIONS

Journal Papers:	Kettenberger, U; Ston, J; Thein, E; Procter, P; Pioletti, DP. Does locally delivered Zoledronate influence peri-implant bone formation? - Spatio-temporal monitoring of bone remodeling in vivo. <i>Biomaterials</i> 2014; 35 (37): 9995-100006 Abdel-Sayed, P; Darwiche, SE; Kettenberger, U; Pioletti, DP. The role of energy dissipation of polymeric scaffolds in the mechanobiological modulation of chondrogenic expression. <i>Biomaterials</i> 2014; 35(6): 1890-97
Conference Abstracts:	Kettenberger, U et al. Development of a nano-composite drug eluting bone plug enhancing fixation of screws in low quality bone. eCM Conference, Davos (Switzerland), 2012 Kettenberger, U et al. Development of a biodegradable drug delivery bone plug enhancing fixation of screws in low quality bone. Tissue Engineering and Regenerative Medicine international Society, Vienna (Austria), 2012 Evaluation of the bisphosphonate-triggered bone remodeling around a bone screw based on time-lapsed microCT scans. Orthopedic Research Society, New Orleans (USA), 2014